



# Cooperative Communications in very large cellular Networks

Luis David Alvarez-Corrales

## ► To cite this version:

Luis David Alvarez-Corrales. Cooperative Communications in very large cellular Networks. Networking and Internet Architecture [cs.NI]. Telecom ParisTech, 2017. English. NNT : . tel-01811833

**HAL Id: tel-01811833**

**<https://hal.science/tel-01811833>**

Submitted on 20 Dec 2018

**HAL** is a multi-disciplinary open access archive for the deposit and dissemination of scientific research documents, whether they are published or not. The documents may come from teaching and research institutions in France or abroad, or from public or private research centers.

L'archive ouverte pluridisciplinaire **HAL**, est destinée au dépôt et à la diffusion de documents scientifiques de niveau recherche, publiés ou non, émanant des établissements d'enseignement et de recherche français ou étrangers, des laboratoires publics ou privés.



EDITE - ED 130

## Doctorat ParisTech

### THÈSE

pour obtenir le grade de docteur délivré par

**TELECOM ParisTech**

*présentée et soutenue publiquement le 14 Novembre 2017 par*

**Luis David ÁLVAREZ CORRALES**

### Titre

**Cooperative Communications in very large cellular Networks**

Directeur de thèse : **Philippe MARTINS**

Co-encadrement de la thèse : **Anastasios GIOVANIDIS**

#### Jury

**M. Anthony BUSSON**, Professeur, Université Claude Bernard Lyon 1  
**M. Marco DI RENZO**, CNRS CR1 avec Habilitation, SUPELEC  
**Mme Catherine GLOAGUEN**, Ingénieur recherche, Orange Labs  
**M. Tijani CHAHED**, Professeur, Télécom SudParis  
**M. Víctor Manuel PÉREZ-ABREU CARRIÓN**, Professeur, CIMAT  
**M. Fabien MATHIEU**, Chercheur, Nokia Bell-Labs Paris  
**M. Philippe MARTINS**, Professeur, Télécom ParisTech  
**M. Anastasios GIOVANIDIS**, Chercheur CR, CNRS-LIP6, Paris  
**M. Paul MUHLETHALER**, Directeur de recherche, Inria

Rapporteur

Rapporteur

Examineur

Examineur

Examineur

Examineur

Directeur de thèse

Co-encadrant

Invité

**TELECOM ParisTech**

école de l'Institut Mines-Télécom - membre de ParisTech

46 rue Barrault 75013 Paris - (+33) 1 45 81 77 77 - [www.telecom-paristech.fr](http://www.telecom-paristech.fr)

## Abstract

Recent studies have set the problem of base station cooperation within the framework of stochastic geometry and point processes. In this way, the irregularity of the base station positions and the randomness of other network parameters can be considered. Existing works study the case when the user can dynamically choose the set of stations cooperating for its service. This assumption, besides being not realistic, saturates the backhaul with intensive communication between the stations. To confront this problem, other authors propose to form the cooperative groups in a static way. These methodologies are, however, not optimal. Instead, static groups must be predefined by means of proximity, with nodes linked by fixed infrastructure. To analyse such a potential work, we propose a grouping method based on node proximity. Actually, it is a variation of the so called *nearest neighbor model*. With the *mutually nearest neighbor relation*, we allow the formation of singles and pairs of nodes. In this way, for a given topology of atoms, two point processes are created: the process of singles and the process of cooperative pairs. We derive structural characteristics for these and analyse the resulting interference fields. The results constitute a novel toolbox towards the performance evaluation of networks with static cooperation.

When the node positions are modelled by a *Poisson point process*, the processes of singles and pairs are not Poisson, complicating the corresponding analysis. The performance of the original model can be approximated by the superposition of two Poisson point processes. This allows the derivation of exact expressions for the coverage probability. Numerical evaluation shows coverage gains from different signal cooperation that can reach up to 15%, compared with the standard noncooperative case. The analysis is general and can be applied to any type of cooperation in pairs of transmitting nodes.

On the other hand, for the cooperation to be meaningful, each station participating in a group should have sufficient available resources to share with other. Thus, we redefine the *mutually nearest neighbor relation* with a metric that considers both geographic proximity and available resources of the stations. When the network is modelled by a Poisson point process, we derive an analysis on the proportion of cooperative pairs or single stations, and the expected sum interference from each of the groups. The results illustrate that cooperation gains strongly depend on the distribution of the available resources over the network.

## Abstrait

Des études ont abordé le problème de la coopération d'antennes d'un réseau cellulaire à l'aide de la géométrie stochastique et des processus ponctuels. Elles considèrent l'irrégularité du positionnement des antennes et la aléatoireité des autres paramètres du réseau. Certains auteurs ont étudié le cas où l'utilisateur choisit dynamiquement l'ensemble des antennes qui le serviront. Cette hypothèse n'est pas réaliste et sature le backhaul en produisant de la communication intensive parmi les antennes. Pour affronter ces problèmes, d'autres auteurs proposent former les groupes d'antennes de façon statique, bien que ces méthodologies statiques ne soient pas optimales. En effet, ces groupes statiques devraient être formés par rapport à la proximité entre les nœuds d'une infrastructure fixée.

Pour analyser le potentiel de ce genre de réseaux coopératifs, nous proposons une méthode basée sur le modèle du voisin le plus proche pour la formation des groupes. La relation de voisin le plus proche aide alors à former des singletons et des paires de nœuds. Ainsi, pour une topologie d'antennes fixe, deux différents processus ponctuels sont définis: le processus de singleton et le processus de paires coopératives. Une analyse des caractéristiques structurelles de ces deux processus est fournie, ainsi qu'une analyse de l'interférence produite par ces derniers. Ces résultats constituent une boîte à outils en direction de l'étude de métriques de performance des réseaux cellulaires coopératifs.

Lorsque le positionnement des antennes est modélisé par un processus de poisson ponctuel, les processus de singletons de paires associées ne suivent pas une loi de Poisson. Ceci complique une analyse plus profonde. Nous pouvons, cependant, rapprocher des métriques de performance du modèle original à l'aide de la superposition de deux mesures aléatoires de Poisson. Il est alors possible de trouver des expressions fermées de la probabilité de couverture. L'évaluation numériques montre des gains de couverture allant jusqu'à 15 % en comparaison du modèle non coopératif standard.

D'autre part, pour que la coopération entre les antennes soit significative, chaque antenne faisant partie d'un groupe devrait, en plus, avoir un nombre de ressources disponibles suffisante pour pouvoir les partager avec les autres. La relation de voisin le plus proche est alors redéfinie avec une métrique qui prend en considération la proximité géographique parmi les antennes et les ressources disponibles de chacune. Lorsque le réseau est modélisé par un processus de Poisson ponctuel, nous fournissons une analyse sur la proportion de singletons et paires en coopération et sur l'interférence de chaque groupe. Ces résultats montrent que les gains d'un réseau coopératif dépendent fortement de la distribution des ressources disponibles dans tout le réseau.

## Résumé

### Résumé court

Des études ont abordé le problème de la coopération d’antennes d’un réseau cellulaire à l’aide de la géométrie stochastique et des processus ponctuels. Elles considèrent l’irrégularité du positionnement des stations de base et la partie aléatoire des autres paramètres du réseau (le *fading*, le *shadowing*, entre autres), pour évaluer la performance chez les utilisateurs [ABG11, BB09]. Ainsi, la performance d’un réseau de télécommunications peut être quantifiée systématiquement. En conséquence, il n’y a pas besoin de tester, travers des simulations, à chaque scénario de la topologie d’un réseau. Les formules fermées obtenues par ces méthodes probabilistes sont très importantes pour un opérateur qui veut planifier et déployer infrastructure, puisqu’elle le fournissent de l’intuition par rapport à l’influence des divers paramètres de la conception d’un réseau cellulaires [BG15, BK15, GZZH16].

Le processus ponctuel de Poisson (PPP) est la classe de mesures ponctuelles la plus étudiée dans la littérature. En effet, tout est connu pour ce processus et ses expressions résultantes sont faciles à implémenter: la loi du processus, sa transformé de Laplace, des moments de tout ordre, sa mesure de Palm, sa représentation chaotique, entre autres. Par suite, pour l’analyse d’un réseau cellulaire modélisé par un PPP, nous avons toute la machinerie fournie par la géométrie aléatoire ou le calcul de Malliavin [ABG11, BK15, DFMTT12, DST16]. De plus, les résultats obtenus par ces formules sont faciles à comparer avec des simulations, puisqu’il est simple de simuler une réalisation d’un PPP. D’ailleurs, l’hypothèse du comportement Poisson est complètement justifiée pour une large classe de réseaux cellulaires. Par exemple, ceux-ci avec qui présentent un très fort *shadowing* [BKK15].

Le plus grand inconvénient de considérer un PPP c’est le fait que le positionnement entre les antennes est indépendant. Cela est dû au fait que, fixe le numéro des atoms sur une surface finie, leur positionnement est indépendant et identiquement distribués. En effet, cela est la façon classique de générer une réalisation d’un PPP. En particulier, la probabilité d’avoir deux nœuds aussi proche que possible est toujours positive. Cette proximité ne suit aucune règle, alors, nous ne pouvons pas parler d’une *attraction* ni d’une *répulsion* entre les atomes. Ils existent des réseaux cellulaires dont le positionnement des nœuds présent, en effet, *repulsion* ou *attraction* parmi eux. C’est pour cela que d’autres classes de processus ponctuels sont considérées aussi dans la littérature [LBDA15]. En particulier, les processus déterminantiaux, qui d’ailleurs sont repulsifs, ont été largement étudiés, spécialement le processus ponctuel  $\beta$ -Ginibre [DZH15].

La façon dont les groupes coopératifs d’antennes seront définis sur cette thèse est fortement dépendante. Par conséquent, pour que il soit possible de faire une analyse de ces réseaux coopératifs, il est impératif de pouvoir utiliser tous les outils analytiques disponibles.

Alors, sur cette thèse nous considérons que le positionnement des antennes suit une loi Poisson. Comme nous avons précisé, les réseaux cellulaires pour lesquels on peut considérer un comportement Poissonnien de ses nœuds constituent une classe assez large. De plus, les réseaux résultants de la superposition des processus ponctuels indépendants et repulsifs sont compatibles avec l’hypothèse Poissonnienne de ses nœuds [DV15].

### 0.0.1 État de l’art et motivation

Des études qui analysent les *réseaux cellulaires en coopération* sont de plus en plus trouvés dans la littérature. Ils montrent que la coopération entre les antennes réduit l’interférence et, par la suite, améliore la capacité du réseau. En plus d’être plus avantageux particulièrement pour les utilisateurs au bord d’une cellule, où d’importants gains en *SINR* s’accomplissent pour le downlink [BG15]. L’idée de coopération joue un rôle très important dans le planning et déploiement d’un réseau cellulaire. Dû à la densification des réseaux par HetNets [DGBA12, CHC14], la coopération devient, en effet, de plus en plus nécessaire. Il existe une quantité considérable de recherche sur la coopération, reliée à la conception du CoMP [IDM<sup>+</sup>11, JMZ<sup>+</sup>14], Network MIMO [JJT<sup>+</sup>08, GHH<sup>+</sup>10, GKB12], ou C-RAN [CCY<sup>+</sup>15, LAL16].

De façon générale, on peut décrire la coopération dans les réseaux cellulaires de la façon suivante:

*Un groupe coordonné d’antennes qui servent un utilisateur.*

Les différentes méthodologies de coopération proposées se distinguent par rapport à *la façon dont le signal est transmis, la quantité d’information échangée, le numéro d’antennes dans les groupes, et, particulièrement, la façon dont les groupes sont définis*. D’ailleurs, les buts des différentes méthodologies de coopération devraient être servir les utilisateurs avec un signal fort et réduire l’interférence .

Les auteurs en [GKB12] proposent la formation des groupes d’antennes d’un point de vue combinatoire, alors qu’en [PGH08], les auteurs analysent un algorithme qui intègre le traitement coopératif multi-cell. Il faut remarquer que ces deux articles ne considèrent aucune aléatorité des antennes. D’autre part, en [BG15, NMH14, BK15, TSAJ14], le positionnement des antennes suit une loi de Poisson. De cette façon, les auteurs se servent de la géométrie aléatoire pour analyser les méthodologies de coopération proposées. En [BG15] l’utilisateur typique est servi par les deux antennes les plus proches de lui, et le reste d’antennes génèrent de l’interférence en paires. Cela améliore la couverture et augmente la cellule de couverture. En [NMH14] l’idée précédente est généralisée, en permettant le groupe qui sert l’utilisateur typique d’avoir plus de deux atomes, tandis que l’interférence est reçue par le reste d’atomes individuellement. Cela améliore la couverture, principalement pour le pire des utilisateurs (*worst-case-user*). Le SINR expérimenté par l’utilisateur typique, lorsqu’il est servi par les  $K$  plus puissants atomes, est étudié en [BK15]. Les auteurs

fournissent d'expressions de la probabilité de couverture, en utilisant la *mesure de moments factoriels* d'un PPP. Un problème similaire est analysé en [TSAJ14], mais en utilisant la transformé de Laplace d'un PPP, pour obtenir des bornes explicites de la probabilité de couverture. Toutes les méthodologies précédentes pour la formation de groupes supposent que c'est l'utilisateur typique c'est celui qui choisit *dynamiquement* l'ensemble d'antennes pour son propre service. Cette façon *dynamique* de définir les groupes coopératifs est directement liée à l'association *utilisateur-antenne* dans un réseau.

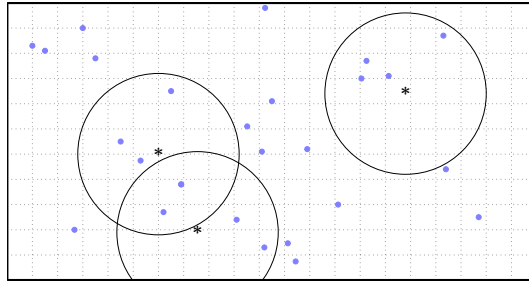
D'autres auteurs proposent de former les groupes d'antennes d'une façon plutôt statique, indépendamment de la configuration d'utilisateurs. De sorte que, fixe une topologie d'antennes, les groupes sont définis a priori, et ils ne changent pas avec le temps. En [AH13] les antennes sont groupées de façon aléatoire autour de centres virtuels, tandis qu'en [ADC16] des antennes sont aléatoirement générées autour de centres virtuels. Les auteurs en [PLH16] proposent la formation des groupes travers la coloration des bords de la graphe dessiné par la triangulation de Delaunay. D'autre part, en [HA11] les groupes sont formés en utilisant une maille hexagonale, lorsque les avantages des groupes déterminés par un processus de Gauss-Poisson son analysées en [GZHZ16]. Les auteurs en [VKG17] créent les groupes d'antennes à l'aide d'une grille carrée et régulière, placée indépendamment du positionnement des antennes.

## 0.1 Méthodologies pour former les groupes d'antennes

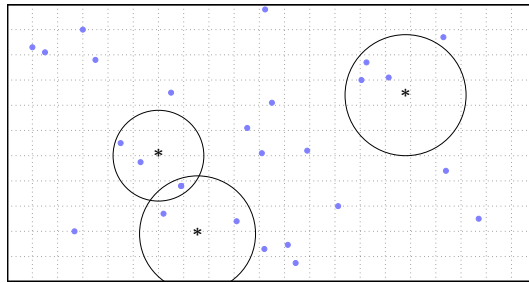
Cette sous-section présente d'exemples différents de méthodologies *dynamiques* et *statiques* pour la formation de groupes coopératifs.

### 0.1.1 Groupes dynamiques

En tant que premier exemple, fixe une configuration d'antennes, nous considérons que chaque utilisateur est servi par les antennes autour de lui, à l'intérieur d'un rayon fixe. La figure 1(a) montre une configuration d'antennes (les points bleus) et d'utilisateurs (les astérisques), ainsi comme les groupes d'antennes générés par cette méthodologie. Remarquons que, s'il n'y a pas d'antennes autour d'un utilisateur dans ce rayon fixe, alors, cet utilisateur n'est pas servi. Pour l'éviter, nous présentons une autre méthodologie dont les groupes d'antennes sont les trois antennes les plus proches de chaque utilisateur. Cet exemple correspond au modèle proposé en [NMH14], avec la taille de groupes 3. La figure 1(b) montre la même configuration d'antennes et d'utilisateurs, et les groupes formés avec ce dernier modèle. D'ailleurs, remarquons que dans les deux exemples dans la figure 1 il y a des antennes qui appartiennent à des différents groupes de coopération, ce qui implique les groupes ne sont pas disjoints.



(a)



(b)

Figure 1: Une configuration d'antennes (points bleus) et d'utilisateurs (astérisques). (a) Chaque'un des utilisateurs est servi par les antennes qui l'entourent, dans un rayon fixe. (b) Chaque utilisateur est servi par les trois antennes les plus proches de lui.



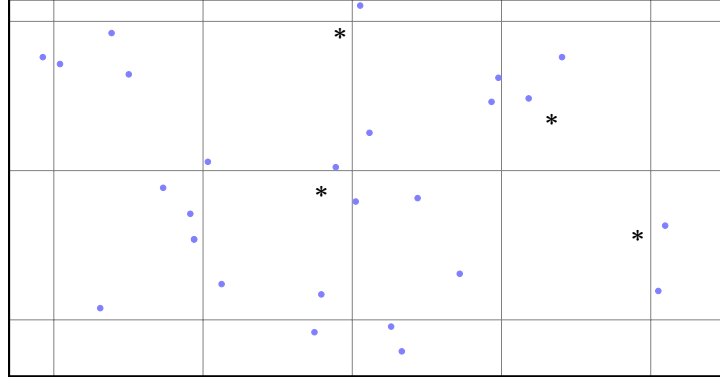


Figure 2: Une configuration d'antennes (les points bleus) et d'utilisateurs (les astérisques). Les antennes qui appartiennent à l'intérieur d'un carré forment un groupe. Chaque utilisateur est servi par le groupe défini par le carré où l'utilisateur est situé.

### 0.1.2 Groupes statiques

Supposons qu'une grille est placée sur le plan. Fixe une configuration d'antennes, indépendamment de la grille, les groupes sont formés par les atomes à l'intérieur de chacune des surfaces délimitées par la grille. Les différents groupes peuvent avoir zéro éléments (il n'y a pas d'atomes dans une de surfaces), 1, 2, 3, etcétera. Les groupes dépendent, évidemment, de la densité des antennes et de la grille, mais pas de la configuration d'utilisateurs. En tant que grille nous pourrions considérer un diagramme de Voronoi, défini par un processus ponctuel de Poisson [AH13], ou une grille régulière et carrée [VKG17]. Fixe maintenant une configuration d'utilisateurs, supposons que chacun est servi par le groupe d'atomes défini par la surface où l'utilisateur se trouve. Vu la façon dont les groupes sont formés, celle-ci est la plus naturelle association utilisateur-groupe. La figure 2 montre une configuration d'antennes (les points bleus), une configuration d'utilisateurs (les astérisques), et les groupes construits par une grille régulière et carrée. Remarquons qu'il y a des utilisateurs sans groupe pour leur servir. De plus, il y a aussi des utilisateurs qui sont plus proches d'autres antennes qui n'appartiennent pas au groupe qui leur serve. En conséquence, l'interférence reçue par ces utilisateurs est plus grande que le signal reçu.

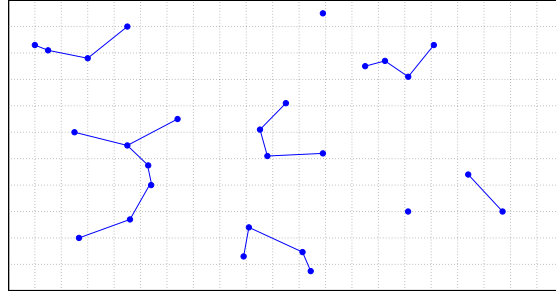
### 0.1.3 Groupes statiques et proximité

Le premier modèle que nous analysons qui prend en compte la proximité entre les antennes pour former les groupes est le *Random Geometric Graph (RGG)*, qui est largement étudié dans la littérature [Pen03, BP14]. Fixe une configuration d'antennes, deux atomes sont connectés si la distance entre eux deux est plus petite qu'un numéro fixe,  $R > 0$ . Alors, un

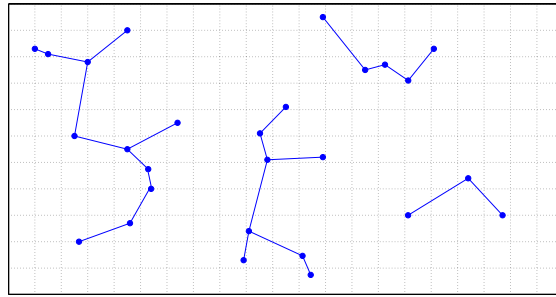
groupe coopératif est composé d'antennes connectées par cette règle. Le RGG remplit les propriétés suivantes :

- La taille de chacun des groupes est égale ou plus grande que 1.
- Pour une antenne fixe, la taille du groupe où elle appartient est une fonction croissante de  $R$ .

Celles-ci tiennent en général. La figure 3 montre une configuration d'antennes (les points bleus) et les groupes correspondant au RGG associé, par deux valeurs différentes de  $R$ . Remarquons qu'il y a d'antennes non connectés, alors, elles n'appartiennent pas à aucun groupe coopératif. Lorsque le positionnement des antennes suit une loi Poisson, il existent des groupes de taille aussi grande que nous voulons, avec une probabilité positive. En fait, fixe la valeur de  $R$ , pour certaines valeurs de la densité des antennes, le RGG *percole*: avec une probabilité positive, il existe une composante de la graphe dont le numéro d'éléments est infini [MR96]. La valeur exacte de la densité critique à partir de laquelle le RGG ne percole pas est inconnue. Pourtant, ils existent de différentes façons de l'approximer.



(a)



(b)

Figure 3: Une configuration d'antennes (les points bleus) et les groupes définis par le RGG, par deux valeurs différentes de  $R$ . La valeur de  $R$  en (a) est plus grande que celle en (b).

Il y a deux autres modèles célèbres aussi dont leur groupes statiques considèrent la proximité entre les antennes: le *Lilypond Model (LLM)* et le *Nearest Neighbor Model (NNM)*, présentés et étudiés en [HM96]. À différence du RGG, la formation des groupes est basée sur la distance relative entre les antennes.

Le LLM est construit de la façon suivante: fixe une configuration d'atomes, on pose sur chaque atome une boule dont le rayon commence à pousser, simultanément et au même taux pour chacun des atomes, et il s'arrête lorsqu'il touche une des autres boules. Les groupes sont formés par les antennes qui sont connectées par les boules qui se touchent.

Le NNM est construit de la façon suivante: fixe une configuration d'atomes, pour chacun d'entre eux, on considère son atome le plus proche. Les groupes sont formés par les séquences d'atomes connectés avec son plus proche.

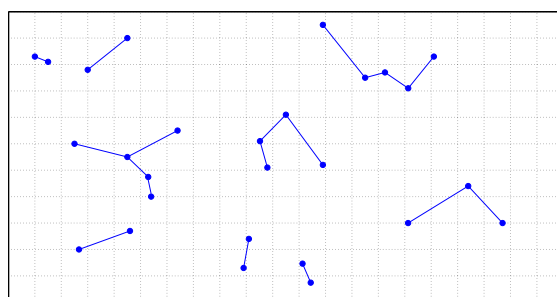
La figure 4 montre une configuration d'antennes, et les groupes générés par le LLM et le NNM. Les deux graphes donnent lieu à différents groupes. Plus précisément, quelques atomes connectés pour le NNM ne sont pas connectés pour le LLM. Néanmoins, les deux modèles partagent les propriétés suivantes:

- Toutes les antennes appartiennent à un des groupes.
- La taille de chaque groupe est égale ou plus grande que 2.
- Les groupes ne contiennent pas de cycles. Ainsi, chaque groupe est un arbre, et le graphe alors est une forêt.

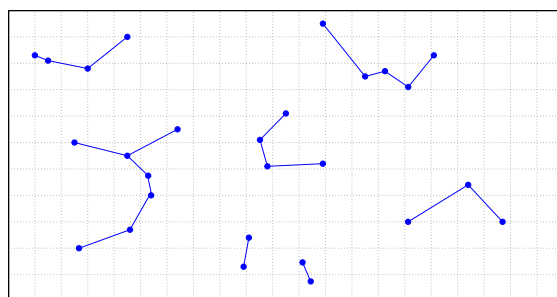
Celles-ci tiennent en général. Par ailleurs, lorsque le positionnement des antennes suit une loi de Poisson, les groupes du LLM et le NNM remplissent encore les suivantes propriétés:

- Les groupes sont indépendants de la densité d'antennes.
- La taille de chaque groupe est finie. Alors, le graphe correspondant ne percole pas et, par conséquence, il est déconnecté.

Ainsi, lorsque les antennes suivent une loi de Poisson, les groupes définis par le LLM et le NNM sont *très réguliers*: nous ne devons pas nous inquiéter par la percolation et les groupes se forment indépendamment de la densité des antennes, au contraire du RGG. Sur la figure 4 nous pouvons remarquer des groupes de taille 2, 3, 4, 5, 6, et 7. En effet, avec probabilité positive, les groupes peuvent avoir une taille aussi grande que nous voulons. En plus, il est évident que le plus grand le groupe, le plus grande la distance entre ces éléments. Cela est dû au fait qu'il n'y a pas de cycles.



(a)



(b)

Figure 4: Une configuration d'antennes (les points bleus) et les groupes définis par (a) le LLM et (b) le NNM.

## 0.2 La façon la plus appropriée de former les groupes

Les différentes problématiques décrites dans la figure 1 par rapport aux groupes dynamiques sont en général aussi présentes dans toutes les méthodologies dynamiques. Cela est dû au fait que c'est l'utilisateur qui choisit les antennes pour son service. Alors, à chaque fois que la configuration d'utilisateurs change, les groupes changent en conséquence. Cela surcharge le backhaul/control channel, avec une intense communication en continue entre les antennes.

En réponse aux inhérentes problématiques des méthodologies dynamiques, d'autres auteurs proposent des méthodologies statiques, indépendamment de la configuration d'utilisateurs. Cependant, soit elles génèrent les groupes d'atomes de façon aléatoire, soit elles génèrent d'atomes de façon aléatoire autour d'un nœud.

Afin d'éviter ces problématiques et garder les avantages de la coopération statique, les groupes doivent être formés d'une façon plus appropriée. Une des alternatives pourrait être considérer la distance relative entre les antennes. La proximité géographique parmi les éléments de chaque groupe coopératif devrait garantir un signal fort, une interférence faible, de la coordination rapide entre les atomes, en plus du fait que les antennes partagent une surface d'intérêt commun. Une méthodologie basée sur la proximité entre les antennes demande, en plus, un minimum d'infrastructure dans le réseau cellulaire.

Le premier modèle qui prend en compte la proximité entre les antennes c'est le RGG. Les groupes présentent quelques problématiques mineures, ils ne sont pas indépendants de la densité des antennes, par exemple. D'autre part, c'est un modèle simple à simuler et à analyser. Malheureusement, un grand problème est difficile à ignorer: la percolation.

Les modèles LLM et le NNM sont deux méthodologies pour générer des groupes statiques, basés aussi sur la proximité parmi les antennes. Lorsque les atomes suivent une loi de Poisson, les groupes sont indépendants de la densité d'antennes et sa taille est finie. Pourtant, le LLM c'est difficile à simuler et à analyser. Alors, le NNM reste le modèle le plus raisonnable pour nos buts particuliers.

Cependant, même lorsque les antennes suivent une loi Poisson, il y a un problème évident à faire face: avec une probabilité positive, il y a des groupes d'antennes d'importe quelle taille. En plus de ne pas être réaliste, le plus grand le groupe, les plus éloignes ses éléments entre eux (figure 4). Celui-ci c'est une conséquence de ne pas avoir de cycles dans les groupes d'antennes. Une analyse de la taille maximale des groupes coopératifs se trouve dans [LHA13]. En effet, c'est important d'étudier la taille maximale des groupes, par rapport à différents paramètres.

Il existe une catégorie de *nearest neighbors*, les *mutually nearest neighbors*. Il s'agit des

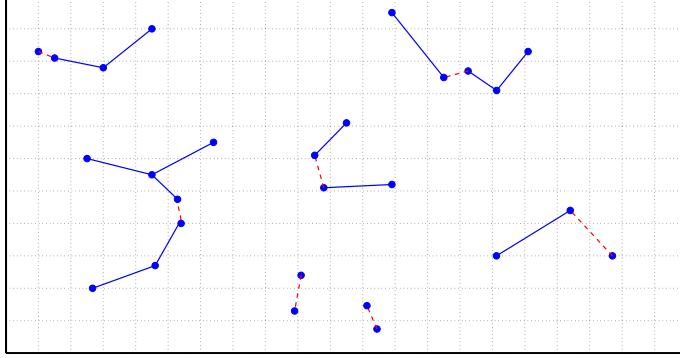


Figure 5: Un déploiement d’antennes (les points bleus) et les clusters définis par le NNM. Les atomes connectés par les lignes pointillées rouges correspondent aux MNN.

paires d’atomes, l’un est le plus proche de l’autre. Dans cette thèse, nous considérons en tant que groupes coopératifs les paires de *mutually nearest neighbors*, et le reste d’antennes restent seuls. De cette façon, nous fixons la taille maximale des groupes par 2 et il n’est pas difficile d’obtenir des premiers résultats. De plus, cette idée est, en effet, facile de généraliser pour des groupes avec une taille maximale plus grande que 2.

Jusqu’à ce point là, nous avons abordé une discussion par rapport aux avantages des groupes statiques, basés sur la proximité entre les antennes. Par contre, il est important, pour créer les groupes coopératifs, considérer si les antennes en question ont les ressources suffisantes pour que sa coopération soit avantageuse. En conséquence, il est impératif une analyse ces réseaux coopératifs pour ceux-ci pour lesquels nous devrions étudier d’autres méthodologies pour former les groupes qui prennent en compte les ressources du réseau.

### 0.3 Contributions et résultats principaux

Cette thèse fournit principalement les contributions suivantes:

- Sur le chapitre II, après une analyse du NNM, nous identifions une classe très importante de sous-groupes: les *mutually nearest neighbors* (MNN) (figure 5). Chaque groupe défini par le NNM contient une unique paire de MNN, et ces sous-groupes définissent un *stable matching*, par rapport à la distance géographique entre les atomes. Alors, les MNN constituent le seuls éléments dans un groupe pour lesquels la coopération entre eux est optimale, par rapport au critère des plus proches.
- Sur le chapitre III, nous exposons les différentes classes de signaux, reçu par l’utilisateur typique, transmis par un atome, une paire, ou un groupe dont la taille est plus grande que deux. Cette analyse peut-être utilisée pour des différents signaux, y compris le cas

directionnel, où le signal transmis dépend du positionnement du groupe d'antennes. Celui-ci demande de l'intégration par rapport aux angles, en compliquant inutilement l'analyse sans une différence considérable. Par conséquent, on considère le cas omnidirectionnel, où le signal transmis vers l'utilisateur typique dépend uniquement de la distance entre les atomes et lui. En plus, nous fournissons des outils qui permettent de prendre en compte diverses stratégies de coopération/coordination, comme celles-ci présentées en [IDM<sup>+</sup>11, JMZ<sup>+</sup>14, GHH<sup>+</sup>10, KG13, Ker13]. Finalement, nous identifions une famille très grande de lois de probabilité qui facilite énormément une analyse de performance d'un réseau omnidirectionnel: les *Phase-type-distribution*. Ces lois de probabilité sont caractérisés par une fonction de répartition comme suit: pour  $n \in \mathbb{N}$  fixe, il existe une fonction mesurable et déterministe  $c : [0, \infty)^m \rightarrow (\mathbb{R})^n$  et une matrice  $M : [0, \infty)^m \rightarrow \mathcal{M}^{n \times n}(\mathbb{R})$ , tels que, pour n'importe quel  $r \in [0, \infty)^m$ ,

$$\mathbb{P}(\tilde{g}(r) > T) = c(r)e^{M(r)T}\mathbf{e},$$

où  $e^{M(r)T}$  désigne l'exponentiel de la matrice  $TM(r)$  [Arn92], et  $\mathbf{e}$  est un vecteur colonne dont sa taille c'est  $m$  et ses entrées sont des numéros 1. La transformé de Laplace de ce genre de lois de probabilité est donnée par

$$\mathbb{E} \left[ e^{-s\tilde{g}(r)} \right] = c(r)(sI - M(r))^{-1}(-M(r))\mathbf{e},$$

où  $I$  désigne la matrice identique et le l'application  $s \mapsto (sI - M(r))^{-1}$  est le *resolvent* de la matrice  $M(r)$  [Arn92].

- Sur le chapitre IV, nous supposons que le positionnement des antennes suit une loi Poisson donnée par le processus  $\Phi$ . Nous formons après des groupes d'antennes qui sont MNN, et tous les autres restent seuls (figure 6). Cet éclaircissage défini naturellement deux processus ponctuels:

$$\Phi^{(1)} := \{x \in \Phi \text{ \& } x \text{ est un singleton}\},$$

$$\Phi^{(2)} := \{x \in \Phi \text{ \& } x \text{ coopère avec un autre élément de } \Phi\}.$$

Par construction des MNN, si  $\Phi$  est *stationnaire*, alors  $\Phi^{(1)}$  and  $\Phi^{(2)}$  les sont aussi.

La plupart de l'analyse est basée sur le résultat suivant.

**Lemma 1.** *Si  $\Phi$  est un PPP, avec densité  $\lambda > 0$ , pour n'importe quels atomes fixes  $x, y \in \mathbb{R}^2$ ,*

$$\mathbb{P} \left( x \overset{\Phi}{\leftrightarrow} y \right) = e^{-\lambda\pi\|x-y\|^2(2-\gamma)},$$

où  $\|\cdot\|$  désigne la distance Euclidienne, et  $\gamma := \frac{2}{3} - \frac{\sqrt{3}}{2\pi}$ .

Tout d'abord, il nous permet d'avoir le suivant résultat.

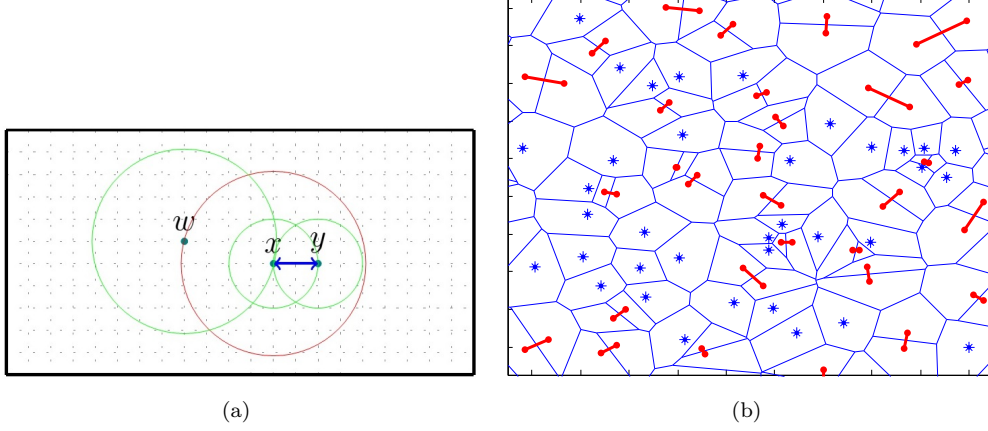


Figure 6: (a) Les atomes  $x$  et  $y$  sont MNN, alors, ils forment une paire coopérative. L'atome  $x$  est le plus proche de l'atome  $w$ , par contre,  $w$  n'est pas le plus proche de  $x$ , donc  $w$  est un singleton. (b) Une configuration Poissonnienne. Les astérisques correspondent aux singletons, et les points connectés aux paires coopératives.

**Theorem 1.** Si  $\Phi$  est un PPP, avec densité  $\lambda > 0$ , pour n'importe quel atome fixe  $x \in \mathbb{R}^2$ , il existe un numéro  $\delta > 0$ , indépendant de  $\lambda$  et  $x$ , tel que,

$$\mathbb{P}(x \in \Phi^{(2)}) = \delta, \quad \mathbb{P}(x \in \Phi^{(1)}) = 1 - \delta.$$

Spécifiquement,  $\delta = \frac{1}{2-\gamma} \approx 0.6215$ .

Ce numéro  $\delta$  est très important sur cette thèse. Le Théorème précédent dit que dans un réseau Poissonnien, donné la position d'une antenne, avec probabilité  $\delta \approx 0.6215$  cette antenne appartient dans une paire, ou avec probabilité  $1 - \delta \approx 0.3875$  elle est un singleton. Nous remarquons que ce résultat est *local*: la position de l'antenne est fixe. Pourtant, il est possible d'obtenir un résultat *global*: le Théorème 2.

Considérons que le signal reçu par l'utilisateur typique, émis par un singleton (paire coopérative), est désigné par  $f(x)$  ( $g(x, y)$ ), où  $x$  ( $x, y$ ) désigne sa position. Supposons que l'interférence générée par  $\Phi^{(1)}$  et  $\Phi^{(2)}$ , vers l'utilisateur typique, est désignée par  $\mathcal{I}^{(1)}$  and  $\mathcal{I}^{(2)}$ , respectivement, cet à dire,

$$\begin{aligned} \mathcal{I}^{(1)} &= \sum_{x \in \Phi^{(1)}} f(x), \\ \mathcal{I}^{(2)} &= \frac{1}{2} \sum_{x \in \Phi^{(2)}} \sum_{y \in \Phi^{(2)} \setminus \{x\}} g(x, y) \mathbf{1}_{\{x \leftrightarrow y\}}, \end{aligned} \tag{1}$$

On a le résultat suivant.



**Theorem 2.** Si  $\Phi$  est un PPP, avec densité  $\lambda > 0$ , alors,

$$\begin{aligned}\mathbb{E}[\mathcal{I}^{(1)}] &= (1 - \delta) \int_{\mathbb{R}^2} \mathbb{E}[f(x)] \lambda dx, \\ \mathbb{E}[\mathcal{I}^{(2)}] &= \frac{1}{2} \int_{\mathbb{R}^2} \int_{\mathbb{R}^2} \mathbb{E}[g(x, y)] e^{-\lambda \pi |x-y|^2 (2-\gamma)} \lambda dy \lambda dx.\end{aligned}\tag{2}$$

En particulier, si  $M^{(1)}$  and  $M^{(2)}$  désignent les mesures d'intensité des processus  $\Phi^{(1)}$  and  $\Phi^{(2)}$ , respectivement, alors,

$$M^{(1)}(dx) = (1 - \delta)\lambda dx, \quad M^{(2)}(dx) = \delta\lambda dx.$$

Le dernier résultat nous indique que, effectivement, dans un réseau Poissonnien, en moyenne,  $\delta \approx 0.6215$  pour cent des antennes sont dans une paire coopérative, et le  $1 - \delta \approx 0.3875$  pour cent sont des singletons. Ses pourcentages restent pareils pour d'autres réseaux pas Poissonnien, comme le modèle de grille hexagonale (figure 7).

Avec ce résultat il est possible aussi de prouver que les processus  $\Phi^{(1)}$  et  $\Phi^{(2)}$ , malheureusement, ils sont loin de suivre une loi de Poisson.

Il est possible d'obtenir d'autres résultats analytiques. Par exemple, une représentation explicite de la probabilité de Palm des processus  $\Phi^{(1)}$  et  $\Phi^{(2)}$  avec laquelle nous montrons le suivant résultat.

**Theorem 3.** Si  $\Phi$  est un PPP, avec densité  $\lambda > 0$ , alors, la distance entre deux antennes qui forment une paire coopérative a comme fonction de distribution

$$F(r) = 1 - e^{-\lambda \pi r^2 (2-\gamma)},\tag{3}$$

where  $\gamma$  is the same constant as in Lemma 1.

C'est à dire, dans un réseau Poissonnien, la variable aléatoire de la distance entre deux antennes en coopération suit une loi Rayleigh, de paramètre  $\alpha := (2\lambda\pi(2-\gamma))^{-1/2}$ .

Il est possible aussi de faire une analyse de fenêtre finie (*finite window*) pour approcher la transformé de Laplace des processus  $\Phi^{(1)}$  et  $\Phi^{(2)}$ : Soit  $A \subset \mathbb{R}^2$  un sous-ensemble régulier et fini, nous définissons les processus

$$\begin{aligned}\Phi_A^{(1)} &:= \{\text{les antennes seules de la configuration finie } \Phi(A)\}, \\ \Phi_A^{(2)} &:= \{\text{les atomes qui sont } \textit{mutually nearest neighbors} \text{ dans la configuration finie } \Phi(A)\}\end{aligned}\tag{4}$$

Si nous considérons  $A_n$  comme la boule, avec radius  $n$  et centrée à l'origine, on a le résultat suivant.

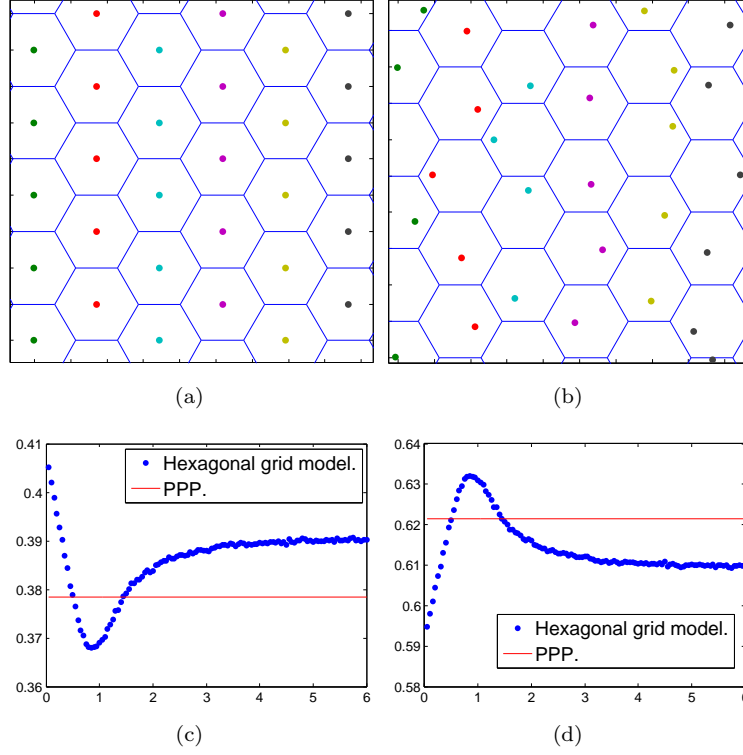


Figure 7: (a) Une grille hexagonale, sans perturbation, où les centres des hexagones représentent les antennes. (b) Une grille hexagonale, avec perturbation, où les antennes (les centres des hexagones) sont perturbés aléatoirement autour des centres avec un paramètre  $H > 0$ . (c) Le pourcentage singletons en fonction du paramètre  $H$ . (d) Le pourcentage d'antennes dans une paire en fonction du paramètre  $H$ .

**Theorem 4.** Si  $\Phi$  est un PPP, avec densité  $\lambda > 0$ . Alors, pour  $i = 1, 2$ ,

$$\lim_{n \rightarrow \infty} \Phi_{A_n}^{(i)} = \Phi^{(i)}.$$

où la convergence est une convergence étroite.

Puisque la convergence étroite de processus ponctuels est équivalente à la convergence de la transformé de Laplace [Kal84], il est possible d'approcher la transformé de Laplace de  $\Phi^{(i)}$  par la transformé de Laplace de  $\Phi_A^{(i)}$ , pour  $A$  grand et régulier. On a le résultat suivant.

**Theorem 5** (Laplace transform). Soit  $\Phi$  est un PPP, avec densité  $\lambda > 0$ , et soit  $A \subset \mathbb{R}^2$  un sous-ensemble fini et régulier. Soit aussi  $f : \mathbb{R}^2 \rightarrow \mathbb{R}^+$  une fonction mesurable. Alor, la transformé de Laplace du processus  $\Phi_A^{(1)}$ , évaluée en  $f(x)$ , a la suivante représentation

$$\begin{aligned} \mathbb{E} \left( e^{-\sum_{x \in \Phi_A^{(1)}} f(x)} \right) = & e^{-\lambda \mathcal{S}^{(2)}(A)} \left( 1 + \lambda \int_A e^{-f(x)} dx + \frac{(\lambda \mathcal{S}^{(2)}(A))^2}{2} \right. \\ & \left. + \sum_{n=3}^{\infty} \frac{\lambda^n}{n!} \int_A \dots \int_A e^{-F^{(n)}(x_1, \dots, x_n) \cdot H^{(n)}(x_1, \dots, x_n)} dx_1 \dots dx_n \right) \end{aligned} \quad (5)$$

ou  $F^{(n)}(x) := (f(x), \dots, f(x))$  et  $H^{(n)}$  est une fonction binaire explicitement donnée, et  $\mathcal{S}(\cdot)$  désigne la mesure de Lebesgue 2-dimensionnel.

La transformé de Laplace du processus  $\Phi_A^{(2)}$ , évaluée en  $f(x)$ , a la suivante représentation

$$\begin{aligned} \mathbb{E} \left( e^{-\sum_{x \in \Phi_A^{(2)}} f(x)} \right) = & e^{-\lambda \mathcal{S}^{(2)}(A)} \left( 1 + \lambda \mathcal{S}^{(2)}(A) + \frac{\lambda^2}{2} \int_A \int_A e^{-(f(x)+f(y))} dy dx \right. \\ & \left. + \sum_{n=3}^{\infty} \frac{\lambda^n}{n!} \int_A \dots \int_A e^{-F^{(n)}(x_1, \dots, x_n) \cdot I^{(n)}(x_1, \dots, x_n)} dx_1 \dots dx_n \right) \end{aligned} \quad (6)$$

ou  $I^{(n)}$  est une fonction binaire explicitement donnée.

Ces expressions des transformés de Laplace des processus  $\Phi_A^{(1)}$  et  $\Phi_A^{(2)}$  sont parfaitement calculables. Par contre, nos résultats numériques nous montrent que la vitesse de convergence (de la série et de l'expression elle-même) dépend fortement de la fenêtre  $A$  et aussi cette représentation n'est pas fermée, ainsi que sa complexité numérique est considérable.

- Puisque les processus  $\Phi^{(1)}$  et  $\Phi^{(2)}$  ne suivent pas une loi de Poisson, alors, il est difficile d'avoir faire une étude approfondie de ces deux processus. En particulier, cela empêche d'analyser la performance d'un réseau cellulaire avec les règles de coopération

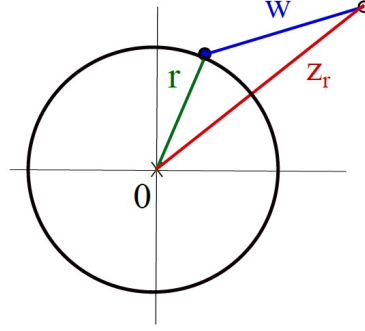


Figure 8: Deux antennes en coopération, où  $r$  et  $Z_r$  représentent leurs distances à l'origine, et  $W$  la distance entre elles.

que nous proposons. Cependant, il est possible de construire un modèle qui imite  $\Phi^{(1)}$  et  $\Phi^{(2)}$  pour lequel il est possible d'effectuer une analyse de performance.

En effet, nous considérons  $\hat{\Phi}^{(1)}$ , un PPP de densité  $\lambda(1-\delta)$ . Alors,  $\hat{\Phi}^{(1)}$  et  $\Phi^{(1)}$  ont les deux le même premier moment. Pour imiter le processus de paires, on considère  $\hat{\Phi}^{(2)}$ , un PPP marqué avec densité  $\lambda\delta/2$ . Les points de ce processus nous les appelons *les parents*, et les marques *les filles*. L'idée c'est que chaque paire (*parent, fille*) représente une de paires coopératives du premier modèle. C'est pour cela que la loi des marques est un élément très importante dans notre analyse. Alors, supposons que un des *parent* est à distance  $r > 0$  de l'origine (l'utilisateur typique). Alors, la distance de sa fille à l'origine, représentée par la variable aléatoire  $Z$ , a comme fonction de distribution

$$f(z|r) = \frac{z}{\alpha^2} e^{-\frac{z^2+r^2}{2\alpha^2}} I_0\left(\frac{zr}{\alpha^2}\right), \quad (7)$$

où  $I_0(x)$  c'est la fonction de Bessel modifiée de premier type, d'ordre zéro [Leb65]. Ainsi,  $Z$  suit une loi de Rice, de paramètre  $(r, \alpha)$ . En particulier, la distance entre chaque *parent* et sa *fille* suit une loi Rayleigh de paramètre  $\alpha$ .

À l'aide de ces outils, une analyse entière de la couverture est effectuée, pour deux différentes associations utilisateur-antenne.

- Si nous supposons que l'utilisateur typique est servi par un seul émetteur fixe, et toutes les antennes en paire et les singletons génèrent de l'interférence, alors, on a le suivant résultat.

**Proposition 1.** *La probabilité de couverture est donnée par l'expression suivante,*

$$\mathbb{P}(\text{SINR} > T) = e^{-\frac{T\sigma^2 r_0^\beta}{p}} \mathcal{L}_{\hat{\mathcal{X}}^{(1)}}\left(\frac{Tr_0^\beta}{p}\right) \mathcal{L}_{\hat{\mathcal{X}}^{(2)}}\left(\frac{Tr_0^\beta}{p}\right), \quad (8)$$

où  $SINR$  c'est le *Signal-to-interference-plus-noise ratio* expérimenté par l'utilisateur typique, et  $\mathcal{L}_{\hat{T}(1)}(\cdot)$  et  $\mathcal{L}_{\hat{T}(2)}(\cdot)$  c'est des fonctions déterministes explicitement données.

- Si nous considérons que l'utilisateur typique est servi par un singleton, si elle est la plus proche, ou par une paire, si le *parent* définissant cette paire ou sa fille sont les plus proches. Alors, on a le résultat suivant.

**Proposition 2.** *La probabilité de couverture est donné par l'expression suivante,*

$$\mathbb{P}(SINR > T) = \mathbb{E}[G(R_1)] + \mathbb{E}[H(R_2, Z_2)] + \mathbb{E}[K(R_2, Z_2)],$$

où  $SINR$  c'est le *Signal-to-interference-plus-noise ratio* expérimenté par l'utilisateur typique, les fonctions  $G : [0, \infty) \rightarrow \mathbb{R}^+$  et  $H, K : [0, \infty) \times [0, \infty) \rightarrow \mathbb{R}^+$  sont déterministes et explicitement donnés, et la loi du vecteur aléatoire  $(R_1, R_2, Z_2)$  est aussi explicitement donnée.

La figure 9 montre les graphiques qui compare la probabilité de couverture, entre le premier modèle (des simulations) et le modèle alternatif (les formules analytiques), pour les deux cas d'association. Nous remarquons que, pour le cas de l'émetteur fixe, la différence entre les deux est presque nulle. Cela nous indique que nous avons bien approximé l'interférence. Cependant, pour le cas du groupe le plus proche, nous remarquons que il y a des grands espaces entre les deux graphes. Cela arrive car nous ne considérons pas le cas de la fille la plus proche de l'utilisateur typique.

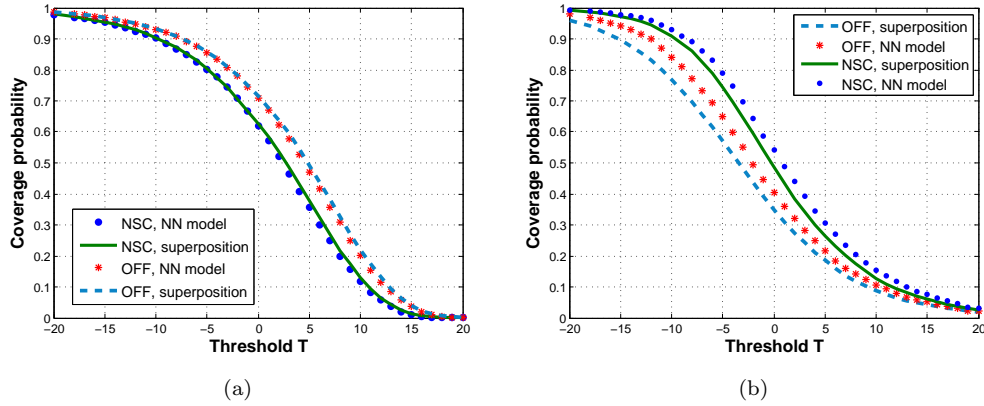


Figure 9: Proximité du modèle alternatif et le modèle précédent pour  $\beta = 3$ . (a) émetteur fixe et (b) le groupe le plus proche.

D'autre part, la figure 10 montre les comparaisons des formules analytiques obtenues et les simulations Monte Carlo, qui sont pratiquement les mêmes.

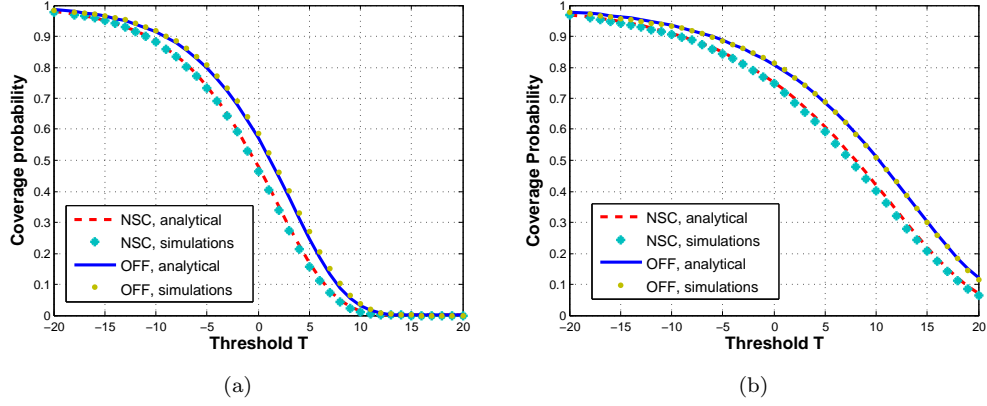


Figure 10: Validation de l'analyse pour l'émetteur fixe pour (a)  $\beta = 2.5$  (b)  $\beta = 4$ .

Finalement, la figure 11 montre les gains de la coopération de la superposition proposée, par rapport au modèle non coopératif. Ils peuvent arriver à un absolu de 15%.

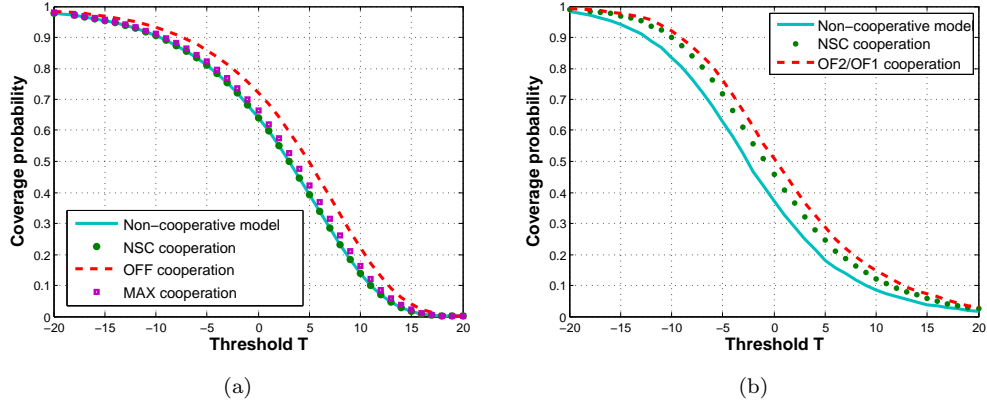


Figure 11: Bénéfices de la superposition Poisson en couverture, par rapport au modèle non coopératif. (a) Émetteur fixe (b) L'émetteur le plus proche.

- Pour que la coopération entre les antennes soit significative, chacune des antennes faisant partie d'un groupe devrait avoir des ressources disponibles suffisantes à partager avec les autres. Un exemple est illustré dans la figure 12

Alors, la mutually nearest neighbor relation est redéfini avec une métrique qui prend en considération la proximité géographique parmi les antennes et les ressources disponibles de chacune. En particulier, cette nouvelle métrique forme des paires d'antennes tels

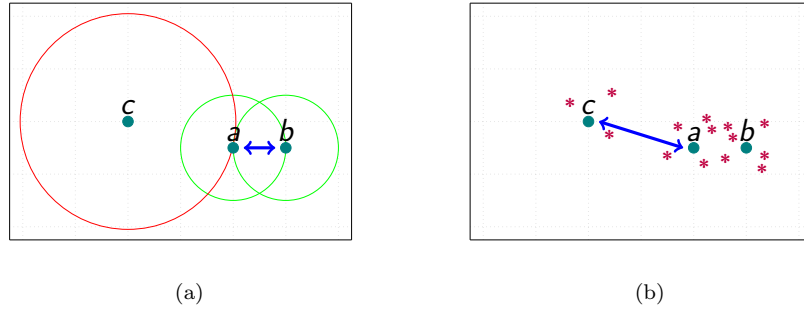


Figure 12: (a) Les atomes  $a$  et  $b$  forment une paire de mutually nearest neighbors, et  $c$  a comme plus proche l'atome  $a$ . (b) Les astérisques représentent des utilisateurs associés à ces atomes. Vu que  $a$  et  $b$  servent un grand numéro d'utilisateurs, leurs ressources sont bas. Si  $c$  ne serve pas aucun utilisateur, il a beaucoup de ressources, alors, la coopération alternative entre  $a$  et  $c$  pourrait bénéficier les utilisateurs de  $a$  et l'interférence gagnée par  $b$  n'est pas assez grande, grace à la proximité.

quels

- (1) elles sont géographiquement proches,
- (2) le produit de ses ressources est assez large,
- (3) la quantité de ressources des deux est pareille.

La figure 13 montre une configuration Poisson et (a) les groupes des paires et des singletons du premier modèle et (b) les paires et les singletons de ce nouveau modèle.

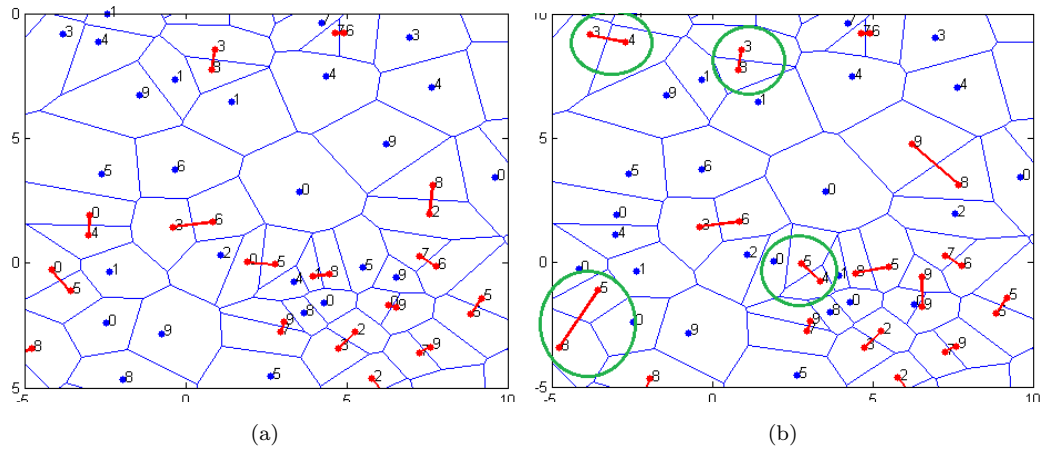


Figure 13: Différences entre les deux modèles de MNN.

Nous pouvons, en plus, ajouter des contraintes supplémentaires: (a) contraintes normales (b) contraintes supplémentaires.

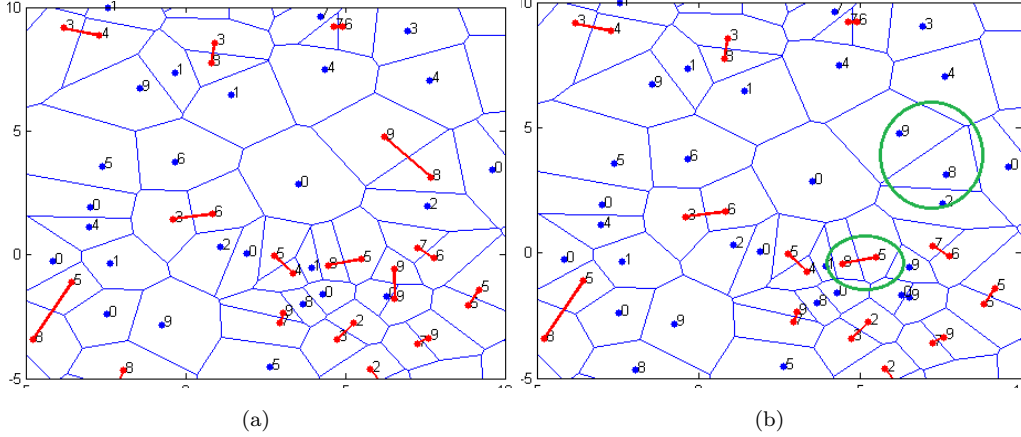


Figure 14: Sans contraintes supplémentaires vs contraintes supplémentaires

Lorsque le réseau suit une loi de Poisson, nous avons le résultat suivant.

**Theorem 6.** *Donnés deux atomes  $a$  et  $b$ , avec des ressources  $z$  et  $\tilde{z}$ . La probabilité que  $a$  soit en coopération avec  $b$  est donné par*

$$\mathbb{P}^{a,b} \left( a \overset{\Phi, \mathcal{D}}{\longleftrightarrow} b \right) = e^{-\lambda F(d_E^{(2)}(a,b), z, \tilde{z})} \mathbf{1}_{\{(z, \tilde{z}) \in \mathcal{D}\}}, \quad (9)$$

où  $d_E^{(2)}(a, b)$  est la distance géographique entre  $a$  et  $b$ , et la fonction  $F : (0, \infty)^3 \rightarrow (0, \infty)$  est explicitement donnée.

Alors, nous fournissons une analyse sur la proportion de singletons et pairs en coopération, et sur l'interférence de chaque groupe. Ces résultats montrent que les gains d'un réseau coopératif dépendent fortement de la distribution des ressources disponibles de tout le réseau.

- Nous généralisons aussi l'idée des clusters par rapport à la proximité entre les atomes pour des tailles plus grandes que 2. Même s'il n'est pas possible de faire une analyse entière, nous fournissons les idées théoriques pour le faire et des résultats par simulations.
- En conclusion, cette thèse présente divers outils en direction de l'analyse des réseaux coopératifs, dont leurs groupes sont formés à l'aide de la proximité parmi les atomes et/ou les ressources disponibles de chacune. Les résultats présentés peuvent être utilisés par un opérateur qui voudrait déployer un réseau cellulaire coopératif, et alors il voudrait tester les avantages qui pourraient gagner. De plus, si l'opérateur a déjà



déployé un réseau cellulaire, il pourrait utiliser aussi ces résultats pour la distribution des ressources bloqué dans chaque groupe coopératif. Notamment pour trouver des méthodes robustes contre l'inexactitude de la calibration des différents paramètres du réseau.

La plupart de notre analyse considère que le réseau suit une loi de Poisson stationnaire. Il est possible, pourtant, de les généraliser pour des réseaux Poissonniens non stationnaires ou pour des réseaux qui présentent de la répulsion ou de l'attraction entre ces atomes. Cela dépend du genre d'analyse que nous voudrions faire et de la complexité que nous voudrions ajouter.

# Contents

<b>Introduction</b>	<b>5</b>
1.1 Wireless Networks and Stochastic Geometry . . . . .	5
1.2 Cooperation in Wireless Networks . . . . .	6
1.3 Clustering methods . . . . .	7
1.3.1 Dynamic Clusters . . . . .	7
1.3.2 Static Clusters . . . . .	7
1.3.3 Static Clusters by means of proximity . . . . .	9
1.4 Appropriate Clustering . . . . .	11
1.5 Thesis contributions . . . . .	15
<b>The Nearest Neighbor Model</b>	<b>17</b>
2.1 Nearest Neighbors . . . . .	17
2.2 The Nearest Neighbor Model . . . . .	19
2.3 Mutually Nearest Neighbors . . . . .	21
2.4 The Matching Problem . . . . .	22
<b>Cooperative Signals</b>	<b>25</b>
3.1 Emitted signal to the typical user . . . . .	25
3.2 Single atoms . . . . .	26
3.3 Pair cooperation . . . . .	26
3.4 Cooperation between $m$ nodes . . . . .	27
<b>Characteristics of the Mutually Nearest Neighbors</b>	<b>31</b>
4.1 Singles and pairs . . . . .	31
4.2 Palm Probabilities . . . . .	34
4.3 The $G$ function of the process of cooperative pairs . . . . .	36
4.4 Size of the Voronoi Cells . . . . .	37
4.5 Further Results . . . . .	39
4.6 Interference Analysis . . . . .	39
4.6.1 Expected value . . . . .	40
4.6.2 Laplace functional . . . . .	42

4.7	Numerical Evaluation . . . . .	45
4.7.1	Expected value of the Interference field . . . . .	45
4.7.2	Laplace transform appoximation . . . . .	45
4.8	Conclusions . . . . .	47
<b>Coverage Analysis</b>		<b>49</b>
5.1	Poisson Superposition Model . . . . .	49
5.2	The Distribution of The Closest Distances . . . . .	50
5.3	Interference Field . . . . .	51
5.4	Coverage Probability . . . . .	53
5.4.1	Fixed Single Transmitter . . . . .	53
5.4.2	Closest Transmitter cluster . . . . .	53
5.5	Numerical Evaluation . . . . .	55
5.5.1	Closeness of the Poisson superposition . . . . .	55
5.5.2	Validity of the numerical analysis . . . . .	55
5.5.3	Cooperation gains . . . . .	55
5.6	Conclusions . . . . .	57
5.7	Additional material . . . . .	58
5.7.1	Proof of Proposition 6 . . . . .	58
5.7.2	Proof of Lemma 2 . . . . .	61
<b>Mutually Nearest Neighbors with resource constraints</b>		<b>65</b>
6.1	The choice of the new distance . . . . .	65
6.2	Hyperbolic proximity . . . . .	66
6.3	Singles and cooperative pairs . . . . .	67
6.3.1	Examples . . . . .	69
6.4	Analytic results . . . . .	70
6.4.1	A key property of the hyperbolic half-space . . . . .	71
6.4.2	The probabillity of two atoms being in cooperation . . . . .	72
6.4.3	Interference analysis . . . . .	74
6.4.4	Intensity measure and the percentage of singles and pairs . . . . .	76
6.4.5	Proportion of singles and cooperative pairs . . . . .	79
6.4.6	Expected value of the interference field . . . . .	79
6.4.7	The $\Lambda$ -volume of $C(a, b)$ . . . . .	80
6.5	Conclusions . . . . .	86
6.6	Additional material . . . . .	86
6.6.1	Uniqueness of the hyperbolic nearest neighbor . . . . .	86
6.6.2	The height of a lens . . . . .	88

<b>Generalisation for clusters larger than pairs, a discussion</b>	<b>91</b>
7.1 The $K$ -NNM . . . . .	91
7.2 Properties . . . . .	92
7.3 Non tractability of the $K$ -NNM and related problems . . . . .	94
7.4 Conclusions . . . . .	98
<b>General conclusions</b>	<b>99</b>
8.1 Summary . . . . .	99
8.2 Future work . . . . .	100
<b>Appendix</b>	<b>103</b>
9.1 List of publications . . . . .	103
9.2 Table of Abbreviations . . . . .	104
9.3 Table of Figures . . . . .	105
9.4 Table of Symbols . . . . .	107



# Introduction

## 1.1 Wireless Networks and Stochastic Geometry

Recent studies analyse wireless networks with the aid of *stochastic geometry*. In this way, the irregularity of the BS locations is modeled via a point process. It allows further to introduce the randomness of other parameters of the telecommunication network (e.g. fading, shadowing), in the model and to evaluate the users' performance [ABG11, BB09]. In this fashion, the performance of a wireless network can be quantified in a systematic way, so there is no need to test each different instance of the network topology by simulations. The *closed formulas* obtained are very important for an operator that wants to plan and deploy infrastructure, since these can provide intuition on the relative influence of various design parameters [BG15, BK15, GZH16].

For its tractability, the Poisson point process (PPP) is, notably, the most used point process along the literature. Indeed, everything is known for this process and the resulting expressions are tractable: *probability distribution, Laplace functional, factorial moment measures, Palm measures, Wiener chaos expansion, etc.* Hence, for the study of wireless networks, the PPP allows the use of all the powerful machinery stochastic geometry or Malliavin calculus provide [ABG11, BK15, DFMTT12, DST16], among others. Moreover, since it is simple to simulate a PPP-realisation, it is easy to compare the analytical formulas provided by the PPP-analysis against simulations. On the other hand, the assumption of the Poissonian behavior of the BS locations is based on studies stating that it is true for a large class of wireless networks. For instance, those with sufficiently strong shadowing [BKK15].

The major disadvantage of considering the Poissonian behavior of a network, is the fact that the position of every node is independent of the position of the rest of the nodes. Which is due to the fact that, given the number of nodes over a finite region, their position is independent and identically distributed (iid) (this is actually the classical way to generate a PPP realisation). In particular, the probability of having two different atoms as close as possible in a Poissonian network is always positive. Further, this *closeness* does not follow any rule, it just happens, independently of the BS positions. In some wireless networks, the position of the nodes often presents repulsion or attraction with respect to the other

BS positions. This is the main reason why other classes of point process with repulsion or attraction among the nodes have been proposed [LBDA15]. Particularly, the class of the determinantal process, which is repulsive, has been widely studied, notably the  $\beta$ -Ginibre point process [DZH15] for its tractability.

In this thesis, we assume that the BS positions are modeled by a PPP. The rules to form cooperative clusters, that will be defined later, translate into strongly dependent thinnings. Thus, for a proper analysis of such cooperative networks, we need to make use of every available analytical tool. And, as mentioned above (again, see [BKK15]), for a large class of wireless networks, it is possible to assume the Poissonian behavior of the nodes. Moreover, it has been proven that for very large cellular networks, that result from the superposition of independent point process with internal repulsion, these turn out to be compatible with the null hypothesis of being Poissonian [DV15].

## 1.2 Cooperation in Wireless Networks

Cooperation between base stations (BSs) is a topic of considerable ongoing research in cellular networks. It is considered as a way to reduce intercell interference and, consequently, improve network capacity. Furthermore, it is particularly beneficial for users located at the cell-edge, where significant SINR gains can be achieved in the downlink (for instance, see [BG15]). The cooperation concept is expected to play a significant role in future planning and deployment, as well as being absolutely necessary in the near future, due to the coming densification of networks by HetNets [DGBA12, CHC14]. There is a considerable amount of research on the topic, related to the concept of CoMP [IDM<sup>+</sup>11, JMZ<sup>+</sup>14], Network MIMO [JJT<sup>+</sup>08, GHH<sup>+</sup>10, GKB12], or C-RAN [CCY<sup>+</sup>15, LAL16].

Generally speaking, we can describe cooperation in a wireless network as follows:

*A Coordinated Group of BSs Serving a User.*

The different cooperation methodologies proposed differ in *the type of transmitted signal cooperation, the amount of information exchange, the number of cooperating nodes, and, notably, the way the groups of BSs are formed*. On the other hand, a common purpose of cooperation is to offer to the user a *strong signal*, with *reduced interference*.

In [GKB12] a combinatorial approach to form cooperative clusters of BSs is proposed, whereas in [PGH08], the authors analyse a clustering algorithm incorporating multi-cell cooperative processing. These two works do not consider any randomness for the BS positions. On the other hand, in [BG15, NMH14, BK15, TSAJ14], the BS positions are assumed to be distributed as a PPP. In this way, the authors benefit from stochastic geometry to analyse the cooperative schemes they propose. In [BG15] it is analysed the case where a typical user is served by its two closest BSs, and the interference is received by pairs of BSs, showing coverage improvements and an increase of the coverage cell. The authors in [NMH14] generalize the previous idea of a bigger cluster serving a typical user, but the interference is received by all the other BSs individually, showing absolute gains in coverage, mostly for the

worst case user. The SINR experienced by a typical user, when served by the  $K$  strongest BSs, is considered in [BK15]. The authors here derive tractable expressions of the coverage probability, with the aid of factorial moment measures. A similar problem is analysed in [TSAJ14], where the authors use the Laplace Transform of a PPP to give explicit bounds and approximations for the coverage probability. What they have in common these clustering criteria is that the user *dynamically selects* the set of stations cooperating for its service. The way the dynamic clusters are defined is straightforwardly related to the user-antenna association of the network.

Other authors propose to group the BSs *in a static way*, independently of the user configuration. In this fashion, given a topology for the BSs, the clusters are defined apriori, and do not change over time. For instance, in [AH13], the authors randomly group BSs around virtual centers, whereas in [ADC16] the clusters are formed by BSs randomly generated around virtual centers. In [PLH16], the clusters are formed using an edge-coloring for a graph drawn by the Delaunay triangulation. The authors in [HA11] cluster the BSs using a hexagonal lattice. The benefit of the clusters formed by a Gauss-Poisson process is analysed in [GZHZ16]. The authors in [VKG17] cluster BSs with the aid of a regular square-grid, placed independently of the BS positions, to analyse the performance of a cooperative cloud network.

## 1.3 Clustering methods

This subsection is devoted to illustrate some examples of *dynamic* and *static* clustering methodologies.

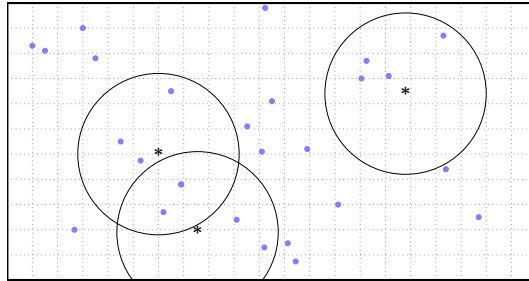
### 1.3.1 Dynamic Clusters

As a first example, given a deployment of users and BSs, consider that each user is served by the BSs lying around it, within a fixed radius. Figure 1.1(a) shows a deployment of BSs (blue dots) and users (asterisks), and the cooperative clusters formed by this methodology. Notice that, if there are no BSs around a user within this fixed radio, then it has no BSs for its service. To prevent this, let us consider the methodology proposed in [NMH14], for which the clusters are formed by the  $n$ -closest BSs of each user. Figure 1.1(b) displays the same deployment of users and BSs, but now showing the cooperative groups defined by this new methodology, for the case  $n = 3$ . Notice that, in both examples, there are BSs that belong to two different cooperative clusters (see Figure 1.1), meaning that the clusters are not disjoint BS sets.

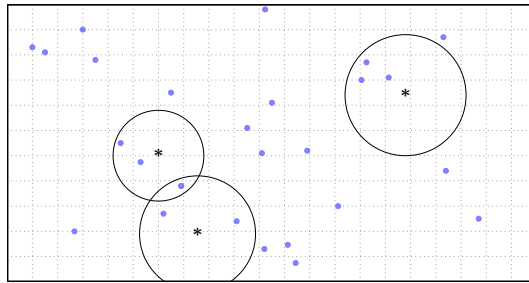
### 1.3.2 Static Clusters

Suppose there is a (possibly irregular) grid over the plane. Given a deployment of BSs, the cooperative clusters are formed by the BSs lying inside each one of the surfaces defined by





(a)



(b)

Figure 1.1: A deployment of BSs (blue dots) and users (asterisks). (a) Each user is served by all the surrounding BSs around a fixed radio. (b) Each user is served by its three closest BSs.

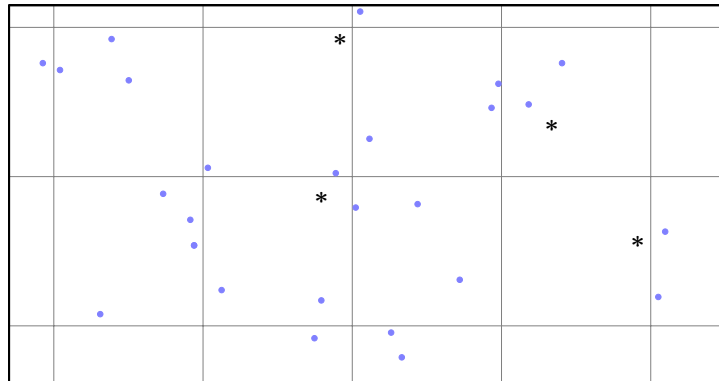


Figure 1.2: A deployment of BSs (blue dots) and users (asterisks). The BSs lying within a square-area belong to a cooperative cluster. A user is served by the cluster defined by the square-area where it is placed.

the grid. The clusters can be of size 0 (no BSs inside a particular surface), 1,2,3, etc. The size of the clusters depends, of course, on the density of the BSs and the grid. Further, notice that the clusters are determined only by the deployment of BSs and the grid, independently of the user configuration. For instance, it is possible to consider a Voronoi grid defined by a PPP independent of the BS positions, as in [AH13], or a regular square-grid, independent of the BS positions, as in [VKG17]. For a deployment of users in this network, suppose that each one of them is served by the cluster determined by the surface where the user lies. This is the natural user-cluster association, given the way the clusters are formed. Figure 1.2 shows a deployment of BSs (blue dots) and users (asterisks), and the clusters formed by the particular case of the regular square-grid. The Figure shows some users without any associated cluster of BSs. On the other hand, there are some users having BSs closer than those belonging to their serving cluster, which results in received interference higher than the received signal.

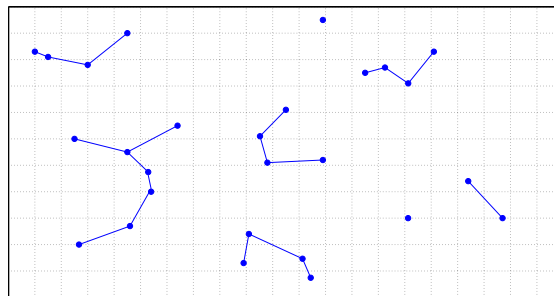
### 1.3.3 Static Clusters by means of proximity

The first model of a static clustering methodology considering the geographical distance between the BSs is the *Random Geometric Graph (RGG)*, highly studied in the literature [Pen03, BP14]. In this model, given a deployment of BSs, two nodes are connected if their distance is smaller than a fixed number,  $R$ . Each cooperative cluster consists of all the BSs connected by the previous criterion. We have the following list of properties for the RGG:

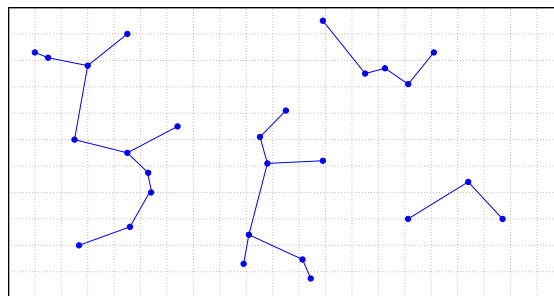
- The cardinality of each cluster is bigger or equal to 1.
- Given a BS, the cardinality of its corresponding cluster associated to the RGG is an

increasing function of  $R$ .

The previous properties hold in general. Figure 1.3 shows a deployment of BSs (blue dots) and the clusters derived from the RGG, for two different values of  $R$ . In the Figure we distinguish some BSs not connected to any atom, meaning that there are BSs not belonging to a cooperative cluster. When the BS positions are modeled by a PPP, there exist clusters of size as big as possible, with a positive probability. Actually, given a value for  $R$ , for certain values of the BS density, the corresponding RGG *percolates*: With a positive probability, there exists a component of the graph whose number of elements is infinite [MR96]. The exact value for the BS density of the critical point from which the RGG does not percolate is not known. Nevertheless there exist some limit Theorems from which it is possible to approximate it. There are two other notable models of static clusters by means of geograph-



(a)



(b)

Figure 1.3: A deployment of BSs (blue dots) and the clusters defined by the RGG for two different values of  $R$ . The value for  $R$  in (a) is smaller than the corresponding value of  $R$  in (b) .

ical proximity between the BSs: the *Lilypond Model (LLM)* and the *Nearest Neighbor Model (NNM)*, both presented and studied in [HM96]. As the RGG, the way the cooperative BSs are grouped is based on the distance with respect to the other BSs, but it is not restricted to the BSs being within a fixed distance.

The LLM is constructed as follows: Given a deployment of BSs, there is a ball, centered on each BS, whose radius starts growing, simultaneously and at the same rate for all the nodes, and it stops growing when it hits one of the other balls. The cooperative clusters consist of those BSs whose respective balls touch each other.

The NNM is constructed in the following way: Given a deployment of BSs, for each one of them, we consider its nearest BS. The cooperative clusters consist of those sequences of BSs connected each with their nearest neighbor.

Figure 1.4 shows a deployment of BSs, and the cooperative groups formed by the LLM 1.4(a) and the NNM 1.4(b). The two graphs result in different clusters of cooperative BSs. More precisely, some atoms connected in the NNM are disconnected in the LLM. Nevertheless, they share certain properties:

- All the BSs belong to a cooperative cluster.
- The cardinality of each cluster is greater or equal to 2.
- The clusters do not contain cycles, that is, each cluster is a tree, and hence the corresponding graph is a forest.

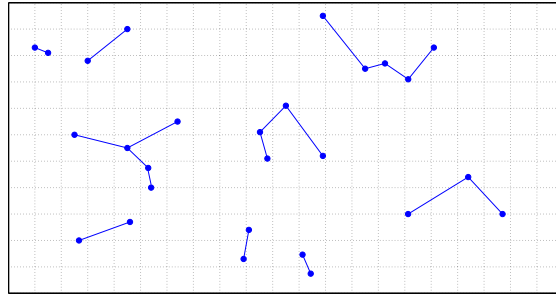
These three properties hold in general. Additionally, when the BS positions are modeled by a stationary PPP, we can add the following two properties for the cooperative clusters defined by the LLM or the NNM.

- The cluster formation is independent of the density of the BSs.
- The cardinality of each cluster is finite. That is, the corresponding graph does not percolate. In particular, the resulting graph is disconnected.

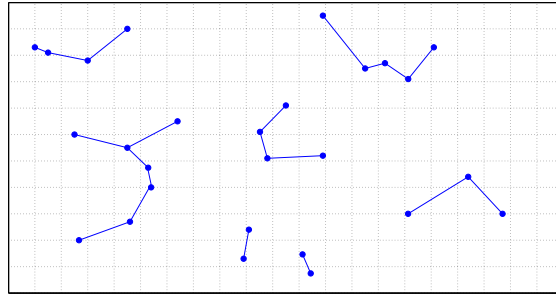
Thus, when the BS positions are Poisson distributed, the clusters defined by both models, the LLM and NNM, are *highly regular*. Meaning that we do not have to deal with percolation, as opposed to the RGG. In Figure 1.4, we recognize cooperative clusters of size 2, 3, 4, 5, 6, and 7. Actually, the cluster size can be as large as possible, with positive probability. Notice, as well, that the bigger the cluster, the bigger the distance between some of its elements.

## 1.4 Appropriate Clustering

The modeling of wireless networks with the aid of stochastic geometry is crucial for an operator that wants to deploy infrastructure. The closed formulas obtained with this tool provide intuition of various design parameters, among others. It is then important to choose a class of point processes modeling the BS positions allowing a minimum of tractability. Being the PPP the most appropriate choice for this duty.



(a)



(b)

Figure 1.4: A deployment of BSs (blue dots) and the clusters defined by the (a) LLM and (b) NNM.

Cooperation in wireless networks is a current topic in the recent literature. It has been proven to be beneficial for cellular networks, as well as being absolutely necessary for the near future. The benefits differ, mostly, in the way the groups of BSs are formed. The clustering criteria can be split mainly into two different types: *dynamic clusters*, where it is the user who selects the BSs working for its service, and *static clusters*, defined apriori, not changing over time, and independent of the user configuration.

In Figure 1.1 we have two different examples of dynamic clustering criteria. Notice that, in both, there is one BS belonging to two different cooperative clusters. This translates into the fact that this BS must serve two different users at the same time, hence, it should share its time or more general resources between the two clusters. The latter leads into spectral efficiency degradation. Actually, this is a general problem present in dynamic clustering criteria, due to the fact that it is the user that leads the cluster formation. Remark, as well, that this method results in changing the cooperative groups, with every different configuration of users. This demands high flexibility in the inter-cell communication, as well as a large amount of information exchange, which overburdens the backhaul/control channel, not always possible.

In response to the inherent problems of the dynamic cluster methodologies, other authors propose to group the BSs in a static way, independently of the user configuration. Since the clusters are defined apriori, and they do not change over time, this translates into reasonable information exchange between the BSs and low backhaul costs. Further, the resource-sharing can be avoided due to the disjoint cluster formation, and one controller per cluster can program and coordinate them. Figure 1.2 illustrates an example of static cooperation. Notice that, for some users, BSs belonging to a different cooperative cluster not serving them can be closer. Thus, the signal received by these users is weaker than the interference they receive. Moreover, there are some users without any associated cluster.

The problems portrayed by the previous example are generally present in the static clustering methodologies along the literature. This is due to the fact that either the BSs are grouped in a random way, or the cooperative BSs are randomly generated around a node. To avoid these problems, and keep the benefits of static cooperation, the clusters should be generated in a more appropriate manner. Considering the relative geographical position among the BSs to form the static cooperative groups can be the answer. The geographical proximity between their elements should grant a strong cooperative signal, a weak interference, fast coordination, and, in this way, the cooperative BSs share a planar area of common interest. Moreover, static clustering criteria based on node proximity requires minimum additional infrastructure in a cellular network: Only communication links between the cooperating BSs are required to be installed. It is desirable also that the cluster formation is independent of the variable parameters of the telecommunication system.

The first analysed clustering methodology that considers proximity between the BSs is the RGG. This model is simple to simulate, since it connects only nodes closer than some given distance  $R$ . However, this adds another complexity: What is the suitable value for

$R$  to group the BSs? On the other hand, when the BSs are distributed as a PPP, there exist values for the BS density for which the probability of having an infinite component is positive. Hence, the RGG differs considerably from a real cooperative wireless network. The choice of BS density and the choice of cluster mechanism are two problems that can or cannot be related. The RGG is a mechanism that relates both. A density independent clustering methodology can simplify the network deployment, while maintaining the benefits of static clusters, by means of proximity.

The LLM and the NNM are two clustering criteria based on node-proximity, that group nodes in a more appropriate way. When the BSs are distributed as a PPP, the corresponding clusters are finite and are independent of the BS density. In spite of this, the LLM is difficult to program and simulate, as opposed to the NNM, which only considers first neighbours. For the same reason, it is natural to analyse, with the aid of stochastic geometry, a cooperative cellular network modeled by the NNM. That being said, as a first approach, the clusters defined by the NNM seem to be appropriate for our particular purposes.

For the NNM model, even under the Poissonian assumption, there is an evident problem: with a positive probability, there exist clusters of size as large as possible. This is not practical, nor convenient. Notice from Figure 1.4 that bigger clusters have atoms which are far away from other atoms within the same cluster. This is, partly, due to the fact that there are no cycles within the clusters. An analysis about how large should the size of a cluster must be can be found in [LHA13]. Thus, it could be interesting to consider models that allow a controlled maximum cluster size.

There exists a relevant class of nearest neighbors, the so called *mutually nearest neighbors*. These are pairs of atoms, each one being the nearest neighbor of the other one. In this Thesis, we consider the cooperative groups as pairs of mutually nearest neighbors, and the rest of the atoms remain single. In this fashion, we have a fixed maximum cluster size, it is easier to derive first results, among other benefits. It is actually easy to generalize this idea for clusters of size greater than two, as we will see at the end of this work.

Up to this point, it has been widely discussed the several benefits of static clustering criteria, based on node proximity. Figure 1.5 illustrates a situation where only the geographical proximity between the BS locations is not enough to ensure a better service, since we do not take into account whether the members of a group have sufficient resources to make their cooperation beneficial. Thus, it is important: (a) to propose alternative clustering criteria, (b) that consider more than the geographical proximity between the nodes, (c) forming appropriate groups of atoms, (d) and analyse the benefits of these alternative cooperations. Moreover, it is imperative an analysis to identify the cellular networks for which it is appropriate to apply these alternative methodologies, and those for which it is not.

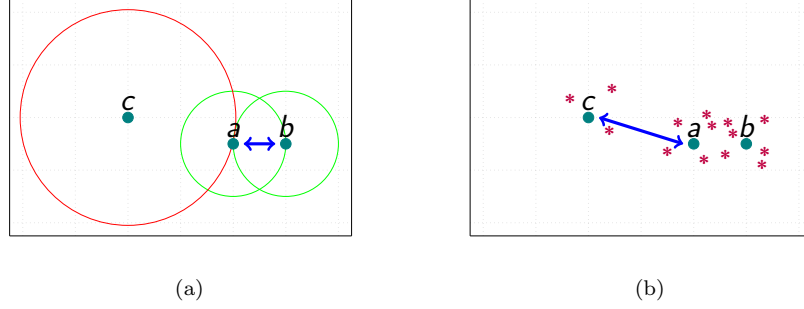


Figure 1.5: Consider a static clustering criterion forming cooperative pairs of mutually nearest neighbors, and the rest of the atoms remain single. (a) The atoms  $a$  and  $b$  belong to a cooperative pair, since  $a$  is the nearest neighbor of  $b$ , and  $b$  is the nearest neighbor of  $a$ . Since  $a$  is the nearest neighbor of  $c$ , but  $c$  is not the nearest neighbor of  $a$ , then  $c$  remains single. (b) If  $a$  and  $b$  serve a large number of users, the asterisks, the available remaining resources of both are low. If  $c$  does not serve as many users, it has a considerable amount of unused resources. Since  $c$  is close to  $a$ , their alternative cooperation can allow users of  $a$  to be partly served from both  $a$  and  $c$ , while the signals from  $c$  can be sufficiently strong, due to proximity.

## 1.5 Thesis contributions

This thesis provides the following contributions:

- We identify a class of nearest neighbors, that work as a root for each cluster defined by the NNM (Chapter 2). With the aid of this, we introduce the *Mutually Nearest Neighbor Relation*, a grouping method for BSs with two types of clusters: Single nodes, operating individually, and pairs of nodes, cooperating with each other. An analysis of cooperative wireless networks of this type is provided (Chapter 4).
- Our analysis is done in a general sense, without restricting ourselves to specific co-operating signal schemes (Chapter 3). Altogether, we provide the analytical tools that evaluate various strategies for transmitter cooperation/coordination, as those in [IDM<sup>+</sup>11, JMZ<sup>+</sup>14, GHH<sup>+</sup>10, KG13, Ker13].
- A complete analysis of the coverage probability is provided, for two different scenarios of user-to-BS association (Chapter 5). This analysis is done via an approximate model: The superposition of two independent PPPs. The model is based on the provided structural characteristics of the singles and the cooperative pairs (Chapter 4).
- To face the problems that naturally arise from clusters that consider only relative geographical proximity, we redefine the Mutually Nearest Neighbor Relation. The atoms are considered within a larger space, and the formation of cooperative pairs and single



BSs takes into account both, the *geographical proximity* and the *available resources* of the BSs (Chapter 6). An interference analysis for cooperative cellular networks under these new rules is provided, assuming that the BSs are modeled by a marked PPP. We make, as well, a comparison of cooperative cellular networks under the classical Mutually Nearest Neighbor Relation and that one considering the available resources of the BSs.

- A wide discussion to generalise the Mutually Nearest Neighbor Relation for clusters of size bigger than 2 (Chapter 7), for the purely geometric model and also for the one considering resource availability.

# The Nearest Neighbor Model

The results along this Chapter constitute a focused study of the works [HM96, KMN06, Gio16]. The Chapter also contains original material and proofs not included in these works.

## Abstract

The current Chapter studies the *NNM*, a clustering methodology based on node proximity. Our aim is to introduce an important class of its subclusters, on which the whole thesis focus: The *mutually nearest neighbors*. Each cluster of the NNM contains exactly one pair of these atoms. Moreover, the mutually nearest neighbors define a *stable matching*, with respect to the relative distance between the atoms of a configuration. For these reasons, they constitute a root of the NNM: the mutually nearest neighbors are the only elements within a cluster for which their cooperation is optimal, according to the nearest neighbor criterion.

## 2.1 Nearest Neighbors

Throughout this thesis,  $\phi$  denotes a simple, locally finite, point configuration in the  $d$ -dimensional Euclidean space  $\mathbb{R}^d$ . Unless otherwise specified, each element of  $\phi$  represents the position of a BS. In this way,  $\phi$  represents a possible deployment of single antenna. Denote by  $\|\cdot\|_d$  the  $d$ -dimensional Euclidean distance.

**Definition 1.** For a given atom  $x \in \phi$ , we say that  $y \in \phi \setminus \{x\}$  is the *Nearest Neighbor* of  $y$  if

$$y = \operatorname{argmin}_{z \in \phi \setminus \{x\}} \|x - z\|_d$$

We denote this by  $x \xrightarrow{\phi} y$ . In telecommunications terms, we say that  $y$  communicates with  $x$ .

The nearest neighbor is not always unique. For example, within the finite configuration  $\phi = \{(0,0), (1,0), (0,1)\}$ , the Euclidean origin is in NNR with both  $(1,0)$  and  $(0,1)$ . For many reasons, it is crucial for the nearest neighbor relation to be uniquely determined.

Moreover, given the irregularity of real cellular networks, we would expect the distance between every different pair of atoms being distinct. Henceforth, in this work, we only consider configurations  $\phi$  fulfilling the previous property. Since our goal is to extend these concepts to point processes, it is then natural to ask ourselves what is the class of point processes  $\Phi = \{\phi\}$  whose configurations  $\phi$  fulfil the above property (almost surely).

**Theorem 1.** *Let be  $\Phi$  either a general stationary point process, or a PPP whose intensity measure is absolutely continuous with respect to the Lebesgue measure. Then, there are no two different pairs of atoms whose distance between their elements is the same,  $\mathbb{P}$ -a.s.*

*Proof.* Let  $\Lambda(\cdot)$  be the intensity measure of  $\Phi$ . Denote

$$\begin{aligned} \mathcal{B} &:= \{\text{There exist different } x, y, z, w \in \Phi, \text{ such that } \|x - z\|_d = \|y - w\|_d\} \\ &= \bigcup_{x \in \Phi} \left( \bigcup_{y \in \Phi \setminus \{x\}} \left( \bigcup_{z \in \Phi \setminus \{x, y\}} \left( \bigcup_{w \in \Phi \setminus \{x, y, z\}} \{\|x - z\|_d = \|y - w\|_d\} \right) \right) \right). \end{aligned}$$

We will prove that  $\mathbb{P}(\mathcal{B}) = 0$ . Let us suppose first that  $\Phi$  is a PPP, whose intensity measure is absolutely continuous with respect to the Lebesgue measure. Let  $\mu^p(\mathbb{R}^d)$  be the space of point configurations over  $\mathbb{R}^d$ . Let  $g : \mathbb{R}^d \times \mu^p(\mathbb{R}^d) \rightarrow [0, \infty)$  such that, for every  $(x, \phi) \in \mathbb{R}^d \times \mu^p(\mathbb{R}^d)$ ,

$$g(x, \phi) := \sum_{y \in \phi} \sum_{z \in \phi \setminus \{y\}} \sum_{w \in \phi \setminus \{y, z\}} \mathbf{1}_{\{\|x - z\|_d = \|y - w\|_d\}}.$$

Hence,

$$\begin{aligned} \mathbb{P}(\mathcal{B}) &= \mathbb{E} \left[ \mathbf{1}_{\{\bigcup_{x \in \Phi} (\bigcup_{y \in \Phi \setminus \{x\}} (\bigcup_{z \in \Phi \setminus \{x, y\}} (\bigcup_{w \in \Phi \setminus \{x, y, z\}} \{\|x - z\|_d = \|y - w\|_d\})))\}} \right] \\ &\leq \mathbb{E} \left[ \sum_{x \in \Phi} \sum_{y \in \Phi \setminus \{x\}} \sum_{z \in \Phi \setminus \{x, y\}} \sum_{w \in \Phi \setminus \{x, y, z\}} \mathbf{1}_{\{\|x - z\|_d = \|y - w\|_d\}} \right] \\ &= \mathbb{E} \left[ \sum_{x \in \Phi} g(x, \Phi \setminus \{x\}) \right] \\ &\stackrel{(a)}{=} \int_{\mathbb{R}^d} \mathbb{E}[g(x, \Phi)] \Lambda(dx) \\ &= \int_{\mathbb{R}^d} \mathbb{E} \left[ \sum_{y \in \Phi} \sum_{z \in \Phi \setminus \{y\}} \sum_{w \in \Phi \setminus \{y, z\}} \mathbf{1}_{\{\|x - z\|_d = \|y - w\|_d\}} \right] \Lambda(dx) \\ &\stackrel{(b)}{=} \mathbb{E} \left[ \sum_{y \in \Phi} \sum_{z \in \Phi \setminus \{y\}} \sum_{w \in \Phi \setminus \{y, z\}} \int_{\mathbb{R}^d} \mathbf{1}_{\{\|x - z\|_d = \|y - w\|_d\}} \Lambda(dx) \right] \\ &= \mathbb{E} \left[ \sum_{y \in \Phi} \sum_{z \in \Phi \setminus \{y\}} \sum_{w \in \Phi \setminus \{y, z\}} \int_{\mathbb{R}^d} \Lambda(\{x \in \mathbb{R}^d \mid \|x - z\|_d = \|y - w\|_d\}) \Lambda(dx) \right], \end{aligned}$$

where (a) follows after considering Campbell's formula and Slivnyak-Mecke Theorem [BB09], and (b) follows after Tonelli's Theorem [Rud87].

For fixed  $y, z, w \in \mathbb{R}^d$ , the set  $\{x \in \mathbb{R}^d \mid \|x - z\|_d = \|y - w\|_d\}$  describes a circumference in  $\mathbb{R}^d$ , centered at  $z$ , and with radius  $\|y - w\|_d$ , that is, a  $(d-1)$ -dimensional object. Since the measure  $\Lambda(\cdot)$  is absolutely continuous, with respect to the  $d$ -dimensional Lebesgue measure, then we have that  $\Lambda(\{x \in \mathbb{R}^d \mid \|x - z\|_d = \|y - w\|_d\}) = 0$ . Thus, the previous inequality implies that  $\mathbb{P}(B) = 0$ .

When  $\Phi$  is a general stationary point process, to prove that  $\mathbb{P}(\mathcal{B}) = 0$ , we have to use the fact that its intensity measure is a multiple of the Lebesgue measure [BB09], and the stationary version of the Campbell's formula (see the more general proof in subsection 6.6.1).  $\square$

**Corollary 1.** *Let be  $\Phi$  either a general stationary point process, or a PPP whose intensity measure is absolutely continuous with respect to the Lebesgue measure. Then, the nearest neighbor of every element of  $\Phi$  is unique,  $\mathbb{P}$ -a.s.*

In particular, the nearest neighbor is unique for every PPP, whose intensity measure has the form  $f(x)dx$ , where the measurable function  $f : \mathbb{R}^d \rightarrow [0, \infty)$  is locally-integrable. Or for every stationary point process, the class of stationary determinantal point processes included. To adapt the same proof of this result to other classes of point process, we would have to make use of their Palm measure. For instance, the explicit expression presented in [LMR14] of the Palm measure of a non stationary determinantal point process, whose intensity measure is absolutely continuous to the Lebesgue measure.

## 2.2 The Nearest Neighbor Model

To group the BSs in a static way, the idea is to split the atoms in  $\phi$  into finite cooperative clusters  $C_m \subset \phi$ , with possibly different sizes. In addition, the clusters  $(C_m)_{m=1}^\infty$  must be a partition of  $\phi$ , that is, two different clusters do not share atoms and their union exhausts the set of atoms  $\phi$ :

$$\begin{aligned} C_m \cap C_k &= \emptyset, \text{ for } m \neq k, \\ \bigcup_{m=1}^{\infty} C_m &= \phi, \end{aligned}$$

where  $\emptyset$  denotes the empty set.

Our aim is to form such static cooperative clusters with rules depending only on the relative distance between the set of atoms, independently of the BS density, allowing a minimum of tractability, and easy to program and simulate. As stated in the Introduction, an appropriate choice is the *Nearest Neighbor Model* [HM96].

**Definition 2** (The Nearest Neighbor Model). *The Nearest Neighbor Model (NNM) consists of clusters  $C$  whose elements are connected, by a direct edge, to their nearest neighbor. That is,  $x \in C$  if, and only if, there exists  $y \in C$  such that  $x \xrightarrow{\phi} y$  or  $y \xrightarrow{\phi} x$ .*

We have the following properties.

**Proposition 1.** *The clusters defined by the NNM fulfill the following properties:*

1. *Each element of the configuration belongs to a cluster.*
2. *The cardinality of each cluster is larger or equal to 2.*
3. *Each cluster does not contain cycles, that is, each cluster is a tree, and hence the NN-graph is a forest.*

*Proof.* First, since any element of a configuration has a nearest neighbor (we are only considering non-trivial configurations, of course), hence, every atom belongs to a cluster.

On the other hand, by definition, every (non empty) cluster contains at least two different elements: the atom and its nearest neighbor.

To prove the last assertion, we need to see that it is impossible for every cluster  $C$  having different atoms  $x_1, x_2, \dots, x_n$ , where  $n \geq 3$ , such that  $x_1 \rightarrow x_2$ ,  $x_2 \rightarrow x_3$ ,  $\dots$ ,  $x_n \rightarrow x_1$ . For this task, we prove the simplest case: There exist three different atoms  $x_1, x_2, x_3$  such that  $x_1 \rightarrow x_2$ ,  $x_2 \rightarrow x_3$ ,  $x_3 \rightarrow x_1$ . Without loss of generality, suppose that  $\|x_1 - x_2\|_d < \min\{\|x_2 - x_3\|_d, \|x_3 - x_1\|_d\}$  (every triangle has a minimum side). However, since  $x_2 \rightarrow x_3$ , from Definition 1, in particular we have that  $\|x_2 - x_3\|_d < \|x_2 - x_1\|_d$ , which is a contradiction. The proof is practically the same for cycles of size bigger than three.  $\square$

The previous result holds for every locally finite configuration, for which two different pairs of atoms do not have the same distance between them. The following result holds for configurations in the PPP case.

**Theorem 2.** *When the BS positions are modeled by a stationary PPP, the clusters defined by the NNM have, in addition, the following properties:*

1. *The cluster formation is independent of the density.*
2. *The cardinality of each cluster is finite,  $\mathbb{P}$ -a.s. That is, the corresponding graph does not percolate. In particular, the resulting NN-graph is disconnected.*

For the proof of the previous Theorem, see [HM96]. Figure 2.1 shows a deployment of BSs, represented by the blue dots, connected by their corresponding nearest neighbor. We can then appreciate the different clusters generated by the NNM.

Even considering the Poissonian behaviour of the BS positions, there are some evident problems. Having cooperative groups of size as large as possible leads into several inconveniences. Applied to a cellular network, this would imply having a big number of BSs serving only one user at each time. Other problem is that the bigger the cluster, the further away

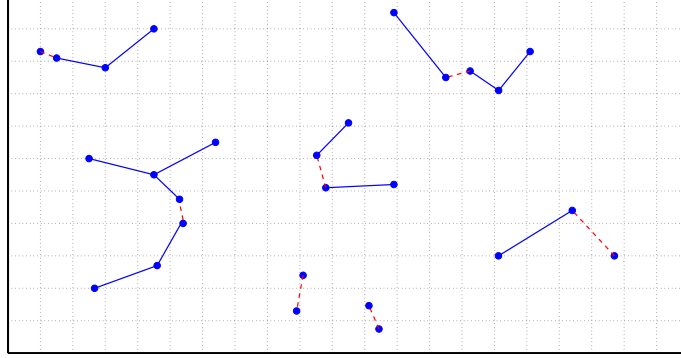


Figure 2.1: A deployment of BSs (blue dots) and the corresponding NNM. The atoms connected by the red-dashed lines are the pair of mutually nearest neighbors within each one of the clusters defined by the NNM.

from each other are the atoms within this cluster, making more complicated, and expensive, the communication among them. This is, partly, due to the fact that there are no cycles in the clusters defined by the NNM.

## 2.3 Mutually Nearest Neighbors

In the NNM, there exists a relevant class of nearest neighbors.

**Definition 3.** *Two atoms  $x, y$  in  $\phi$  are said to be mutually nearest neighbors if, and only if,  $x \xrightarrow{\phi} y$  and  $y \xrightarrow{\phi} x$ .*

A particularity of the mutually nearest neighbors is that they must have the same distance between them. Hence, these are restricted only to pairs of atoms, given the class of configurations we are considering. Figure 2.1 shows a deployment of atoms, the corresponding clusters defined by the NNM connected by blue lines, and the mutually nearest neighbors connected by red dash-dotted lines. We can distinguish clusters of size 2, whose elements are mutually nearest neighbors. Moreover, each cluster has one pair of mutually nearest neighbors. Actually, this happens in every finite cluster defined by the NNM.

**Proposition 2.** *In the NNM, every finite cluster contains exactly one pair of mutually nearest neighbors.*

*Proof.* Let  $C$  be a finite cluster of nearest neighbors, with cardinality  $N \geq 2$ . When  $N = 2$ , that is,  $C = \{x, y\}$ , then,  $x \rightarrow y$  and  $y \rightarrow x$ , meaning that  $x$  and  $y$  are mutually nearest neighbors. Now, let us suppose that  $N > 2$ . Suppose that there are no pair of mutually nearest neighbors. Then, there must exist different  $x_1, \dots, x_m$  in  $C$ ,  $m > 2$ , such that  $x_1 \rightarrow x_2 \rightarrow \dots \rightarrow x_{m-1} \rightarrow x_m \rightarrow x_1$  (it is constructed iteratively, in a finite number of steps).

Hence,  $C$  contains a cycle, which, according to Proposition 1, is impossible. Thus,  $C$  must contain a pair of mutually nearest neighbors.

To prove the uniqueness of the pair, we only need again to use the fact that the nearest neighbor is unique and that there are no cycles in  $C$ , which makes impossible to connect to different pairs of mutually nearest neighbors.  $\square$

The existence of a pair of mutually nearest neighbors is restricted to finite clusters. It is easy to construct an infinite family of atoms, all connected by their nearest neighbor, and not having a pair of mutually nearest neighbors.

Consider a finite cluster of the NNM. The only atoms, within this cluster, whose distance to its nearest neighbor is minimal, are those from the respective unique pair of mutually nearest neighbors. Therefore, the mutually nearest neighbors are the subclusters of the NNM for which the cooperation is optimal, with respect to the nearest neighbor criterion. Thus, the mutually nearest neighbors can be considered as the root of the NNM.

From the above discussion, we are interested in a variation of the NNM, with maximum clustersize 2: pairs of mutually nearest neighbors, and the rest of the atoms remain single. In this way, given a deployment of nodes, we have single atoms, operating individually, and pairs of atoms, cooperating with each other. These cooperative pairs constitute a base for every finite cluster defined by the NNM. Thus, this variation is a starting basic model, that has a fixed maximum clustersize, it is easier to obtain first and highly satisfactory results (via simulations and analysis), and it is simple to generalize the same idea for a maximum cluster size larger than 2.

On the other hand, this clustering methodology can be seen as a *matching* between the elements of a realisation.

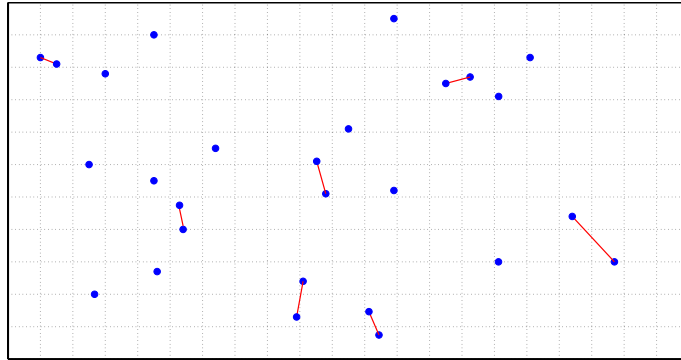
## 2.4 The Matching Problem

This subsection is influenced by the *marriage problem*, investigated by Gale and Shapley in [GS62]. The aim of this discussion is to give a different insight into the way the mutually nearest neighbors are formed.

Suppose that there are exactly  $n$  persons who wish to be paired with each other. If the persons are seen as vertices, a *matching* is a set of edges, without common vertices, where each edge represents a pair of persons, and the whole set of edges represents a way of pairing the set of  $n$  persons.

As an example, consider a configuration of  $n$  atoms. Two atoms are paired if they are mutually nearest neighbors. Figure 2.2 shows a deployment of BSs (blue dots), and the pairs of mutually nearest neighbors are connected by red lines (the edges of the graph defining the matching). Notice that not all the atoms are paired.

**Definition 4.** *Given a configuration of  $n$  persons and a matching. The matching is said to be perfect, if the  $n$  persons are paired.*



The matching generated by the mutually nearest neighbors is not perfect, which is not surprising, given the irregularity of the considered configurations. On the other hand, this implies less infrastructure within the network. Hence, as long as the benefits of cooperation remain, what better than to make cooperate only a part of the BSs. In Chapter 4 we will prove that, if the BSs positions are modeled by a PPP, around 62% of them belong to a pair of mutually nearest neighbors. Actually, for other families of point processes, the respective percentage of mutually nearest neighbors oscillates around 62%. In Chapter 6 we will propose a variation of the mutually nearest neighbors. The corresponding matching is not perfect either. Nevertheless, the extra factor added gives more flexibility to the model and allows the operator to play more with the formation of the cooperative pairs and then with its corresponding percentage.

Eventhough the mathching generated by the mutually nearest neighbors is not perfect, it is actually an optimal way of pairing, with respect to the relative distance between atoms. Suppose that each atom ranks the remaining  $n-1$  atoms with respect to its relative distance to them, where the lower ranking corresponds to its nearest neighbor. Given a pair of mutually nearest neighbors, each one of its elements cannot be better matched with respect to each one's ranking.

**Definition 5.** Given a configuration of  $n$  persons and a matching, suppose that each persons ranks the remaining  $n - 1$  persons, with respect to a particular criterion. The matching is said to be stable, with respect to this criterion, if it does not exist any match by which both elements would be individually better off this pair than they are with the element to which they are currently matched.

As stated above, the matching generated by the mutually nearest neighbors is stable, with respect to the relative distance between the atoms. In [Irv85], the authors suggest an algorithm, given a set of  $n$  persons and a ranking for each, to find a stable matching, with



respect to the given ranking.

# Cooperative Signals

Part of the discussion in this Chapter has been published within the following two articles, the first one presented at IEEE Globecom 2016, at Washington, D.C., USA:

- *Coverage Gains from the Static Cooperation of Mutually Nearest Neighbors*,
- *Analysis of Static Cellular Cooperation between Mutually Nearest Neighbors Nodes*, submitted Journal paper, arXiv:1611.02614v1.

## Abstract

The current Chapter is devoted to the modeling of the received signal, at the typical user, when transmitted either by a single BS, or a cooperative pair, or a cooperative group of BSs of larger size. The analysis can be applied to any type of antennas, including directional BSs, for which the emitted signal, received at the typical user, depends on the positions of the cooperative group of BSs. The directional case requires extra integration with respect to angles, which unnecessarily complicates the analysis, without substantial difference. Thus, for simplicity of presentation, we consider for the examples the omnidirectional case, where the emitted signal depends only on the distance of the BS from the typical user.

## 3.1 Emitted signal to the typical user

The way the cooperative signals are modeled in this Chapter is independent of the BS deployment and of the way the BSs are grouped. Our goal is to present these signals in a general fashion, then illustrate the ideas with examples, and finally give conditions offering the possibility of a tractable analysis. The discussion comprises the received signals emitted by single BSs, cooperative pairs, already presented in [ACGM16, ACGMD16]. And we include a new discussion for clusters of size bigger than 2.

In what follows, we will introduce explicit examples. For these, let us consider an i.i.d. family  $(h_r)_{r>0}$  of positive exponential random variables, with parameter 1, also independent of the BS deployment. Given  $p > 0$ , the couple  $(h_r, p)$  represents the random propagation effects and the power signal emitted to the typical user from a BS whose distance from

the origin is  $r > 0$ . Let us also choose the *path-loss* function as  $l(r) := \frac{1}{r^\beta}$ , with *path loss exponent*  $\beta > 2$ .

### 3.2 Single atoms

Consider  $f : \mathbb{R}^2 \rightarrow [0, \infty)$  and  $\tilde{f} : [0, \infty) \rightarrow \mathbb{R}^+$  two generic random fields. The quantity  $f(x)$  (and  $\tilde{f}(r)$ ) represents the received signal at the typical user, when transmitted by a single BS, whose position is  $x$  (or its distance from the origin is  $r > 0$ ). For a single BS we could, for example, consider

$$\tilde{f}(r) = p \frac{h_r}{r^\beta}, \quad (3.1)$$

which follows an exponential distribution, with parameter  $\frac{r^\beta}{p}$ .

### 3.3 Pair cooperation

Consider  $g : \mathbb{R}^2 \times \mathbb{R}^2 \rightarrow \mathbb{R}^+$  and  $\tilde{g} : [0, \infty) \times [0, \infty) \rightarrow \mathbb{R}^+$  two generic random fields, both independent of the BS deployment. The quantity  $g(x, y)$  (and  $\tilde{g}(r, z)$ ) represents the received signal at the typical user, when transmitted by a pair of BSs whose positions are  $x$  and  $y$  (or their distance from the origin are  $r > 0$  and  $z > 0$ ), respectively. The received signal can take the following example expressions, which refer to different types of cooperation or coordination,

$$\tilde{g}(r, z) = \begin{cases} p \frac{h_r}{r^\beta} + p \frac{h_z}{z^\beta}, & \text{[NSC]} \\ \mathbf{1}_{on_r} p \frac{h_r}{r^\beta} + (1 - \mathbf{1}_{on_r}) p \frac{h_z}{z^\beta}, & \text{[OFF]} \\ \max \left\{ p \frac{h_r}{r^\beta}, p \frac{h_z}{z^\beta} \right\}, & \text{[MAX]} \\ \left| \sqrt{p \frac{h_r}{r^\beta}} e^{i\theta_r} + \sqrt{p \frac{h_z}{z^\beta}} e^{i\theta_z} \right|^2 & \text{[PH]} \end{cases} \quad (3.2)$$

In the above,  $(\mathbf{1}_{on_r})_{r>0}$  and  $(\theta_r)_{r>0}$  are two different families of indexed identically distributed random variables (r.v.), independent of the other random objects. They follow a Bernoulli distribution, with parameter  $q \in (0, 1)$  ( $\bar{q} := 1 - q$ ), and a general distribution over  $[0, 2\pi)$ , respectively. [NSC] refers to non-coherent joint transmission, as in [NMH14, BK15, TSAJ14, GZHZ16], where each of the two BSs transmits an orthogonal signal, and the two are added at the receiver side. [OFF] refers to the case where one of the two BSs is active and the other inactive, according to an independent Bernoulli experiment, independent of the BS positions. [MAX] refers to the case where the BS with the strongest signal is actively serving a user, while the other is off. The [OFF] and [MAX] cases are relevant to energy saving operation. In the [PH] case, two complex signals are combined in phase (see [BG15, NMH14]), in particular, when  $\cos(\theta_r - \theta_z) = 1$ , the two signals are in the same direction, and they add up coherently at the receiver (user side), giving the maximum cooperating signal.

Table 3.1: Expressions for the CCDF and the LT

	$\mathbb{P}(g(r, z) > T)$	$\mathbb{E}[e^{-sg(r, z)}]$
<b>[NSC]</b>	$\frac{z^\beta}{p(r^\beta - z^\beta)} \left( e^{-\frac{r^\beta}{p}T} - e^{-\frac{z^\beta}{p}T} \right)$	$\frac{r^\beta}{sp + r^\beta} \frac{z^\beta}{sp + z^\beta}$
<b>[OFF]</b>	$qe^{-\frac{r^\beta}{p}T} + \bar{q}e^{-\frac{z^\beta}{p}T}$	$q \frac{r^\beta}{sp + r^\beta} + \bar{q} \frac{z^\beta}{sp + z^\beta}$
<b>[MAX]</b>	$e^{-\frac{r^\beta}{p}T} + e^{-\frac{z^\beta}{p}T} - e^{-\left(\frac{r^\beta}{p} + \frac{z^\beta}{p}\right)T}$	$\frac{r^\beta}{sp + r^\beta} + \frac{z^\beta}{sp + z^\beta} - \frac{r^\beta + z^\beta}{sp + r^\beta + z^\beta}$

The above expressions in (3.2) are merely examples of the cooperation signals. A more general family can be proposed with specific properties. For instance, for some  $n \in \mathbb{N}$ , consider  $c_i : [0, \infty) \times [0, \infty) \rightarrow \mathbb{R}$ , and  $d_i : [0, \infty) \times [0, \infty) \rightarrow \mathbb{R}^+$ , for  $1 \leq i \leq n$ , some *deterministic* and measurable functions, such that

$$\mathbb{P}(\tilde{g}(r, z) > T) = \sum_{i=1}^n c_i(r, z) e^{-d_i(r, z)T}. \quad (3.3)$$

The tail probability distribution functions (CCDF) of  $\tilde{g}(r, z)$  for **[NSC]**, **[OFF]**, and **[MAX]** fulfils equation (3.3) (see Table 3.1). On the contrary, the CCDF of  $\tilde{g}(r, z)$  for **[PH]** does not necessarily have the form of equation (3.3). Notice, as well, that the cluster size, in this case 2, is independent of the number of addends in (3.3) (again, see Table 3.1 for **[MAX]**). In general, the function defined in (3.3) is not necessarily a CCDF. For this to hold, some extra conditions must be imposed to the functions  $c_i(r, z)$  and  $d_i(r, z)$ . For instance, a necessary condition is that  $\sum_{i=1}^n c_i(r, z) = 1$ . However, the functions  $c_i(r, z)$  do not need to be all positive (see Table 3.1 **[OFF]** for all the functions  $c_i(r, z)$  being positive, and **NSC** and **[MAX]** two examples of not all the functions  $c_i(r, z)$  being positive).

When analysing performance related to coverage probability, the CCDF for the signals that can be written as (3.3) lead easier to numerically tractable formulas. In the following subsection we introduce a class of probability distributions that generalizes those characterized by equation (3.3), and that facilitate the performance analysis of a network.

Table 3.1 shows expressions for  $\mathbb{E}[e^{-sg(r, z)}]$ , for every  $s > 0$ , that will be useful for the numerical evaluation in Chapter 5. For the analysis that follows, we consider a general expression.

### 3.4 Cooperation between $m$ nodes

Fix  $m \in \mathbb{N}$ . Consider  $g : (\mathbb{R}^2)^m \rightarrow \mathbb{R}^+$  and  $\tilde{g} : [0, \infty)^m \rightarrow \mathbb{R}^+$ , two generic random fields, both independent of the BS deployment. The quantity  $g(x_1, \dots, x_m)$  (and  $\tilde{g}(r_1, \dots, r_m)$ ) represents the received signal at the typical user, when transmitted by a group of BSs whose positions are  $x_1, \dots, x_m$  (or their distance from the origin are  $r_1, \dots, r_m$ ), respectively. For a fixed  $1 \leq k \leq m$  and  $r = (r_1, \dots, r_m) \in [0, \infty)^m$ , the received signal can take the following

example expressions, which refer to different types of cooperation or coordination,

$$\tilde{g}(r) = \begin{cases} \sum_{i=1}^m \frac{h_{r_i}}{r_i^\beta}, & [\mathbf{NSC}^{(m)}] \\ \sum_{i=1}^m V_i^{(k)} p \frac{h_{r_i}}{r_i^\beta}, & [\mathbf{OFF}^{(m,k)}] \\ \sum_{i=1}^m W_i^{(k)} p \frac{h_{r_i}}{r_i^\beta}, & [\mathbf{OFF}_2^{(m)}] \\ \max \left\{ p \frac{h_{r_1}}{r_1^\beta}, \dots, p \frac{h_{r_m}}{r_m^\beta} \right\}, & [\mathbf{MAX}^{(m)}] \end{cases}. \quad (3.4)$$

In the above,  $(V_1^{(k)}, \dots, V_m^{(k)})$  is a random vector, independent of the other random objects, such that

$$\mathbb{P}(V_1^{(k)} = i_1, \dots, V_m^{(k)} = i_m) = \begin{cases} \frac{1}{\binom{m}{k}}, & \text{if } i_j \in \{0, 1\} \text{ and } \sum_{j=1}^m i_j = k \\ 0, & \text{otherwise.} \end{cases}$$

$(W_1, \dots, W_m)$  is an independent random vector, independent of the other random objects, such that each  $W_i$  is a Bernoulli random variable, with parameter  $q \in (0, 1)$ .  $[\mathbf{NSC}^{(m)}]$  refers to non-coherent joint transmission, as in [NMH14, BK15, TSAJ14, GZHZ16], where each of the  $m$  BSs transmits an orthogonal signal, and the  $m$  signals are added at the receiver side.  $[\mathbf{OFF}^{(m,k)}]$  refers to the case where  $k$  of the  $m$  BSs are active, transmitting an orthogonal signal, and the other  $m - k$  are inactive, according to a random experiment.  $[\mathbf{OFF}_2^{(m)}]$  refers to the case where, according to a binomial experiment, for some  $0 \leq \ell \leq m$ ,  $\ell$  of the  $m$  BSs are active, transmitting an orthogonal signal, and the other  $m - \ell$  are inactive.  $[\mathbf{MAX}^{(m)}]$  refers to the case where the BS with the strongest signal is actively serving a user, while the others are off. Notice that  $[\mathbf{NSC}^{(m)}]$  is special cases of  $[\mathbf{OFF}^{(m,k)}]$ , for  $k = m$ .  $[\mathbf{OFF}^{(m,k)}]$ ,  $[\mathbf{OFF}_2^{(m)}]$ , and  $[\mathbf{MAX}^{(m)}]$  are relevant to energy saving operation.

A more general family can be proposed with specific properties. Denote by  $\mathcal{M}^{n \times n}(\mathbb{R})$  the space of square matrices. Suppose that, for some  $n \in \mathbb{N}$ , there exist *deterministic* and measurable functions  $c : [0, \infty)^m \rightarrow (\mathbb{R})^n$  and  $M : [0, \infty)^m \rightarrow \mathcal{M}^{n \times n}(\mathbb{R})$ , such that, for every  $r \in [0, \infty)^m$ ,

$$\mathbb{P}(\tilde{g}(r) > T) = c(r) e^{M(r)T} \mathbf{e}, \quad (3.5)$$

where  $e^{M(r)T}$  denotes the exponential of the matrix  $TM(r)$  [Arn92], and  $\mathbf{e}$  is a column vector of ones of size  $m$ . The CCDF of  $\tilde{g}(r, z)$  for  $[\mathbf{NSC}^{(m)}]$ ,  $[\mathbf{OFF}^{(m)}]$ ,  $[\mathbf{OFF}^{(m,k)}]$ ,  $[\mathbf{OFF}_2^{(m)}]$ , and  $[\mathbf{MAX}^{(m)}]$  cases fulfils equation (3.5). For instance, for  $[\mathbf{OFF}^{(m)}]$ , we have that  $n = m$ , and, for every  $r = (r_1, \dots, r_m)$ ,

$$c(r_1, \dots, r_m) = \left( \frac{1}{m}, \dots, \frac{1}{m} \right)$$

$$M(r_1, \dots, r_m) = \begin{pmatrix} -\frac{r_1^\beta}{p} & 0 & \dots & 0 & 0 \\ 0 & -\frac{r_2^\beta}{p} & \dots & 0 & 0 \\ \dots & \dots & \dots & \dots & \dots \\ 0 & 0 & \dots & -\frac{r_{m-1}^\beta}{p} & 0 \\ 0 & 0 & \dots & 0 & -\frac{r_m^\beta}{p} \end{pmatrix}$$

Table 3.2: Expressions for the CCDF and the LT

	$c(r, z)$	$M(r, z)$
<b>[NSC]</b>	$(1, 0)$	$\begin{pmatrix} -\frac{r_2^\beta}{p} & \frac{r_2^\beta}{p} \\ 0 & -\frac{z_2^\beta}{p} \end{pmatrix}$
<b>[OFF]</b>	$(q, \bar{q})$	$\begin{pmatrix} -\frac{r_2^\beta}{p} & 0 \\ 0 & -\frac{z_2^\beta}{p} \end{pmatrix}$
<b>[MAX]</b>	$(1, 1, -1)$	$\begin{pmatrix} -\frac{r_2^\beta}{p} & 0 & 0 \\ 0 & -\frac{z_2^\beta}{p} & 0 \\ 0 & 0 & -\frac{r_2^\beta}{p} - \frac{z_2^\beta}{p} \end{pmatrix}$

For **[NSC]<sup>(m)</sup>**, we have that  $n = m$ , and, for every  $r = (r_1, \dots, r_n)$ ,

$$c(r_1, \dots, r_m) = (1, 0, \dots, 0)$$

$$M(r_1, \dots, r_m) = \begin{pmatrix} -\frac{r_1^\beta}{p} & \frac{r_1^\beta}{p} & 0 & 0 & \dots & 0 & 0 & 0 \\ 0 & -\frac{r_m^\beta}{p} & \frac{r_m^\beta}{p} & 0 & \dots & 0 & 0 & 0 \\ \dots & \dots & \dots & 0 & \dots & \dots & \dots & \dots \\ 0 & 0 & 0 & 0 & \dots & 0 & -\frac{r_{m-1}^\beta}{p} & \frac{r_{m-1}^\beta}{p} \\ 0 & 0 & 0 & 0 & \dots & 0 & 0 & -\frac{r_m^\beta}{p} \end{pmatrix}$$

Generally, the cluster size  $m$ , could be different of  $n$  in (3.5). Interestingly, for cluster size 2, **[NSC]**, **[OFF]**, and **[MAX]** fulfil equation (3.5) (see Table 3.2). Moreover, every distribution whose CCDF can be written as in (3.3), can be rewritten as in (3.5).

When analysing performance related to coverage probability, the CCDF for the signals that can be written as (3.5) lead easier to numerically tractable formulas. The family of probability distributions whose CCDF has the form of (3.5) are called *Phase-type-distribution* [BKF14]. **[OFF]<sub>2</sub><sup>(m)</sup>** is related to the hyperexponential distribution, and **[NSC]<sup>(m)</sup>** to the hypoexponential distribution. The Laplace transform of probability distribution characterized by equation (3.5) is given by

$$\mathbb{E} \left[ e^{-s\tilde{g}(r)} \right] = c(r)(sI - M(r))^{-1}(-M(r))\mathbf{e}, \quad (3.6)$$

where  $I$  is the identity matrix. The application  $s \mapsto (sI - M(r))^{-1}$  is known as the resolvent of the matrix  $M(r)$  [Arn92].



# Characteristics of the Mutually Nearest Neighbors

This Chapter resulted in the following article, presented at WiOpt 2015, at Mumbai, India:

- *Analysing interference from static cellular cooperation using the Nearest Neighbor Model.*

And part of this Chapter has been published also within the following two articles, the first one presented at IEEE Globecom 2016, at Washington, D.C., USA:

- *Coverage Gains from the Static Cooperation of Mutually Nearest Neighbors,*
- *Analysis of Static Cellular Cooperation between Mutually Nearest Neighbors Nodes,* submitted Journal paper, arXiv:1611.02614v1.

## Abstract

Suppose that the BSs positions are modeled by a point process. We group the BSs into *cooperative groups*, formed by mutually nearest neighbors, and the rest remain single, operating individually. From the dependent thinning specified by the above clustering criterion, it is possible to define two point processes: The process of *singles*, and the process of *cooperative pairs*. The current Chapter is devoted to present results about the structural characteristics of to these two point processes. Mainly when the process modeling the BS positions is a PPP. All these results lead to the performance analysis of a cooperative cellular network.

## 4.1 Singles and pairs

Consider a point processes  $\Phi = \{\phi\}$ , modeling the BS locations, and whose realisations fulfill the *uniqueness* of the nearest neighbor a.s. (Corollary 1). For our particular purposes, we suppose that  $\Phi$  takes values in the 2-dimensional Euclidean space. Nevertheless, all the results holds for every dimension larger than 2, and can be straightforwardly obtained.



In Chapter 2 we introduced the cooperative groups of atoms we are interested in: Pairs of atoms in MNNR, the so called *mutually nearest neighbors*. And all the other BSs remain single, operating individually.

**Definition 6.** An atom  $x \in \phi$  is called *single* iff it is not in MNNR (does not cooperate) with any other atom in  $\phi$ . That is, if for every  $y \in \phi$  such that  $x \xrightarrow{\phi} y$ , then  $y \not\xrightarrow{\phi} x$ .

Figure 4.1 shows a deployment of BSs, where the blue dots represent the single atoms, and the pairs of connected red dots represent the cooperative groups. When the BS positions are modeled by a point process, for each one of its realisation, we can easily identify the singles and pairs. Thus, we define the corresponding processes of singles and cooperative pairs.

**Definition 7.** Given a point process  $\Phi$ , define two new point processes  $\Phi^{(1)}$  and  $\Phi^{(2)}$ :

$$\Phi^{(1)} := \{x \in \Phi \text{ \& } x \text{ is single}\},$$

$$\Phi^{(2)} := \{x \in \Phi \text{ \& } x \text{ cooperates with another element of } \Phi\}.$$

The way  $\Phi^{(1)}$  and  $\Phi^{(2)}$  are defined depend only on the relative distance between the elements of  $\Phi$ . As a consequence, if the original process is stationary, then the two resulting processes are *stationary* as well.

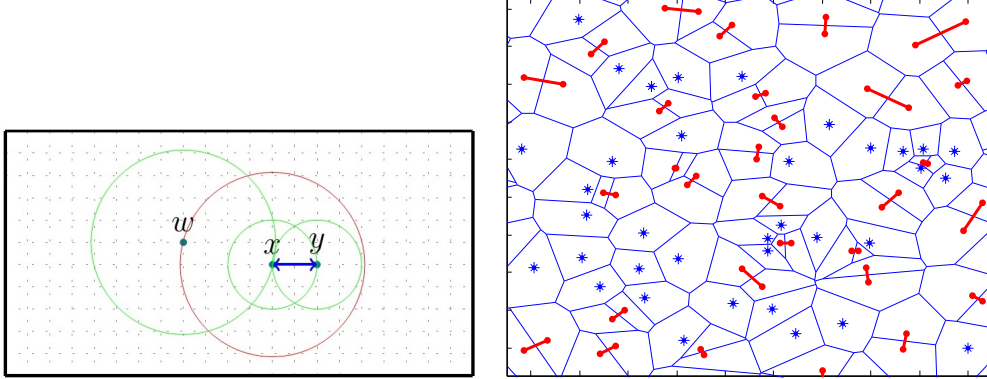


Figure 4.1: (Left) The atoms  $x$  and  $y$  are mutually nearest neighbors, so, they work in pair. The atom  $x$  is the nearest neighbor of  $w$ , but  $w$  is not the closest atom to  $x$ , thus  $w$  is single. (Right) A Poisson realisation with its corresponding Voronoi diagram. The asterisks are the single BSs, the connected dots are the cooperating pairs.

As a starting point to study some properties of the processes of singles and cooperative pairs, we wish to give an equivalence, in geometrical terms, for two different atoms being in MNNR, with respect to a given configuration. For this task, denote by  $\mathcal{S}^{(2)}(\cdot)$  the 2-dimensional Euclidean surface, by

$$B_E^{(2)}(x, r) := \{y \in \mathbb{R}^2 \mid \|x - y\|_2 < r\}$$

the 2-dimensional Euclidean ball, centered at  $x$ , and radius  $r > 0$ . And denote the planar area

$$C(x, y) := B_E^{(2)}(x, \|x - y\|_2) \cup B_E^{(2)}(y, \|x - y\|_2).$$

The relation  $x \xrightarrow{\phi} y$  holds iff the disc  $B_E^{(2)}(x, \|x - y\|)$  is empty of atoms from  $\phi$ . Consequently, the relation  $x \xleftrightarrow{\phi} y$  holds iff, there are no atoms from  $\phi$  inside  $C(x, y)$ . An illustration of this is given in Figure 4.1. Thus, if the empty space function of a point process is known, it is possible to give an expression for the probability of two given atoms being in cooperation. For instance, when  $\Phi = \{\phi\}$  is a PPP, the Euclidean surface of  $C(x, y)$  is

$$\mathcal{S}^{(2)}(C(x, y)) = \pi \|x - y\|^2 (2 - \gamma),$$

where  $\gamma := \frac{2}{3} - \frac{\sqrt{3}}{2\pi}$  is a constant number equal to the surface, divided by  $\pi$ , of the intersection of two discs with unit radius and centres lying on the circumference of each other. Hence, we have the following result.

**Lemma 1.** *Given a PPP  $\Phi$ , with density  $\lambda > 0$ , for two different and fixed atoms  $x, y \in \mathbb{R}^2$ ,*

$$\mathbb{P}\left(x \xleftrightarrow{\Phi} y\right) = e^{-\lambda \pi \|x - y\|^2 (2 - \gamma)}.$$

When  $\Phi$  is a PPP, from the previous Lemma, we have the following result.

**Theorem 3.** *Given a PPP  $\Phi$ , with density  $\lambda > 0$ , for every fixed atom  $x \in \mathbb{R}^2$ , there exists a constant  $\delta > 0$ , independent of  $\lambda$  and  $x$ , such that*

$$\mathbb{P}\left(x \in \Phi^{(2)}\right) = \delta, \quad \mathbb{P}\left(x \in \Phi^{(1)}\right) = 1 - \delta.$$

Specifically,  $\delta = \frac{1}{2 - \gamma} \approx 0.6215$ .

*Proof.* By definition of  $\Phi^{(2)}$ ,

$$\mathbb{P}\left(x \in \Phi^{(2)}\right) = \mathbb{E}\left(\mathbf{1}_{\{x \xleftrightarrow{\Phi} y, \text{ for some } y \in \Phi \setminus \{x\}\}}\right) \stackrel{(a)}{=} \mathbb{E}\left(\sum_{y \in \Phi} \mathbf{1}_{\{x \xleftrightarrow{\Phi} y\}}\right),$$

where (a) holds because for PPPs the nearest neighbor is a.s. unique. Using Campbell-Little-Mecke formula and Slyvniak's Theorem [BB09] for a PPP,

$$\mathbb{E}\left(\sum_{y \in \Phi} \mathbf{1}_{\{x \xleftrightarrow{\Phi} y\}}\right) = \int_{\mathbb{R}^2} \mathbb{P}\left(x \xleftrightarrow{\Phi} y\right) \lambda dy \stackrel{(b)}{=} \lambda \int_{\mathbb{R}^2} e^{-\lambda \pi \|x - y\|^2 (2 - \gamma)} dy = \frac{1}{2 - \gamma},$$

where (b) follows from Lemma 1. □

The constant  $\delta$  from the previous Theorem is crucial within this work. The above Theorem states that, given the position of a BS (in a PPP), its probability of being in a cooperative pair is  $\delta \approx 0.6215$ , otherwise, its probability of being single is  $1 - \delta \approx 0.3785$ , irrespective of the value of the density  $\lambda > 0$ . Since we are fixing the atom location, this

result should be interpreted from a local point of view. Nevertheless, in Section 4.6.1 we will prove that, given a density  $\lambda > 0$  for the PPP, the intensities of  $\Phi^{(1)}$  and  $\Phi^{(2)}$  are actually  $(1 - \delta)\lambda$  and  $\delta\lambda$ , respectively. The former can be interpreted from a global point of view: over any planar area in  $\mathbb{R}^2$ , in average, 37.85% of atoms are singles and 62.15% belong to a cooperative pair.

When  $\Phi$  is a PPP, it is natural to wonder if  $\Phi^{(1)}$  and  $\Phi^{(2)}$  are also PPPs. As a matter of fact, they are not (we could have expected this, since they were defined by a strongly dependent thinning). Suppose that  $\Phi^{(2)}$  is actually a PPP. As shown in Theorem 3, for every atom in  $\Phi^{(2)}$ , there is a positive probability of this point not being in MNNR with another point of  $\Phi^{(2)}$ . However, by definition, all the elements of  $\Phi^{(2)}$  are in MNNR with another element of  $\Phi^{(2)}$ , which is a contradiction. We conclude that the process  $\Phi^{(2)}$  is not a PPP. For  $\Phi^{(1)}$  the argumentation is not as simple. We can show using the Kolmogorov-Smirnov test [She07] that the number of  $\Phi^{(1)}$  atoms within a finite window is not Poisson distributed. Moreover, Monte Carlo simulations estimate that the average proportion of single atoms from  $\Phi^{(1)}$  is far from the 37.85%.

The percentages in Theorem 3 are not valid just for PPPs. Take the hexagonal grid model. This is commonly used by industry related research teams to model the BS positions, and then evaluate a system deployment and performance via Monte Carlo methods. The hexagonal grid's centers should represent the BS locations. This is an ideal scenario (the BSs are never that regular). We introduce another point process, based on the hexagonal grid, that actually allows for randomness of the BS positions. Starting from the grid placement, let the position of each BS be randomly perturbed, independently of the others. For example, consider as BS location the point whose polar coordinates around each hexagon's center follow two uniform random variables (r.v.s), one angular over  $[0, 2\pi)$  and the radial one over  $[0, Q]$  (see Figure 4.2). Figure 4.2 shows how the average percentage of singles and pairs for the hexagonal grid model changes when varying the parameter  $Q > 0$ . Remark that these numbers are very close to the respective average percentages we found when  $\Phi$  is a PPP.

## 4.2 Palm Probabilities

We can interpret the Palm probability of a stationary point process as the conditional probability, given that the process has a point inside an infinitesimal neighborhood around a fixed atom [BB09]. Denote by  $\mathbb{P}^0$ ,  $\mathbb{P}^{(1),0}$ , and  $\mathbb{P}^{(2),0}$  the Palm probabilities of the stationary point processes  $\Phi$ ,  $\Phi^{(1)}$ , and  $\Phi^{(2)}$ , respectively. Let  $A_0 := \{\Phi \in \mathcal{A}_0\}$ ,  $B_0 := \{\Phi \in \mathcal{B}_0\}$  be two events, where

$$\begin{aligned}\mathcal{A}_0 &:= \{\phi \mid 0 \in \phi \text{ and } 0 \text{ is single} \}, \\ \mathcal{B}_0 &:= \{\phi \mid 0 \in \phi \text{ and } 0 \text{ cooperates with another atom of } \phi \}.\end{aligned}$$

We have the following result [BB03, pp.35, Ex.142].

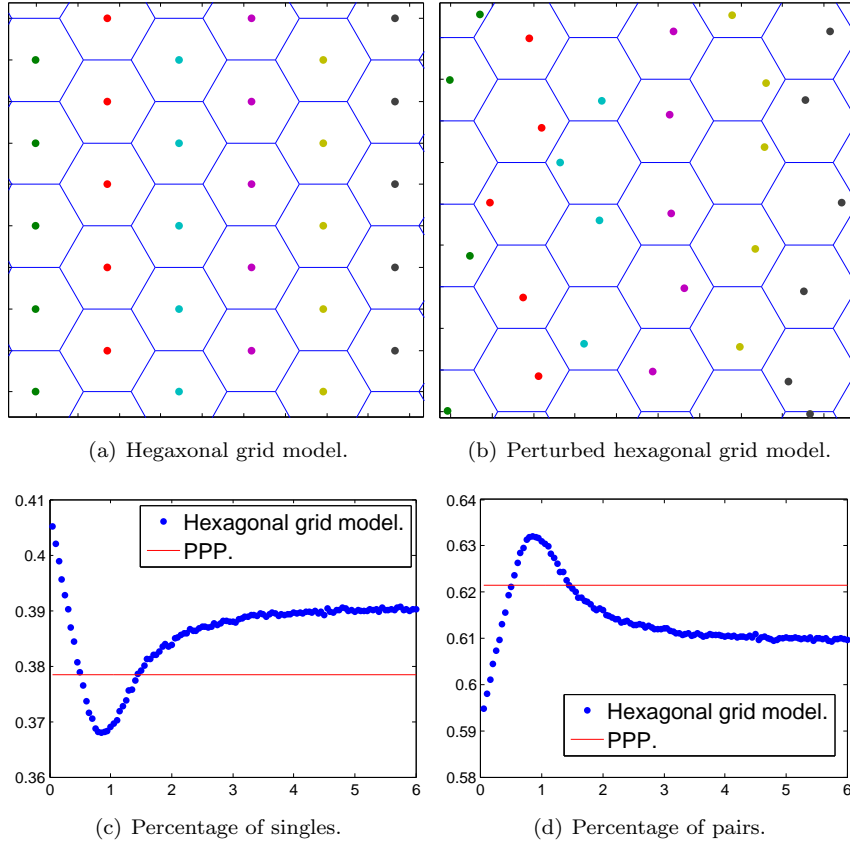


Figure 4.2: Figures (a) and (b) show, respectively, the hexagonal grid model without perturbation and with the center being perturbed after a random experiment. On the other hand, figures (c) and (d) present, respectively, in the vertical axis the average percentages of singles and pairs, for the hexagonal grid model, against different values for the parameter  $Q > 0$  in the horizontal axis.

**Theorem 4.** *Let  $\Phi$  be a stationary point process such that  $\mathbb{P}^0(A_0) > 0$  and  $\mathbb{P}^0(B_0) > 0$ . Therefore, for every  $C \in \Omega$ ,*

$$\mathbb{P}^{(1),0}(C) = \mathbb{P}^0(C|A_0), \quad \mathbb{P}^{(2),0}(C) = \mathbb{P}^0(C|B_0).$$

When  $\Phi$  is a PPP,  $\mathbb{P}^0(A_0) = 1 - \delta > 0$  and  $\mathbb{P}^0(B_0) = \delta > 0$  (Theorem 3). Then, for every  $C \in \mathcal{F}$ ,

$$\mathbb{P}^{(1),0}(C) = \frac{\mathbb{P}^0(C, A_0)}{1 - \delta}, \quad \mathbb{P}^{(2),0}(C) = \frac{\mathbb{P}^0(C, B_0)}{\delta}. \quad (4.1)$$

### 4.3 The $G$ function of the process of cooperative pairs

The  $G$  function is the cumulative distribution function (CDF) of the distance from a typical atom of the process to its nearest neighboring point [Bad07]. Denote by  $G^{(2)}(r)$  the  $G$  function of  $\Phi^{(2)}$ , then,  $G^{(2)}(r) := \mathbb{P}^{(2),0}(d(0, \Phi^{(2)} \setminus \{0\}) \leq r)$ , for every  $r > 0$ . Applying equation (4.1) to this expression, we have the following result.

**Theorem 5.** *For a PPP  $\Phi$ , the  $G$  function of  $\Phi^{(2)}$  is*

$$G^{(2)}(r) = 1 - e^{-\lambda \pi r^2 (2 - \gamma)}, \quad (4.2)$$

where  $\gamma$  is the same constant as in Lemma 1.

*Proof.* Notice that  $A_0 = \bigcup_{y \in \Phi \setminus \{0\}} \{0 \overset{\Phi}{\leftrightarrow} y\}$ , where, since the nearest is unique, this union is mutually disjoint, and  $A_0$  is the event from Theorem 4, and . For  $r > 0$  fixed,

$$\begin{aligned} G^{(2)}(r) &= \mathbb{P}^{(2),0} \left( d(0, \Phi^{(2)} \setminus \{0\}) \leq r \right) \\ &\stackrel{(a)}{=} \mathbb{P}^0 \left( d(0, \Phi^{(2)} \setminus \{0\}) \leq r, A_0 \right) \frac{1}{\delta} \\ &= \mathbb{E}^0 \left( \sum_{y \in \Phi \setminus \{0\}} \mathbf{1}_{\{d(0, \Phi^{(2)} \setminus \{0\}) \leq r, 0 \overset{\Phi}{\leftrightarrow} y\}} \right) \frac{1}{\delta} \\ &\stackrel{(b)}{=} \mathbb{E} \left( \sum_{y \in \Phi} \mathbf{1}_{\{d(0, \Phi^{(2)} \setminus \{0\}) \leq r, 0 \overset{\Phi}{\leftrightarrow} y\}} \right) \frac{1}{\delta}, \end{aligned}$$

where (a) follows from equation (4.1) and (b) from Slivnyak-Mecke's Theorem [BB09]. Observe that, if there is some  $y \in \Phi$  being the mutually nearest neighbor of the atom 0, that is  $0 \overset{\Phi}{\leftrightarrow} y$ , then,

$$d(0, \Phi^{(2)} \setminus \{0\}) = d(0, \Phi \setminus \{0\}) = \|y\| \quad a.s.$$

Using this, Campbell-Little-Mecke formula and Lemma 1,

$$\begin{aligned}
\mathbb{E}\left(\sum_{y \in \Phi} \mathbf{1}_{\{d(0, \Phi^{(2)} \setminus \{0\}) \leq r, 0 \leftrightarrow y\}}\right) \frac{1}{\delta} &= \mathbb{E}\left(\sum_{y \in \Phi} \mathbf{1}_{\{\|y\| \leq r, 0 \overset{\Phi}{\leftrightarrow} y\}}\right) \frac{1}{\delta} \\
&= \mathbb{E}\left(\sum_{y \in \Phi} \mathbf{1}_{\{\|y\| \leq r\}} \mathbf{1}_{\{0 \overset{\Phi}{\leftrightarrow} y\}}\right) \frac{1}{\delta} \\
&= \int_{\mathbb{R}^2} \mathbb{E}\left(\mathbf{1}_{\{\|y\| \leq r\}} \mathbf{1}_{\{0 \overset{\Phi}{\leftrightarrow} y\}}\right) \lambda dy \frac{1}{\delta} \\
&= \int_{\mathbb{R}^2} \mathbf{1}_{\{\|y\| \leq r\}} \mathbb{E}\left(\mathbf{1}_{\{0 \overset{\Phi}{\leftrightarrow} y\}}\right) \lambda dy \frac{1}{\delta} \\
&= \frac{\lambda}{\delta} \int_{\{\|y\| \leq r\}} \mathbb{P}(0 \overset{\Phi}{\leftrightarrow} y) dy \\
&= \frac{\lambda}{\delta} \int_{\{\|y\| \leq r\}} e^{-\lambda \pi \|y\|^2 (2-\gamma)} dy \\
&\stackrel{(c)}{=} \frac{\lambda 2\pi}{\delta} \int_0^r e^{-\lambda \pi s^2 (2-\gamma)} s ds \\
&= 1 - e^{-\lambda \pi r^2 (2-\gamma)},
\end{aligned}$$

where (c) follows from the change of variable to polar coordinates.  $\square$

The last Theorem states that, in the PPP case, the distance between cooperative atoms is Rayleigh distributed, with scale parameter  $\alpha := (2\lambda\pi(2-\gamma))^{-1/2}$ .

## 4.4 Size of the Voronoi Cells

A Voronoi cell of an atom  $x \in \phi$  is defined to be the geometric locus of all planar points  $z \in \mathbb{R}^2$  closer to this atom than to any other atom of  $\phi$  [dBCvKO08]. In a wireless network the Voronoi cell is important when answering the question 'which user should be associated with which station?'. Thus, it follows naturally to investigate the size of Voronoi cells associated with single atoms or pairs.

In a stationary framework, we examine the network performance at the Cartesian origin, the *typical user approach*. Let  $\{0 \curvearrowright \Phi^{(1)}\}$  (resp.  $\{0 \curvearrowright \Phi^{(2)}\}$ ) denote the event that the typical user belongs to the Voronoi cell of some atom of  $\Phi^{(1)}$  (resp.  $\Phi^{(2)}$ ). For the PPP case we have the following result.

**Proposition 3.** *Suppose that  $\Phi$  is a PPP, with density  $\lambda > 0$ . There exists a measurable function  $F : [0, \infty) \times [0, \infty) \times [0, 2\pi) \times [0, 2\pi) \rightarrow [0, \infty)$ , independent of the density  $\lambda$ , such that*

$$\mathbb{P}(0 \curvearrowright \Phi^{(2)}) = \lambda^2 \int_0^\infty \int_0^\infty \int_0^{2\pi} \int_0^{2\pi} s r e^{-\lambda F(r, s, \theta, \varphi) - \lambda \pi r^2} d\varphi d\theta dr ds \quad (4.3)$$

*Proof.* Denote by  $(R, \Theta)$  the polar coordinates of the closest  $\Phi$  atom from the typical user. The r.v.  $R$  is Rayleigh distributed, with scale parameter  $(\lambda 2\pi)^{-1/2}$ . Because of the isotropy of a stationary PPP,  $R$  and  $\Theta$  are independent r. v. and  $\Theta$  is uniformly distributed over  $[0, 2\pi)$ . Therefore, the density function of the random vector  $(R, \Theta)$  is

$$f_{(R, \Theta)}(r, \theta) = \lambda r e^{-\lambda \pi r^2} \mathbf{1}_{\{r > 0\}} \mathbf{1}_{\{\theta \in [0, 2\pi)\}}$$

Hence,

$$\begin{aligned} \mathbb{P}(0 \curvearrowright \Phi^{(2)}) &= \mathbb{E} \left( \mathbb{P}(0 \curvearrowright \Phi^{(2)} | R, \Theta) \right) \\ &= \int_0^\infty \int_0^{2\pi} \mathbb{P}(0 \curvearrowright \Phi^{(2)} | R = r, \Theta = \theta) \lambda r e^{-\lambda \pi r^2} d\theta dr \end{aligned}$$

Fix a realisation  $\phi$ , whose nearest neighbor to the origin, denoted by  $x$ , has  $(r, \theta)$  as its polar coordinates. Consider  $y$  another atom from  $\phi$ , whose polar coordinates are  $(s, \varphi)$ . If  $\rho$  denotes the Euclidean distance between  $x$  and  $y$ , then,

$$\rho^2 = r^2 + s^2 - 2rs \cos(\theta - \varphi)$$

Given that  $x$  is the nearest neighbor atom from  $\phi$  to the origin, hence,  $x$  and  $y$  are in MNRR iff

$$D(x, y) := (B_E^{(2)}(x, \rho) \cup B_E^{(2)}(y, \rho)) \setminus B_E^{(2)}(0, r) \quad (4.4)$$

is empty of atoms from  $\phi \setminus \{x, y\}$ . Denote by  $F(r, s, \theta, \varphi)$  the Euclidean surface of  $D(x, y)$ , the empty space function of a PPP implies that

$$\mathbb{P}(0 \curvearrowright \Phi^{(2)} | R = r, \Theta = \theta) = \int_0^\infty \int_0^{2\pi} e^{-\lambda F(r, s, \theta, \varphi)} s ds d\varphi,$$

and therefore,

$$\mathbb{P}(0 \curvearrowright \Phi^{(2)}) = \lambda^2 \int_0^\infty \int_0^{2\pi} \int_0^\infty \int_0^{2\pi} e^{-\lambda F(r, s, \theta, \varphi) - \lambda \pi r^2} r s ds d\varphi d\theta dr$$

Notice that the function  $F(r, s, \theta, \varphi)$  is independent of the density  $\lambda$ . In some cases, it is possible to find explicit values for  $F(r, s, \theta, \varphi)$ . For instance, if  $\rho \geq 2r$  implies that  $B(0, r) \subset B(x, \rho)$ . Hence,

$$\mathcal{S}^{(2)}(D(x, y)) = \mathcal{S}^{(2)}(B_E^{(2)}(y, \rho) \setminus B_E^{(2)}(x, \rho)) + \mathcal{S}^{(2)}(B_E^{(2)}(x, \rho)) - \mathcal{S}^{(2)}(B_E^{(2)}(0, r))$$

Since

$$\begin{aligned} \mathcal{S}^{(2)}(B_E^{(2)}(y, \rho) \setminus B_E^{(2)}(x, \rho)) &= \pi \rho^2 (1 - \gamma), \\ \mathcal{S}^{(2)}(B_E^{(2)}(x, \rho)) - \mathcal{S}^{(2)}(B_E^{(2)}(0, r)) &= \pi \rho^2 - \pi r^2, \end{aligned}$$

then, when  $\rho \geq 2r$ ,

$$F(r, s, \theta, \varphi) = \pi \rho^2 (2 - \gamma) - \pi r^2.$$

Unfortunately, in other cases is arduous to obtain  $F(r, s, \theta, \varphi)$ . □

Since  $\mathbb{P}(0 \curvearrowright \Phi^{(1)}) = 1 - \mathbb{P}(0 \curvearrowright \Phi^{(2)})$ , we have also an analytic representation for  $\mathbb{P}(0 \curvearrowright \Phi^{(1)})$ . The function  $F(r, s, \theta, \varphi)$  is not explicitly given, being the Euclidean surface of three overlapping discs. This is an example of the complications that arise from the MNMR, due to numerical issues related to integration over multiple overlapping circles. Such complications led us to the approximate model in Chapter 5.

**Numerical Result 1.** *Given a PPP  $\Phi$ , the average surface proportion of Voronoi cells associated with single atoms, and that associated with pairs of atoms, is independent of the parameter  $\lambda$ . By Monte Carlo simulations, we find that*

$$\mathbb{P}(0 \curvearrowright \Phi^{(1)}) \approx 0.4602, \quad \mathbb{P}(0 \curvearrowright \Phi^{(2)}) \approx 0.5398.$$

Interestingly, although the ratio of single atoms to pairs is  $0.3785/0.6215 \approx 0.6090$ , the ratio of the associated Voronoi surface is  $0.4602/0.5398 \approx 0.8525$ , implying that the typical Voronoi cell of a single atom is larger than that of an atom from a pair, as Figure 4.1 shows. The last remark gives a first intuition that there is attraction between the cooperating atoms in pair and repulsion among the singles.

## 4.5 Further Results

The *empty space function (ES)*, commonly denoted by  $F$ , is the CDF of the distance from the typical user to the nearest atom of the point process considered [Bad07]. The two functions NN and ES can be combined into a single expression known as the *J function*. The latter is a tool introduced by van Lieshout and Baddeley [Bad07] to measure repulsion and/or attraction between the atoms of a point process. It is defined as

$$J(r) = \frac{1 - G(r)}{1 - F(r)}, \tag{4.5}$$

for every  $r > 0$ . In the case of the PPP,  $G(r) \equiv F(r)$  and  $J(r) = 1$ , as a consequence of the fact that the reduced Campbell measure is identical to the original measure. Hence the  $J$  function quantifies the differences of any process with the PPP. When  $J(r) > 1$ , this is an indicator of repulsion between atoms, whereas  $J(r) < 1$  indicates attraction. We use Monte Carlo simulations to plot the  $J$  function of both processes (see Figure 4.3). From the figures we conclude that  $\Phi^{(1)}$  *exhibits repulsion for every  $r \geq 0$ , and  $\Phi^{(2)}$  attraction everywhere*. However, notice that the attraction in the case  $\Phi^{(2)}$  is due to the way the pairs are formed. If we consider a new process having as elements the middle points between each one of the cooperating pairs, this process exhibits repulsion everywhere as well.

## 4.6 Interference Analysis

The purpose of the analysis up to this point was to develop some structural results for the processes of singles and cooperative pairs. These were motivated within a communication



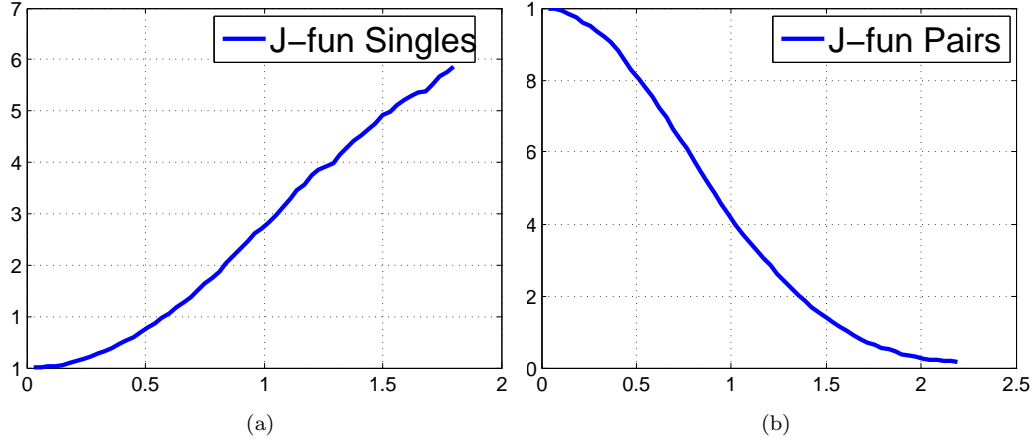


Figure 4.3: (a) The J function of the process  $\Phi^{(1)}$ . (b) The J function of the process  $\Phi^{(2)}$ .

context, ideally to derive results related to cooperative cellular networks. As shown in the previous Sections, the cooperative pairs will have a different influence on a user in the network, than those operating individually. The current Section will focus on the *interference field* generated by  $\Phi^{(1)}$  and  $\Phi^{(2)}$ , received by a typical user.

Consider that the received signal, to a typical user, emitted by each single BS (cooperative pair) is represented by  $f(x)$  ( $g(x, y)$ ), where  $x$  ( $x, y$ ) corresponds to its position (see Chapter 3). If we denote by  $\mathcal{I}^{(1)}$  and  $\mathcal{I}^{(2)}$ , the interference field generated by the elements of  $\Phi^{(1)}$  and  $\Phi^{(2)}$ , then,

$$\begin{aligned}\mathcal{I}^{(1)} &= \sum_{x \in \Phi^{(1)}} f(x), \\ \mathcal{I}^{(2)} &= \frac{1}{2} \sum_{x \in \Phi^{(2)}} \sum_{y \in \Phi^{(2)} \setminus \{x\}} g(x, y) \mathbf{1}_{\{x \leftrightarrow y\}},\end{aligned}\tag{4.6}$$

The  $1/2$  in front of the summation prevents us from considering a pair twice. Remark that we can consider here any type of signal (directional or not).

#### 4.6.1 Expected value

The next Theorem gives an exact integral expression to the expected value of the interference field generated by the singles and the pairs, when the BS positions are modeled by a PPP.

**Theorem 6.** *For a PPP  $\Phi$ , the expected value of the interference field generated by  $\Phi^{(1)}$  and  $\Phi^{(2)}$  is given by*

$$\begin{aligned}\mathbb{E}[\mathcal{I}^{(1)}] &= (1 - \delta) \int_{\mathbb{R}^2} \mathbb{E}[f(x)] \lambda dx, \\ \mathbb{E}[\mathcal{I}^{(2)}] &= \frac{1}{2} \int_{\mathbb{R}^2} \int_{\mathbb{R}^2} \mathbb{E}[g(x, y)] e^{-\lambda \pi |x-y|^2 (2-\gamma)} \lambda dy \lambda dx.\end{aligned}\tag{4.7}$$

*Proof.* Let us start with  $\mathcal{I}^{(1)}$ . Since the nearest neighbor is unique,

$$\mathcal{I}^{(1)} = \sum_{x \in \Phi^{(1)}} f(x) = \sum_{x \in \Phi} f(x) \mathbf{1}_{\{x \in \Phi^{(1)}\}} = \sum_{x \in \Phi} f(x) (1 - \mathbf{1}_{\{x \in \Phi^{(2)}\}})$$

After applying the reduced Campbell-Little-Mecke formula and Slivnyak-Mecke's Theorem

$$\begin{aligned} \mathbb{E} [\mathcal{I}^{(1)}] &= \mathbb{E} \left[ \sum_{x \in \Phi} f(x) (1 - \mathbf{1}_{\{x \in \Phi^{(2)}\}}) \right] \\ &\stackrel{(a)}{=} \int_{\mathbb{R}^2} \mathbb{E} [f(x)] (1 - \mathbb{P}(x \in \Phi^{(2)})) \lambda dx \\ &\stackrel{(b)}{=} (1 - \delta) \int_{\mathbb{R}^2} \mathbb{E} [f(x)] \lambda dx, \end{aligned}$$

where (a) follows because  $f(x)$  is independent of  $\Phi$  and (b) after Theorem 3.

For  $\mathcal{I}^{(2)}$ , we make the observation that

$$\sum_{x \in \Phi^{(2)}} \sum_{y \in \Phi^{(2)} \setminus \{x\}} g(x, y) \mathbf{1}_{\{x \overset{\Phi}{\leftrightarrow} y\}} = \sum_{x \in \Phi} \sum_{y \in \Phi \setminus \{x\}} g(x, y) \mathbf{1}_{\{x \overset{\Phi}{\leftrightarrow} y\}},$$

and iterating the reduced Campbell-Little-Mecke formula and Slivnyak-Mecke's Theorem,

$$\begin{aligned} \mathbb{E} [\mathcal{I}^{(2)}] &= \mathbb{E} \left[ \sum_{x \in \Phi} \sum_{y \in \Phi \setminus \{x\}} g(x, y) \mathbf{1}_{\{x \overset{\Phi}{\leftrightarrow} y\}} \right] \\ &= \int_{\mathbb{R}^2} \int_{\mathbb{R}^2} \mathbb{E} [g(x, y) \mathbf{1}_{\{x \overset{\Phi}{\leftrightarrow} y\}}] \lambda dy \lambda dx \\ &\stackrel{(a)}{=} \int_{\mathbb{R}^2} \int_{\mathbb{R}^2} \mathbb{E} [g(x, y)] \mathbb{P} \left( x \overset{\Phi}{\leftrightarrow} y \right) \lambda dy \lambda dx \\ &\stackrel{(b)}{=} \int_{\mathbb{R}^2} \int_{\mathbb{R}^2} \mathbb{E} [g(x, y)] e^{-\lambda \pi \|x-y\|^2 (2-\gamma)} \lambda dy \lambda dx, \end{aligned}$$

where (a) follows because  $g(x, y)$  is independent of  $\Phi$  and (b) after Lemma 1.  $\square$

The expected value can be finite or infinite, depending on the choice of  $f(x)$  and  $g(x, y)$ . Observe that for [NSC] and [PH] the expected interference has the same value.

**Corollary 2.** *For a PPP  $\Phi$ , let  $M^{(1)}$  and  $M^{(2)}$  be the intensity measures of  $\Phi^{(1)}$  and  $\Phi^{(2)}$ . Then,*

$$M^{(1)}(dx) = (1 - \delta) \lambda dx, \quad M^{(2)}(dx) = \delta \lambda dx.$$

*Proof.* Let  $A$  be a regular subset of  $\mathbb{R}^2$ . For the choice  $f(x) = \mathbf{1}_A^x$  (and  $g(x, y) = \mathbf{1}_A^x \mathbf{1}_A^y$ ), the random variable  $\mathcal{I}^{(1)}$  (and  $\mathcal{I}^{(2)}$ ) counts the number of singles (pairs) within  $A$ . Applying directly the preceding Theorem, and remarking that  $\int_{\mathbb{R}^2} e^{-\lambda \pi \|x-y\|^2 (2-\gamma)} \lambda dy = \delta$ , for every  $x \in \mathbb{R}^2$ , we have the desired result.  $\square$

The previous Corollary confirms that, in the PPP case,  $(1 - \delta) \lambda$  and  $\delta \lambda$  are the intensities of  $\Phi^{(1)}$  and  $\Phi^{(2)}$ , as stated in Section 4.1.

### 4.6.2 Laplace functional

In this Section, we present our findings related to the LT of the interference from  $\Phi^{(1)}$  and  $\Phi^{(2)}$ , when  $\Phi$  is a PPP. Fix a measurable set  $A \subset \mathbb{R}^2$  (window). Recall that  $\Phi(A)$  denotes all the atoms of  $\Phi$  inside  $A$ . We define the point processes

$$\Phi_A^{(1)} := \left\{ \text{single atoms of } \Phi(A) \right\}, \quad \Phi_A^{(2)} := \left\{ \text{atoms of } \Phi(A) \text{ in } MNNR \right\} \quad (4.8)$$

where the MNNR have been considered only among the  $\Phi$  atoms inside  $A$ . Consider a sequence of finite windows  $(A_n)_{n=1}^\infty$  increasing to  $\mathbb{R}^2$  in an appropriate sense (for example,  $A_n = B_E^{(2)}(0, n)$ ). Denote by  $\stackrel{(d)}{=}$  equality in distribution, we have the following result.

**Theorem 7.** *Given a PPP  $\Phi$ , then, for  $i = 1, 2$ ,*

$$\lim_{n \rightarrow \infty} \Phi_{A_n}^{(i)} \stackrel{(d)}{=} \Phi^{(i)}.$$

*Proof.* For a natural number  $n$ , denote  $B_n := B_E^{(2)}(0, n)$  and fix  $\Phi_n := \Phi_{B_n}^{(1)}$ , as done in equation (4.8). We will prove that, for every compact subset  $E$  of  $\mathbb{R}^2$ ,

$$\begin{aligned} (i) \quad & \lim_{n \rightarrow \infty} \mathbb{P}(\Phi_n(E) = 0) = \mathbb{P}(\Phi^{(1)}(E) = 0), \\ (ii) \quad & \limsup_{n \rightarrow \infty} \mathbb{P}(\Phi_n(E) \leq 1) \geq \mathbb{P}(\Phi^{(1)}(E) \leq 1), \\ (iii) \quad & \lim_{t \nearrow \infty} \limsup_{n \rightarrow \infty} \mathbb{P}(\Phi_n(E) > t) = 0. \end{aligned}$$

The previous being equivalent to convergence in distribution of the sequence of point processes  $(\Phi_n)$  to  $\Phi^{(1)}$  [Kal84]. Fix a compact  $E \subset \mathbb{R}^2$ . Let us start to prove (i). Being  $\Phi_n$  a thinning of the PPP  $\Phi$ ,

$$\begin{aligned} \mathbb{P}(\Phi_n(E) = 0) &= e^{-\lambda S^{(2)}(E)} + \mathbb{P}(\Phi_n(E) = 0, \Phi(E) > 0) \\ &= e^{-\lambda S^{(2)}(E)} + \mathbb{P}(\Phi_n(E) = 0, \Phi^{(1)}(E) = 0, \Phi(E) > 0) \\ &\quad + \mathbb{P}(\Phi_n(E) = 0, \Phi^{(1)}(E) > 0, \Phi(E) > 0) \end{aligned}$$

Given that the compact subset  $E$  is fixed, take a natural number  $n_1$  such that  $n_1 > 3 \sup_{y \in E} \|y\|$ , and such that  $E \subset B_n$ , for every  $n > n_1$ . Therefore, for every atom belonging to  $\Phi^{(1)}$ , but not to  $\Phi_n$ , the distance to its nearest neighbor must exceed  $\frac{2}{3} \sup_{y \in E} \|y\|$ . Thus, there exists a constant  $C_1 > 0$  such that, for every  $n > n_1$ ,

$$\mathbb{P}(\Phi_n(E) = 0, \Phi^{(1)}(E) > 0, \Phi(E) > 0) \leq e^{-\lambda \pi C_1 n^2}$$

In the same fashion,

$$\begin{aligned} \mathbb{P}(\Phi^{(1)}(E) = 0) &= e^{-\lambda S^{(2)}(E)} + \mathbb{P}(\Phi_n(E) = 0, \Phi^{(1)}(E) = 0, \Phi(E) > 0) \\ &\quad + \mathbb{P}(\Phi^{(1)}(E) = 0, \Phi_n(E) > 0, \Phi(E) > 0) \end{aligned}$$

and there must exists a natural number  $n_2$ , and a constant  $C_2 > 0$  such that, for every  $n > n_2$ ,

$$\mathbb{P}(\Phi^{(1)}(E) = 0, \Phi_n(E) > 0, \Phi(E) > 0) \leq e^{-\lambda\pi C_2 n^2}$$

Take  $N = \max\{n_1, n_2\}$ , then, for every  $n > N$ ,

$$|\mathbb{P}(\Phi_n(E) = 0) - \mathbb{P}(\Phi^{(1)}(E) = 0)| \leq e^{-\lambda\pi C_1 n^2} + e^{-\lambda\pi C_2 n^2}$$

We conclude that

$$\lim_{n \rightarrow \infty} \mathbb{P}(\Phi_n(E) = 0) = \mathbb{P}(\Phi^{(1)}(E) = 0)$$

To prove (ii), remark that

$$\begin{aligned} \mathbb{P}(\Phi_n(E) = 1) &= \mathbb{P}(\Phi_n(E) = 1, \Phi^{(1)}(E) \neq 1) + \mathbb{P}(\Phi_n(E) = 1, \Phi^{(1)}(E) = 1) \\ \mathbb{P}(\Phi^{(1)}(E) = 1) &= \mathbb{P}(\Phi^{(1)}(E) = 1, \Phi_n(E) \neq 1) + \mathbb{P}(\Phi^{(1)}(E) = 1, \Phi_n(E) = 1) \end{aligned}$$

hence

$$\begin{aligned} |\mathbb{P}(\Phi_n(E) = 1) - \mathbb{P}(\Phi^{(1)}(E) = 1)| \\ \leq |\mathbb{P}(\Phi_n(E) = 1, \Phi^{(1)}(E) \neq 1) - \mathbb{P}(\Phi^{(1)}(E) = 1, \Phi_n(E) \neq 1)| \end{aligned}$$

In the same way as we did before, we can prove that

$$\lim_{n \rightarrow \infty} |\mathbb{P}(\Phi_n(E) = 1, \Phi^{(1)}(E) \neq 1) - \mathbb{P}(\Phi^{(1)}(E) = 1, \Phi_n(E) \neq 1)| = 0,$$

which leads to

$$\lim_{n \rightarrow \infty} \mathbb{P}(\Phi_n(E) = 1) = \mathbb{P}(\Phi^{(1)}(E) = 1)$$

Finally, we prove (iii). Being  $\Phi_n$  a thinning of the PPP  $\Phi$ ,

$$\mathbb{P}(\Phi_n(E) > t) \leq \mathbb{P}(\Phi(E) > t) \leq \frac{\mathbb{E}\Phi(E)}{t} = \frac{\lambda\mathcal{S}^{(2)}(E)}{t}$$

which goes to zero, as  $t \nearrow \infty$ .

Take a sequence  $(A_n)$  of compact sets. To conclude that  $(\Phi_{A_n}^{(1)})$  converges in distribution to  $\Phi^{(1)}$ , then it must fulfil that, for every natural number  $m$ , there exists another natural number  $N$  such that, for every  $n > N$ , then,  $B_m \subset A_n$ . We can prove that  $(\Phi_{A_n}^{(2)})$  converges in distribution to  $\Phi^{(2)}$ .  $\square$

As convergence in distribution is equivalent to convergence of the LT [Kal84], the previous Theorem states that the LT of  $\Phi_A^{(i)}$  approximates that one of  $\Phi^{(i)}$ , for  $A$  large enough. The benefit of this approach is that, for every finite window  $A$ , we can actually obtain an analytic representation for the LT of  $\Phi_A^{(i)}$ . As a sketch of the proof, fix a finite subset  $A$ . Conditioned on the number of atoms, these are i.i.d. uniformly distributed within  $A$ . Thus, using the law of total probability, we can express the LT as an infinite sum of terms. The

probability of a PPP having a fixed number of atoms within  $A$  is known. We only have left to find expressions for the LT conditioned on the number of points inside  $A$ . For a finite number of different planar points  $x_1, \dots, x_n \in A$ , define  $H^{i,n}(x_1, \dots, x_n)$  as the indicator function of  $x_i$  being in pair with another atom within the configuration  $\{x_1, \dots, x_n\}$  (Definition 3). In the same fashion, define  $I^{i,n}(x_1, \dots, x_n)$  as the indicator function of  $x_i$  being single with respect to  $\{x_1, \dots, x_n\}$  (Definition 6). Let

$$\begin{aligned} H^{(n)}(x_1, \dots, x_n) &:= (H^{(1,n)}(x_1, \dots, x_n), \dots, H^{(n,n)}(x_1, \dots, x_n)), \\ I^{(n)}(x_1, \dots, x_n) &:= (I^{(1,n)}(x_1, \dots, x_n), \dots, I^{(n,n)}(x_1, \dots, x_n)). \end{aligned}$$

We have the following result.

**Theorem 8** (Laplace transform). *Consider a PPP  $\Phi$ , with intensity  $\lambda$ , a regular subset  $A \subset \mathbb{R}^2$ , and a measurable function  $f : \mathbb{R}^2 \rightarrow \mathbb{R}^+$ . Let  $F^{(n)}(x_1, \dots, x_n) := (f(x_1), \dots, f(x_n))$ . The LT of  $\Phi_A^{(1)}$ , evaluated at  $f(x)$ , is equal to*

$$\begin{aligned} \mathbb{E} \left( e^{-\sum_{x \in \Phi_A^{(1)}} f(x)} \right) &= e^{-\lambda \mathcal{S}^{(2)}(A)} \left( 1 + \lambda \int_A e^{-f(x)} dx + \frac{(\lambda \mathcal{S}^{(2)}(A))^2}{2} \right. \\ &\quad \left. + \sum_{n=3}^{\infty} \frac{\lambda^n}{n!} \int_A \dots \int_A e^{-F^{(n)}(x_1, \dots, x_n) \cdot H^{(n)}(x_1, \dots, x_n)} dx_1 \dots dx_n \right) \end{aligned} \quad (4.9)$$

The LT of  $\Phi_A^{(2)}$ , evaluated at  $f(x)$ , is equal to

$$\begin{aligned} \mathbb{E} \left( e^{-\sum_{x \in \Phi_A^{(2)}} f(x)} \right) &= e^{-\lambda \mathcal{S}^{(2)}(A)} \left( 1 + \lambda \mathcal{S}^{(2)}(A) + \frac{\lambda^2}{2} \int_A \int_A e^{-(f(x)+f(y))} dy dx \right. \\ &\quad \left. + \sum_{n=3}^{\infty} \frac{\lambda^n}{n!} \int_A \dots \int_A e^{-F^{(n)}(x_1, \dots, x_n) \cdot I^{(n)}(x_1, \dots, x_n)} dx_1 \dots dx_n \right) \end{aligned} \quad (4.10)$$

*Implementation:* For every natural number  $n$ , it is easy to write a program/algorithm with input  $(x_1, \dots, x_n)$  and output  $H^{(n)}(x_1, \dots, x_n)$  (or  $I^{(n)}(x_1, \dots, x_n)$ ):

1. Define a  $n \times n$  matrix  $D = (d_{i,j})$ , such that  $d_{i,j} = \|x_i - x_j\|$ .
2. Choose a  $n \times 1$  vector  $v$ , such that, for each  $i = 1, \dots, n$ ,  $v(i) = \operatorname{argmin}_{j \in \{1, \dots, n\} \setminus \{i\}} d_{i,j}$ .
3. Define another  $n \times 1$  vector  $u$ , such that, for each  $i = 1, \dots, n$ 
  - **If**  $i = v(v(i))$  (that is,  $x_i$  and  $x_{v(i)}$  are in MNMR), then  $u(i) = 1$ .
  - **Else**  $u(i) = 0$ .

4. **Return**  $u$ .

Fixed  $f(x)$ ,  $F^{(n)}(x_1, \dots, x_n)$  is also known. Thus, for every natural number  $n$ , it is easy to set up a program that numerically approaches

$$\begin{aligned} &\int_A \dots \int_A e^{-F^{(n)}(x_1, \dots, x_n) \cdot H^{(n)}(x_1, \dots, x_n)} dx_1 \dots dx_n, \text{ and} \\ &\int_A \dots \int_A e^{-F^{(n)}(x_1, \dots, x_n) \cdot I^{(n)}(x_1, \dots, x_n)} dx_1 \dots dx_n. \end{aligned}$$

As  $n$  grows, computational time for  $H^{(n)}(x_1, \dots, x_n)$  and  $I^{(n)}(x_1, \dots, x_n)$  grows as well. Further,  $n$ -nested integrals of these functions need to be computed, complicating the problem even more.

## 4.7 Numerical Evaluation

As a final discussion for this Chapter, we present the numerical evaluation of the expressions in Theorem 6 and Theorem 8.

### 4.7.1 Expected value of the Interference field

We first illustrate the validity of the expressions in equation (4.7), and we compare them with simulations. We consider a density for the BSs  $\lambda = 0.25 [km^{-2}]$ , which corresponds to an average closest distance of  $(2\sqrt{\lambda})^{-1} = 1 [km]$  between stations. We also consider that the power is  $p = 1 [Watt]$ .

Given a fixed  $\beta > 2$ , define the random field  $f(x) = \frac{h_{\|x\|}}{\|x\|^\beta} \mathbf{1}_{\{\|x\| > R\}}$ , where  $R$  is a positive number and the family  $(h_r)_{r>0}$  is defined in Chapter 3. The indicator function serves to calculate the interference generated by the singles, outside a ball centred at 0 and radius  $R$ . With the aid of  $f(x)$ , define  $\mathcal{I}^{(1)}$  as in equation (4.6). Using Theorem 6, the numerical evaluation of the expected value of  $\mathcal{I}^{(1)}$  is given in figure 4.4. The expression in (4.7) gives almost identical results with the simulations.

Similarly, with the aid of the random field  $g(x, y) \mathbf{1}_{\{\|x\|, \|y\| > R\}}$ , define  $\mathcal{I}^{(2)}$  as in equation (4.6). For the numerical evaluation, we consider the two cases [NSC] and [MAX]. The interference from [MAX] is always smaller than that one from [NSC], since it is received only from one of the two BSs of each pair, while the other is silent. Figure 4.4 shows that the numerical evaluation of the expression in (4.7) gives almost identical results with the simulations. Remark also that, for  $\beta = 4$ , the two scenarios do not numerically defer much.

### 4.7.2 Laplace transform approximation

The accuracy of the LT approximation, for the processes of singles and pairs, depends on (i) how large the finite window  $A$  is and (ii) the convergence of the series from Theorem 8.

We do not have an exact formula for the LT of  $\Phi^{(1)}$  and  $\Phi^{(2)}$ , and, unfortunately, it is not possible to obtain a rate of convergence, with respect to the finite window  $A$ , from the Theorem 7. Since the original process  $\Phi$  is a PPP, we know an exact analytic formula for its LT, for which it is easy to obtain a convergence rate, with respect to  $A$ . Thus, it is advisable to use the same rate to approximate the LT of  $\Phi^{(1)}$  and  $\Phi^{(2)}$ . Up to this point, it is the only obvious method.

Consider a density  $\lambda = 1$  for  $\Phi$ , and the function  $f(x) = \frac{1}{\|x\|^\beta} \mathbf{1}_{\{\|x\| > 1\}}$  (for  $\beta = 2.5$  and  $\beta = 4$ ). For these choices, a finite window  $A$  with Euclidean surface  $S^{(2)}(A) = 400$  is enough to guarantee an accurate approximation for the LT of  $\Phi$ . Once fixed  $A$ , we need to study

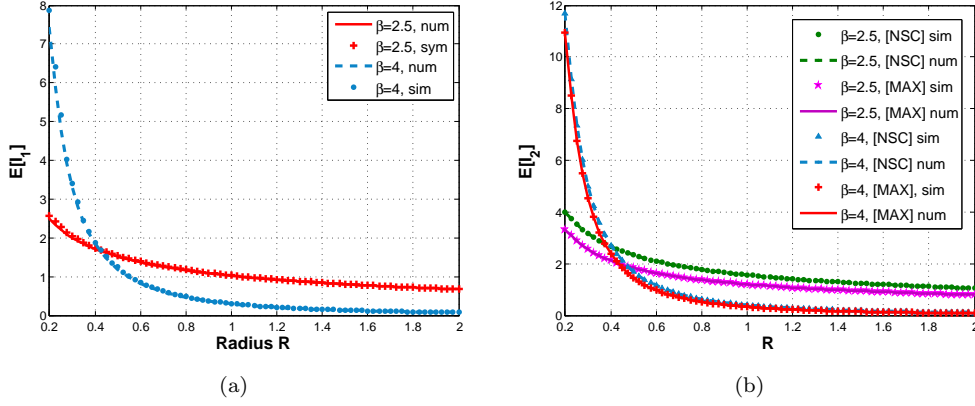


Figure 4.4: (a) Expected value of the interference generated by the single atoms, outside a radius  $R$ , (b) and by the cooperative pairs, outside a radius  $R$ .

the convergence of the series from Theorem 7. Figure 4.5 shows, for the two different values of  $\beta$ , (i) the plots of the LT of  $\sum_{x \in \Phi_A^{(1)}} f(x)$  and  $\sum_{x \in \Phi_A^{(2)}} f(x)$  obtained by simulations, (ii) against the plots of the partial sums of the first  $N$  terms of the series from equation (4.9) and equation (4.10). The Poisson distribution, with parameter  $\lambda S^{(2)}(A) = 400$ , has expected value 400 and standard deviation 20. Actually, the corresponding PDF concentrates in  $\{315, \dots, 485\}$ . This explains why the series approximation is almost constant for  $N < 315$ , and gets close to the values obtained via simulations for  $N > 485$ . This is not numerically tractable, since we need to compute  $K$ -nested integrals, for  $K = 1, \dots, N$ . Let us disregard the fact that we are dealing with a convergence with respect to the finite window  $A$ . Choosing a much smaller  $A$  improves the convergence of the series. However, we are trying to model large cellular networks, then, a small window is out of the scope of this work.

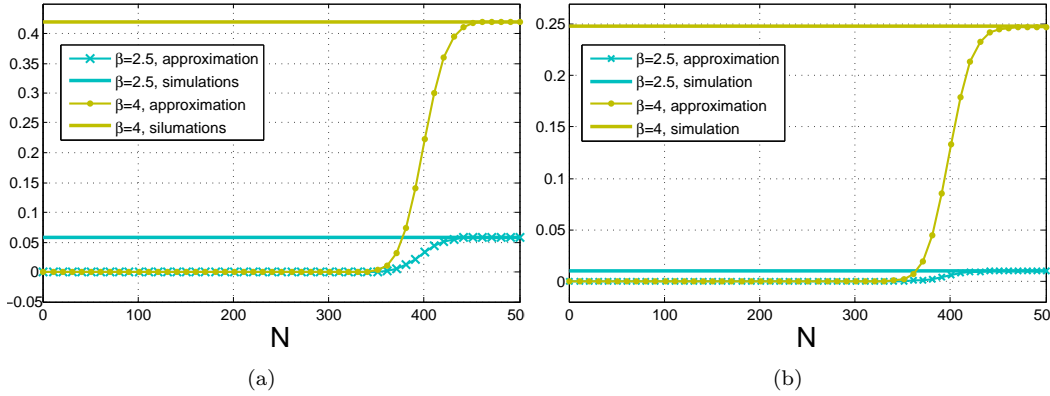


Figure 4.5: The LT for the (a) process of singles and (b) the process of cooperative pairs.

## 4.8 Conclusions

We proposed a clustering methodology to pair BSs in MNRR, and the rest of the atoms remain single. The two point process resulting from this strongly dependent thinning were analysed with the use of stochastic geometry. Relevant properties of these processes were derived, mainly when the point process modeling the BS locations is a PPP: Percentage of atoms, Palm measure, Voronoi cell, repulsion/attraction, first moment, Laplace transform. Due to the nature of the thinning defining the singles and pairs, some of these results lack of tractability. Nevertheless, all of them are useful to the understanding and analysis of a cooperative network based on node proximity. Moreover, they should be contemplated to the performance evaluation of such cooperative networks. Further analysis and applications in this direction should be done.





# Coverage Analysis

This Chapter has been published within the following two articles, the first one presented at IEEE Globecom 2016, at Washington, D.C., USA:

- *Coverage Gains from the Static Cooperation of Mutually Nearest Neighbors*,
- *Analysis of Static Cellular Cooperation between Mutually Nearest Neighbors Nodes*, submitted Journal paper, arXiv:1611.02614v1.

## Abstract

When the BS positions are modeled by a PPP, the non-Poissonian behaviour of the processes of singles and pairs makes difficult a much more detailed study of both processes. Among others, this complicates a complete performance analysis of SINR related metrics, for a cooperative network considering mutually nearest neighbors and single BSs. For instance, the expressions presented in the previous Chapter for the LT are not numerically tractable. Thus, one cannot derive expressions for the coverage probability by classical LT methods, as shown in [ABG11]. It has not been possible either to find expressions for the moment measures of order larger than one for both processes. Hence, an analysis of the coverage probability similar to the approach proposed by the authors in [BK15] is impossible. Nevertheless, the analysis from the previous Chapter allows the construction an alternative model, equipped with the basic structure of the singles and cooperative pairs. The goal of this Chapter is to use this new model to approximate the coverage probability of a cooperative network considering mutually nearest neighbors and single BSs.

## 5.1 Poisson Superposition Model

Given a density for the BS positions,  $\lambda > 0$ , to imitate the processes of singles and pairs,  $\Phi^{(1)}$  and  $\Phi^{(2)}$ , we consider two independent point processes  $\hat{\Phi}^{(1)}$  and  $\hat{\Phi}^{(2)}$ . Eventhough the original processes of singles and pairs are far from being independent, this assumption obviously facilitates the analysis.

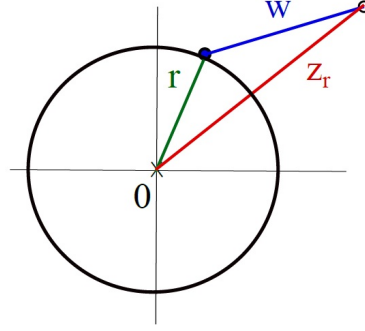


Figure 5.1: Two cooperating BSs, where  $r$  and  $Z_r$  are their distances from the origin, and  $W$  is the distance between them.

We suppose that process  $\hat{\Phi}^{(1)}$  is a PPP, with parameter  $(1 - \delta)\lambda$ . In this way, the new process of singles and  $\Phi^{(1)}$  share the first moment (Corollary 2).

We suppose that the process  $\hat{\Phi}^{(2)}$  is an independently marked PPP, with intensity  $\frac{\delta}{2}\lambda$ . The atoms of this process are called *the parents*, and its respective mark are called *the daughters*. The idea is that each couple (*parent*, *daughter*) imitates a cooperative pair in MNNR. Consider a family of positive r.v.s  $(Z_r)_{r>0}$ , such that each  $Z_r$  follows a Rice distribution, with parameter  $(r, \alpha)$ , where  $\alpha := (2\lambda\pi(2 - \gamma))^{-1/2}$ . Hence, the mark of a parent whose Euclidean distance to the typical user is  $r > 0$ , is distributed as  $Z_r$ .

To understand the choice for the marks distribution, suppose that a BS is placed at the polar coordinates  $(r, \theta)$ , with  $r > 0$  and  $\theta \in [0, 2\pi)$  fixed (see Figure 5.1). Assume also that this BS belongs to a cooperating pair from the Nearest Neighbor model, and let us denote by  $W$  the distance between the stations in pair. Theorem 5 states that  $W$  is Rayleigh distributed, with scale parameter  $\alpha$ . Denote by  $Z$  the distance from the typical user to the second BS. The isotropy of the PPP implies that the distribution of  $Z$  is independent of  $\theta$ . Furthermore, the way the r.v.  $Z$  is defined is actually the classical way a Rician r.v. is constructed [ADC16].

**Proposition 4.** *The r.v.  $Z$  is Rice distributed, with parameters  $(r, \alpha)$ . The probability density function (PDF) of  $Z$  is given by*

$$f(z|r) = \frac{z}{\alpha^2} e^{-\frac{z^2 + r^2}{2\alpha^2}} I_0\left(\frac{zr}{\alpha^2}\right), \quad (5.1)$$

where  $I_0(x)$  is the modified Bessel function, of the first kind, with order zero [Leb65].

## 5.2 The Distribution of The Closest Distances

Let  $R_1$  and  $R_2$  denote the r.v.s of the distances from the closest element of  $\hat{\Phi}^{(1)}$  and  $\hat{\Phi}^{(2)}$  to the origin, respectively. Denote also by  $Z_2$  the mark of the parent at  $R_2$ . It is known

that the r.v.s  $R_1$  and  $R_2$  are Rayleigh distributed [ABG11], with scale parameters  $\xi$  and  $\zeta$ , where  $\xi := ((1-\delta)2\lambda\pi)^{-1/2}$  and  $\zeta := (\delta\lambda\pi)^{-1/2}$ . By definition,  $R_2$  and  $Z_2$  are not mutually independent, but we can derive their joint PDF.

**Lemma 2.** *The joint PDF of the r.v.  $(R_2, Z_2)$  is given by*

$$f(r, z) = \frac{rz}{(\alpha\zeta)^2} e^{-\frac{r^2}{2}\left(\frac{1}{\alpha^2} + \frac{1}{\zeta^2}\right) - \frac{z^2}{2\zeta^2}} I_0\left(\frac{rz}{\zeta^2}\right). \quad (5.2)$$

Furthermore, the r.v.  $Z_2$  is Rayleigh distributed, with scale parameter  $(\alpha^2 + \zeta^2)^{-1/2}$ .

*Proof.* See subsection 5.7.2. □

To make a complete analysis of the coverage probability, we make use of the distribution of the random vector  $(R_1, R_2, Z_2)$ . Because  $R_1$  is independent of  $(R_2, Z_2)$ , the joint PDF is the product of the PDF of  $R_1$  with the joint PDF of  $(R_2, Z_2)$ .

### 5.3 Interference Field

In this subsection we present some expressions of objects related to the interference field of the processes  $\hat{\Phi}^{(1)}$  and  $\hat{\Phi}^{(2)}$ , that will be useful for the coverage analysis. From the way the marks of  $\hat{\Phi}^{(2)}$  were defined, it is clear that we will deal only with omnidirectional BSs, for which the emitted signal, received at the typical user, depends only on the distance of the BSs to the typical user (see Chapter 3).

For  $M \in \mathcal{M}^{m \times m}(\mathbb{R}^2)$ , and  $r > 0$ , denote

$$\mathcal{L}_{\tilde{f}}(M; r) := \mathbb{E} \left[ e^{M\tilde{f}(r)} \right], \quad (5.3)$$

where  $e^{M\tilde{f}(r)}$  denotes the exponential of the matrix  $M\tilde{f}(r)$  [Arn92]. And, for  $\rho > 0$ , denote

$$\mathcal{L}_{\tilde{g}}(M; r, \rho) := \mathbb{E} \left[ e^{M\tilde{g}(r, Z_r)} \mathbf{1}_{\{Z_r > \rho\}} \right] \quad (5.4)$$

where  $e^{M\tilde{g}(r, Z_r)}$  denotes the exponential of the matrix  $M\tilde{f}(r)$  [Arn92]. When  $\rho = 0$ ,  $\mathcal{L}_g(s; r, 0)$  will be denoted just by  $\mathcal{L}_g(s; r)$ . The tractability of the expressions from equations the preceding expressions depends, of course, on the distribution of the random matrix  $e^{M\tilde{f}(r)}$  and  $e^{M\tilde{g}(r, Z_r)} \mathbf{1}_{\{Z_r > \rho\}}$ . As an example, consider that  $M = -s$ , where  $s$  is a positive real number. Taking  $\tilde{f}(r)$  as in equation (3.1), then

$$\mathcal{L}_{\tilde{f}}(-s; r) = \frac{r^\beta}{sp + r^\beta} \quad (5.5)$$

In Table 3.1 we find expressions for  $\mathbb{E}[e^{-s\tilde{g}(r, z)}]$  in the [NSC], [OFF], and [MAX] cases. By remarking that

$$\mathcal{L}_{\tilde{g}}(-s; r, \rho) = \mathbb{E} \left[ \mathbb{E} \left[ e^{-s\tilde{g}(r, Z_r)} \middle| Z_r \right] \mathbf{1}_{\{Z_r > \rho\}} \right],$$

we get analytical expressions for  $\mathcal{L}_{\tilde{g}}(s; r)$  in the [NSC], [OFF], and [MAX]. For instance, for [NSC] we have that

$$\mathcal{L}_{\tilde{g}}(-s; r, \rho) = \frac{r^\beta}{sp + r^\beta} \int_\rho^\infty \frac{z^\beta}{sp + z^\beta} f(z|r) dr,$$

where  $f(z|r)$  is the density function of the Rice r.v.  $Z_r$  from equation (5.1). The [OFF] and [MAX] cases are completely analogous. The general expression for  $\mathcal{L}_{\tilde{g}}(s; r)$  from equation (3.6) allows to give analytical formulas similar to  $\mathcal{L}_{\tilde{g}}(-s; r, \rho)$ . The [PH] case is more complicated and follows another direction. For the case  $\cos(\theta_r - \theta_z) = 1$ , see [BG15, Lem. 3].

Consider the interference fields generated by all the elements of  $\hat{\Phi}^{(1)}$  and  $\hat{\Phi}^{(2)}$ , outside the radii  $\rho_1 \geq 0$  and  $\rho_2 \geq 0$ , respectively,

$$\begin{aligned} \hat{\mathcal{I}}^{(1)}(\rho_1) &:= \sum_{x \in \hat{\Phi}^{(1)}, \|x\| > \rho_1} \tilde{f}(\|x\|), \\ \hat{\mathcal{I}}^{(2)}(\rho_2) &:= \sum_{\substack{y \in \hat{\Phi}^{(2)} \\ \|y\| > \rho_2, Z_{\|y\|} > \rho_2}} \tilde{g}(\|y\|, Z_{\|y\|}). \end{aligned} \quad (5.6)$$

The total interference generated outside different radii for the two processes,

$$\hat{\mathcal{I}}(\rho_1, \rho_2) := \hat{\mathcal{I}}^{(1)}(\rho_1) + \hat{\mathcal{I}}^{(2)}(\rho_2). \quad (5.7)$$

When  $\rho_1 = \rho_2 = 0$ , they are just denoted by  $\hat{\mathcal{I}}^{(1)}$ ,  $\hat{\mathcal{I}}^{(2)}$ , and  $\hat{\mathcal{I}}$ , respectively.

The following gives analytical representations to the LT of the PPP Interference fields [BB09].

**Lemma 3.** *Given  $M \in \mathcal{M}^{m \times m}(\mathbb{R}^d)$ , for  $\rho_1 > 0$ , and  $\rho_2 > 0$ , denote by*

$$\begin{aligned} \mathcal{L}_{\hat{\mathcal{I}}^{(1)}}(M; \rho_1) &:= \mathbb{E} \left[ e^{M\mathcal{I}^{(1)}(\rho_1)} \right] \\ \mathcal{L}_{\hat{\mathcal{I}}^{(2)}}(M; \rho_2) &:= \mathbb{E} \left[ e^{M\mathcal{I}^{(2)}(\rho_2)} \right]. \end{aligned} \quad (5.8)$$

*Then*

$$\begin{aligned} \mathcal{L}_{\hat{\mathcal{I}}^{(1)}}(M; \rho_1) &= e^{-\lambda 2\pi(1-\delta) \int_{\rho_1}^\infty (1 - \mathcal{L}_f(M; r)) r dr}, \\ \mathcal{L}_{\hat{\mathcal{I}}^{(2)}}(M; \rho_2) &= e^{-\pi \lambda \delta \int_{\rho_2}^\infty (1 - \mathcal{L}_g(M; r, \rho_2)) r dr}, \end{aligned} \quad (5.9)$$

The Lemma uses the Poisson properties of  $\hat{\Phi}^{(1)}$  and  $\hat{\Phi}^{(2)}$ . The expressions given in equations (5.9) are the tools which allow us to make an entire analysis of the coverage probability.

As an example, if we replace equation (5.5) in equation (5.9), for  $s > 0$  and  $\rho = 0$  we get the analytical representation  $\mathcal{L}_{\hat{\mathcal{I}}^{(1)}}(-s) = e^{-\frac{\lambda(1-\delta)2\pi^2(sp)^{2/\beta}}{\beta} \text{csc}(\frac{2\pi}{\beta})}$  [ABG11], where  $\text{csc}(z)$  is the cosecant function. In the same fashion, it is possible to obtain expressions for  $\mathcal{L}_{\hat{\mathcal{I}}^{(1)}}(s; \rho)$  and  $\mathcal{L}_{\hat{\mathcal{I}}^{(2)}}(s; \rho)$ .

## 5.4 Coverage Probability

We can now make use of the PPP superposition model to evaluate the performance of the different cooperation (or coordination) types proposed above. The beneficial signal, received at the typical user from a single BS or a pair, will be denoted by  $\tilde{f}(r)$  and  $\tilde{g}(r, z)$ , respectively. These may not be the same functions modeling the interference the typical user receives from other BSs. This is explained by the fact that the interference is the sum of the signals other BSs generate for their own serving users who are not located at the Cartesian origin.

We consider two scenarios of user-to-BS association.

### 5.4.1 Fixed Single Transmitter

Let us suppose that there is one BS serving the typical user, whose distance to the origin is fixed and known  $r_0 > 0$ . Moreover, it serves the typical user independently of the atoms from  $\hat{\Phi}^{(1)}$  and  $\hat{\Phi}^{(2)}$ . Then the signal emitted to the typical user is  $\tilde{f}(r_0)$ , and the Signal-to-Interference-plus-Noise-Ratio (SINR) at the typical user is defined by  $\text{SINR} := \frac{\tilde{f}(r_0)}{\sigma^2 + \hat{\mathcal{I}}}$ , where  $\sigma^2$  is the additive Gaussian noise power at the receiver and  $\hat{\mathcal{I}}$  is the total interference power (see equation (5.7)).

**Proposition 5.** *Suppose  $\tilde{f}(r_0)$  as in (3.1). Then, the success probability is given by the expression*

$$\mathbb{P}(\text{SINR} > T) = e^{-\frac{T\sigma^2 r_0^\beta}{p}} \mathcal{L}_{\hat{\mathcal{I}}^{(1)}}\left(\frac{Tr_0^\beta}{p}\right) \mathcal{L}_{\hat{\mathcal{I}}^{(2)}}\left(\frac{Tr_0^\beta}{p}\right). \quad (5.10)$$

The last proposition allows us to evaluate the coverage probability directly with the help of equation (5.9) for  $\rho = 0$ .

### 5.4.2 Closest Transmitter cluster

We consider that the typical user is connected to the BS at  $R_1$  or to the cooperating cluster (parent, daughter) at  $(R_2, Z_2)$ , from subsection 5.2. The previous association depends on which one of them is closer to the typical user. If  $R_1 < \min\{R_2, Z_2\}$ , the single BS at  $R_1$  serves the typical user, and it emits the signal  $\tilde{f}(R_1)$ . In the opposite case, if  $R_2 \leq R_1$  or if  $Z_2 \leq R_1$ , the cooperating pair at  $(R_2, Z_2)$  serves the user, and it emits the signal  $\tilde{g}(R_2, Z_2)$ . All the BSs not serving the typical user generate interference. Thus,

$$\text{SINR} := \begin{cases} \frac{\tilde{f}(R_1)}{\sigma^2 + \hat{\mathcal{I}}(R_1, R_1)} & ; R_1 < \min\{R_2, Z_2\}, \\ \frac{\tilde{g}(R_2, Z_2)}{\sigma^2 + \hat{\mathcal{I}}(R_2, R_2)} & ; R_2 < \min\{R_1, Z_2\}, \\ \frac{\tilde{g}(R_2, Z_2)}{\sigma^2 + \hat{\mathcal{I}}(Z_2, R_2)} & ; Z_2 < \min\{R_1, R_2\}. \end{cases} \quad (5.11)$$

From equation (5.6), recall that once a *parent* generates interference, its respective *daughter* does it along with it. For the first term of the preceding equation,  $\hat{\mathcal{I}}(R_1, R_1)$  considers that

all the singles and *parents* lying outside  $R_1$  generate interference. For the the second term we use a similar argument. For the third one, the argument is a little bit more delicate. The r.v.  $\hat{I}(Z_2, R_2)$  considers that all the singles lie outside the radius  $Z_2$ , and all of them generate interference. Nevertheless, only the *parents* outside  $R_2$  generate interference (the parent associated to  $R_2$  lies outside  $Z_2$ ). Note that, the way this user-to-BS-association is defined, for the three cases, this is the only way to assure that all the BSs not serving the typical user generate interference.

**Proposition 6.** *Suppose  $f(r)$  and  $g(r, z)$  follow equations (3.1) and (3.5). Given a finite threshold  $T > 0$ , there exist explicit functions  $G : [0, \infty) \rightarrow \mathbb{R}^+$  and  $H, K : [0, \infty) \times [0, \infty) \rightarrow \mathbb{R}^+$  such that*

$$\mathbb{P}(\text{SINR} > T) = \mathbb{E}[G(R_1)] + \mathbb{E}[H(R_2, Z_2)] + \mathbb{E}[K(R_2, Z_2)].$$

*Proof.* See subsection 5.7.1. □

Since we know the distribution of the r.v.  $R_1$  and of the random vector  $(R_2, Z_2)$ , the previous Theorem allows to evaluate the required coverage probability. For instance, it is possible to use

$$\begin{aligned} \mathbb{E}[G(R_1)] &= \int_0^\infty G(r) f_{R_1}(r) dr, \\ \mathbb{E}[H(R_2, Z_2)] &= \int_0^\infty \int_0^\infty H(r, z) f_{R_2, Z_2}(r, z) dz dr, \\ \mathbb{E}[K(R_2, Z_2)] &= \int_0^\infty \int_0^\infty K(r, z) f_{R_2, Z_2}(r, z) dz dr, \end{aligned}$$

where  $f_{R_1}(r)$  and  $f_{R_2, Z_2}(r, z)$  are the density functions of  $R_1$  and  $(R_2, Z_2)$  (see equation (5.2)). Or it is possible to use, as well, Monte Carlo simulations

$$\begin{aligned} \mathbb{E}[G(R_1)] &\approx \frac{\sum_{n=1}^N G(R_1^{(n)})}{N}, \\ \mathbb{E}[H(R_2, Z_2)] &\approx \frac{\sum_{n=1}^N H(R_2^{(n)}, Z_2^{(n)})}{N}, \\ \mathbb{E}[K(R_2, Z_2)] &\approx \frac{\sum_{n=1}^N K(R_2^{(n)}, Z_2^{(n)})}{N}, \end{aligned}$$

where  $(R_1^{(n)})_{n=1}^N$  is an independent sequence of r.v., each one distributed as  $R_1$ , and  $(R_2^{(n)}, Z_2^{(n)})_{n=1}^N$  is an independent sequence of radom vectors, each one distributed as  $(R_2, Z_2)$ . To generate independent copies of  $(R_2, Z_2)$ , there exist several methods: Cholesky decomposition or Gibbs sampling, for instance [RC04].

## 5.5 Numerical Evaluation

Finally, this Section is devoted to the numerical evaluation of the formulas, for the different results along the Chapter. We consider a density for the BSs  $\lambda = 0.25 \text{ [km}^{-2}\text{]}$ , which corresponds to an average closest distance of  $(2\sqrt{\lambda})^{-1} = 1 \text{ [km]}$  between stations. We also consider that the power is  $p = 1 \text{ [Watt]}$ .

### 5.5.1 Closeness of the Poisson superposition

The analysis of the current Chapter is meant to approximate the coverage probability of a cooperative network under the MNNR criterion. The corresponding coverage probability is obtained via simulations, and it is compared with the results from Theorem 5 and Theorem 6. The SINR, of a cellular cooperative network under the MNNR criterion, related to the *single transmitter association*, is constructed in the same way as described in Section 5.4. And the corresponding SINR, related to *closest transmission cluster*, is constructed in the following way: The typical user is served by its closest BS, if this BS is in MNNR with another BS, both of them serve the user, and the rest of the BSs generate interference.

In Figure 5.2 we compare the coverage probabilities, over the threshold  $T$ , for the original model from Chapter 4, and the superposition model, in both association cases. For the *single transmitter association*, the curves match perfectly, meaning that the way the superposition models the interference is the right one. For the "*closest*" *transmission cluster*, the difference between the curves is more evident, because on the one hand the superposition model does not take into account the repulsion between clusters (singles or pairs), and on the other hand the association of a cluster to the user as done in (5.11) for the superposition model, sometimes misses the actual closest daughter to the origin, which is not necessarily the one at  $Z_2$ . This never happens the way we choose the closest cluster in the model from Chapter 5. Hence, the approximative model underestimates the coverage benefits in the closest cluster association.

### 5.5.2 Validity of the numerical analysis

In Figure 5.3, we compare the plots of the coverage probability from the numerical integration, against simulations, of the analytic formula for the coverage probability presented in Proposition 5 and Proposition 6. As we can see, they fit perfectly, both for larger values of  $\beta$ , like  $\beta = 4$ , and for critical ones, like  $\beta = 2.5$ .

### 5.5.3 Cooperation gains

Once validated the formulas from Proposition 5 and Proposition 6, we proceed to study the related possible coverage gains, with respect to the classical non-cooperative model [ABG11]. For this task, we consider the different cooperation schemas presented as examples in Chapter 3 for the signal emitted from a cooperative pair.



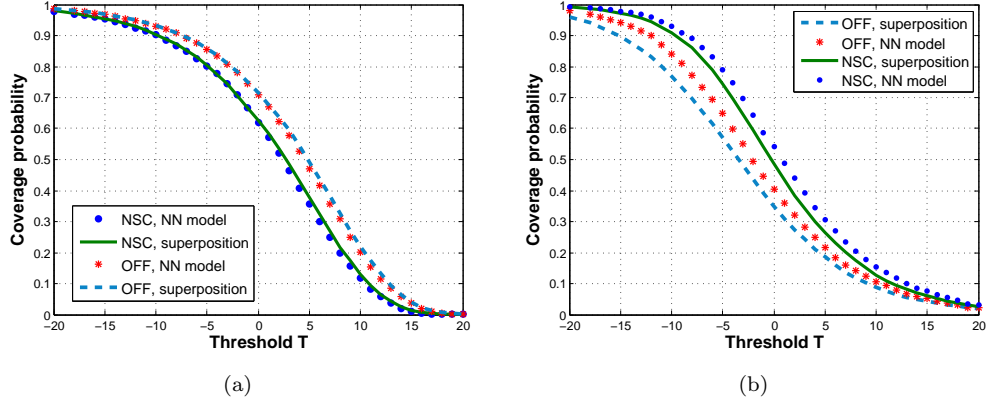


Figure 5.2: Closeness of the approximation between the superposition and the Nearest Neighbor model,  $\beta = 3$ . (a) Fixed transmitter and (b) closest transmitter.

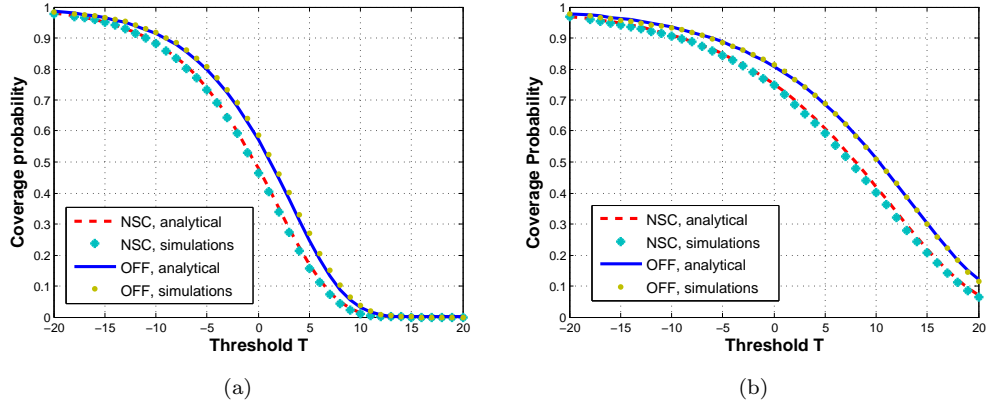


Figure 5.3: Validity of the analysis for the superposition model for the fixed single transmitter. (a)  $\beta = 2.5$  (b)  $\beta = 4$ .

Figure 5.4(a) shows the gains for the fixed transmitter user-to-BS association. Remark that the coverage probabilities corresponding to the [NSC] and to the non-cooperative model are practically the same. The latter is explained since the interference generated in both approaches is practically the same (see equation (5.10)). Notice also that the coverage probability in the [MAX] case is close to the coverage probability in the [NSC] case. This suggests that the strongest signal in each cooperating pair influences interference the most. For the [OFF] case there is a 10% benefit, with respect to the non-cooperative case, in the largest part of the domain in  $T$ .

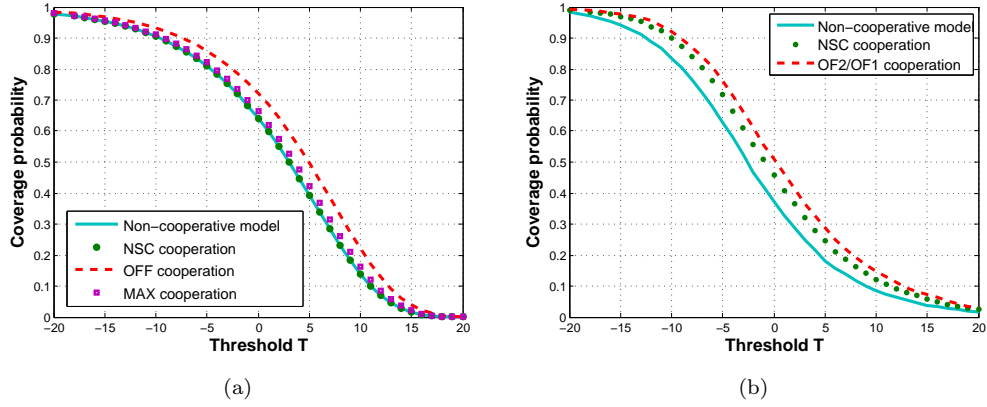


Figure 5.4: Coverage gains for the Poisson superposition compared to no cooperation,  $\beta = 3$ . (a) Fixed transmitter (b) Closest transmitter.

Figure 5.4(a) shows the gains for the closest cluster user-to-BS association. For the SINR, let us call [MAX/OFF] the case where the closest cluster emits a signal to the typical user according to [MAX], i.e. only the max signal is sent, while the pairs generate interference according to [OFF]. The idea is that when all network pairs choose [MAX] cooperation for their own users, this choice of one-station-out-of-two is random for the typical user point of view. This [MAX/OFF] case shows a 15% absolute gain from the non cooperative case, which is around 9% for the [NSC] (see Fig. 5.4(b)). This gain is almost equal with the dynamic clustering in [BG15].

## 5.6 Conclusions

The MNNR is a reasonable methodology to define single BSs and cooperative pairs. In spite of the analytical difficulties, derived from the strongly dependent nature of the criterion, it is possible to provide a complete analysis of SINR-related metrics, via a new model that imitates the structure of the singles and cooperative pairs. The resulting coverage benefits, with respect to the non-cooperative case, can reach a 15% of absolute gain. Similar gains are

achieved by some dynamic clustering methodologies. The gains coming from our model are impressive, considering that only 62% of the BSs cooperate. Different kinds of cooperative signals reported different coverage benefits. Thus, cooperation benefits fundamentally depend on the choice of the grouping method, the allowed maximum cluster size, as well as the appropriate cooperation signals. This work provides an important step towards resolving this complex problem.

## 5.7 Additional material

This final Section is devoted to present the proofs of Proposition 6 and Lemma 2.

### 5.7.1 Proof of Proposition 6

We split the proof in three parts.

#### A first expression

Since the events  $\{R_1 < \min\{R_2, Z_2\}\}$ ,  $\{R_2 < \min\{R_1, Z_2\}\}$ , and  $\{Z_2 < \min\{R_1, R_2\}\}$  are mutually independent, from equation (5.11) we have that

$$\begin{aligned}
\mathbb{P}(\text{SINR} > T) &= \mathbb{P}\left(\frac{\tilde{f}(R_1)}{\sigma^2 + \hat{\mathcal{I}}(R_1, R_1)} > T, R_1 < \min\{R_2, Z_2\}\right) \\
&\quad + \mathbb{P}\left(\frac{\tilde{g}(R_2, Z_2)}{\sigma^2 + \hat{\mathcal{I}}(R_2, R_2)} > T, R_2 < \min\{R_1, Z_2\}\right) \\
&\quad + \mathbb{P}\left(\frac{\tilde{g}(R_2, Z_2)}{\sigma^2 + \hat{\mathcal{I}}(Z_2, R_2)} > T, Z_2 < \min\{R_1, R_2\}\right) \\
&= \mathbb{E}\left[\mathbf{1}_{\left\{\frac{\tilde{f}(R_1)}{\sigma^2 + \hat{\mathcal{I}}(R_1, R_1)} > T\right\}} \mathbf{1}_{\{R_1 < \min\{R_2, Z_2\}\}}\right] \\
&\quad + \mathbb{E}\left[\mathbf{1}_{\left\{\frac{\tilde{g}(R_2, Z_2)}{\sigma^2 + \hat{\mathcal{I}}(R_2, R_2)} > T\right\}} \mathbf{1}_{\{R_2 < \min\{R_1, Z_2\}\}}\right] \\
&\quad + \mathbb{E}\left[\mathbf{1}_{\left\{\frac{\tilde{g}(R_2, Z_2)}{\sigma^2 + \hat{\mathcal{I}}(Z_2, R_2)} > T\right\}} \mathbf{1}_{\{Z_2 < \min\{R_1, R_2\}\}}\right]
\end{aligned} \tag{5.12}$$

For the first term we have that

$$\begin{aligned}
& \mathbb{E} \left[ \mathbf{1}_{\left\{ \frac{\tilde{f}(R_1)}{\sigma^2 + \hat{\mathcal{I}}(R_1, R_1)} > T \right\}} \mathbf{1}_{\{R_1 < \min\{R_2, Z_2\}\}} \right] \\
&= \mathbb{E} \left[ \mathbb{E} \left[ \mathbf{1}_{\left\{ \frac{\tilde{f}(R_1)}{\sigma^2 + \hat{\mathcal{I}}(R_1, R_1)} > T \right\}} \mathbf{1}_{\{R_1 < \min\{R_2, Z_2\}\}} \middle| R_1, R_2, Z_2 \right] \right] \\
&\stackrel{(a)}{=} \mathbb{E} \left[ \mathbf{1}_{\{R_1 < \min\{R_2, Z_2\}\}} \mathbb{E} \left[ \mathbf{1}_{\left\{ \frac{\tilde{f}(R_1)}{\sigma^2 + \hat{\mathcal{I}}(R_1, R_1)} > T \right\}} \middle| R_1, R_2, Z_2 \right] \right] \\
&\stackrel{(b)}{=} \mathbb{E} \left[ \mathbf{1}_{\{R_1 < \min\{R_2, Z_2\}\}} \mathbb{E} \left[ \mathbf{1}_{\left\{ \frac{\tilde{f}(R_1)}{\sigma^2 + \hat{\mathcal{I}}(R_1, R_1)} > T \right\}} \middle| R_1 \right] \right] \\
&= \mathbb{E} \left[ \mathbf{1}_{\{R_1 < \min\{R_2, Z_2\}\}} \mathbb{P} \left( \frac{\tilde{f}(R_1)}{\sigma^2 + \hat{\mathcal{I}}(R_1, R_1)} > T \middle| R_1 \right) \right],
\end{aligned}$$

where (a) comes from the properties of the conditional expectation and (b) follows because the event  $\left\{ \frac{\tilde{f}(R_1)}{\sigma^2 + \hat{\mathcal{I}}(R_1, R_1)} > T \right\}$  is independent of  $R_2$  and  $Z_2$ .

After a similar analysis for the two terms with the cooperative signal, we have that

$$\begin{aligned}
& \mathbb{E} \left[ \mathbf{1}_{\left\{ \frac{\tilde{g}(R_2, Z_2)}{\sigma^2 + \hat{\mathcal{I}}(R_2, R_2)} > T \right\}} \mathbf{1}_{\{R_2 < \min\{R_1, Z_2\}\}} \right] \\
&= \mathbb{E} \left[ \mathbf{1}_{\{R_2 < \min\{R_1, Z_2\}\}} \mathbb{P} \left( \frac{\tilde{g}(R_2, Z_2)}{\sigma^2 + \hat{\mathcal{I}}(R_2, R_2)} > T \middle| R_2, Z_2 \right) \right], \\
& \mathbb{E} \left[ \mathbf{1}_{\left\{ \frac{\tilde{g}(R_2, Z_2)}{\sigma^2 + \hat{\mathcal{I}}(Z_2, R_2)} > T \right\}} \mathbf{1}_{\{Z_2 < \min\{R_1, R_2\}\}} \right] \\
&= \mathbb{E} \left[ \mathbf{1}_{\{Z_2 < \min\{R_1, R_2\}\}} \mathbb{P} \left( \frac{\tilde{g}(R_2, Z_2)}{\sigma^2 + \hat{\mathcal{I}}(Z_2, R_2)} > T \middle| R_2, Z_2 \right) \right]
\end{aligned}$$

### Some functions

Denote by

$$\begin{aligned}
\hat{G}(r) &:= \mathbb{P} \left( \frac{\tilde{f}(R_1)}{\sigma^2 + \hat{\mathcal{I}}(R_1, R_1)} > T \middle| R_1 = r \right), \\
\hat{H}(r, z) &:= \mathbb{P} \left( \frac{\tilde{g}(R_2, Z_2)}{\sigma^2 + \hat{\mathcal{I}}(R_2, R_2)} > T \middle| R_2 = r, Z_2 = z \right), \\
\hat{K}(r, z) &:= \mathbb{P} \left( \frac{\tilde{g}(R_2, Z_2)}{\sigma^2 + \hat{\mathcal{I}}(Z_2, R_2)} > T \middle| R_2 = r, Z_2 = z \right).
\end{aligned}$$

Being  $R_1$  independent of  $\hat{\mathcal{I}}(R_1, R_1)$ , then  $\hat{G}(r) = \mathbb{P} \left( \tilde{f}(r) > T(\sigma^2 + \hat{\mathcal{I}}(r, r)) \right)$  for a given  $r > 0$ . Consider  $\tilde{f}(r)$  as in (3.1), then it follows an exponential distribution with parameter

$\frac{r^\beta}{p}$ . Since  $\hat{\mathcal{I}}(r, r)$  is independent of  $\tilde{f}(r)$ ,

$$\hat{G}(r) = \mathbb{E} \left[ \mathbb{P} \left( \tilde{f}(r) > T \left( \sigma^2 + \hat{\mathcal{I}}(r, r) \right) \middle| \hat{\mathcal{I}}(r, r) \right) \right] = e^{\frac{-Tr^\beta}{p} \sigma^2} \mathcal{L}_{\hat{\mathcal{I}}(1)} \left( \frac{Tr^\beta}{p}; r \right) \mathcal{L}_{\hat{\mathcal{I}}(2)} \left( \frac{Tr^\beta}{p}; r \right),$$

where the deterministic functions  $\mathcal{L}_{\hat{\mathcal{I}}(1)}(s; \rho)$  and  $\mathcal{L}_{\hat{\mathcal{I}}(2)}(s; \rho)$  are given by (5.9).

Again, being  $(R_2, Z_2)$  independent of  $\hat{\mathcal{I}}(R_2, R_2)$ , then  $\hat{H}(r, z) = \mathbb{P} \left( \tilde{g}(r, z) > T \left( \sigma^2 + \hat{\mathcal{I}}(r, r) \right) \right)$  for  $r > 0$  and  $z > 0$ . Using the general expression in (3.5) for  $\tilde{g}(r, z)$ ,

$$\begin{aligned} \hat{H}(r, z) &= c(r, z) e^{M(r, z) T \sigma^2} \mathcal{L}_{\hat{\mathcal{I}}(1)}(M(r, z) T; r) \mathcal{L}_{\hat{\mathcal{I}}(2)}(M(r, z) T; r) \mathbf{e}, \\ \hat{K}(r, z) &= c(r, z) e^{M(r, z) T \sigma^2} \mathcal{L}_{\hat{\mathcal{I}}(1)}(M(r, z) T; z) \mathcal{L}_{\hat{\mathcal{I}}(2)}(M(r, z) T; r) \mathbf{e}. \end{aligned}$$

### Final expression

To complete the analysis, we need to find the coverage probability expressed in equation (5.12), thus, we need expressions for

$$\mathbb{E} \left[ \hat{G}(R_1) \mathbf{1}_{\{R_1 < \min\{R_2, Z_2\}\}} \right], \quad \mathbb{E} \left[ \hat{H}(R_2, Z_2) \mathbf{1}_{\{R_2 < \min\{R_1, Z_2\}\}} \right], \quad \mathbb{E} \left[ \hat{K}(R_2, Z_2) \mathbf{1}_{\{Z_2 < \min\{R_1, R_2\}\}} \right].$$

Let us begin by the first one,

$$\begin{aligned} \mathbb{E} \left[ \hat{G}(R_1) \mathbf{1}_{\{R_1 < \min\{R_2, Z_2\}\}} \right] &\stackrel{(a)}{=} \mathbb{E} \left[ \mathbb{E} \left[ \hat{G}(R_1) \mathbf{1}_{\{R_1 < \min\{R_2, Z_2\}\}} \middle| R_1 \right] \right] \\ &= \mathbb{E} \left[ \hat{G}(R_1) \mathbb{E} \left[ \mathbf{1}_{\{R_1 < \min\{R_2, Z_2\}\}} \middle| R_1 \right] \right] = \mathbb{E} \left[ \hat{G}(R_1) \mathbb{P}(\min\{R_2, Z_2\} > R_1 | R_1) \right], \end{aligned}$$

where (a) follows by properties of the conditional expectation. Define

$$G(r) = \hat{G}(r) \mathbb{P}(\min\{R_2, Z_2\} > R_1 | R_1 = r),$$

we only have left to find an explicit expression for  $\mathbb{P}(\min\{R_2, Z_2\} > R_1 | R_1 = r)$ . Because  $R_1$  is independent of  $(R_2, Z_2)$ ,

$$\mathbb{P}(\min\{R_2, Z_2\} > R_1 | R_1 = r) = \mathbb{P}(\min\{R_2, Z_2\} > r),$$

and then

$$\mathbb{P}(\min\{R_2, Z_2\} > r) = 1 - F_{R_2}(r) - F_{Z_2}(r) + F_{R_2, Z_2}(r, r),$$

where  $F_{R_2}$ ,  $F_{Z_2}$ , and  $F_{R_2, Z_2}$  are the CDF of  $R_2$ ,  $Z_2$ , and  $(R_2, Z_2)$  that can be explicitly obtained from equation (5.2).

In the same fashion,

$$\begin{aligned} \mathbb{E} \left[ \hat{H}(R_2, Z_2) \mathbf{1}_{\{R_2 < \min\{R_1, Z_2\}\}} \right] &= \mathbb{E} \left[ \hat{H}(R_2, Z_2) \mathbb{P}(\min\{R_1, Z_2\} > R_2 | R_2, Z_2) \right], \\ \mathbb{E} \left[ \hat{K}(R_2, Z_2) \mathbf{1}_{\{Z_2 < \min\{R_1, R_2\}\}} \right] &= \mathbb{E} \left[ \hat{K}(R_2, Z_2) \mathbb{P}(\min\{R_1, R_2\} > Z_2 | R_2, Z_2) \right] \end{aligned}$$

Define

$$\begin{aligned} H(r, z) &:= \hat{H}(r, z) \mathbb{P}(\min\{R_1, Z_2\} > R_2 | R_2 = r, Z_2 = z), \\ K(r, z) &:= \hat{K}(r, z) \mathbb{P}(\min\{R_1, R_2\} > Z_2 | R_2 = r, Z_2 = z). \end{aligned}$$

To obtain explicit formulas for  $H(r, z)$  and  $K(r, z)$ , we proceed as before to find out that

$$\begin{aligned} \mathbb{P}(\min\{R_1, Z_2\} > R_2 | R_2 = r, Z_2 = z) &= (1 - F_{R_1}(r)) \mathbf{1}_{\{z > r\}}, \\ \mathbb{P}(\min\{R_1, R_2\} > Z_2 | R_2 = r, Z_2 = z) &= (1 - F_{R_1}(z)) \mathbf{1}_{\{r > z\}}, \end{aligned}$$

where  $F_{R_1}$  is the CDF of  $R_1$ . Define

$$\begin{aligned} \tilde{G}(r) &:= 1 - F_{R_2}(r) - F_{Z_2}(r) + F_{R_2, Z_2}(r, r), \\ \tilde{H}(r, z) &:= (1 - F_{R_1}(r)) \mathbf{1}_{\{z > r\}}, \\ \tilde{K}(r, z) &:= (1 - F_{R_1}(z)) \mathbf{1}_{\{r > z\}}. \end{aligned}$$

The functions  $F_{R_1}(r)$ ,  $F_{R_2}(r)$ , and  $F_{Z_2}(r)$  are the CDF of the random variables  $R_1$ ,  $R_2$ ,  $Z_2$ , which are Rayleigh distributed (see Section 5.2), and  $F_{R_2, Z_2}(r, z)$  is the CDF of the random vector  $(R_2, Z_2)$ , which can be obtained with equation (5.2). Hence, the analytical expressions for  $G(r)$ ,  $H(r, z)$ , and  $K(r, z)$  we have been looking for are given by

$$G(r) = \tilde{G}(r) \hat{G}(r), \quad H(r, z) = \tilde{H}(r, z) \hat{H}(r, z), \quad K(r, z) = \tilde{K}(r, z) \hat{K}(r, z).$$

### 5.7.2 Proof of Lemma 2

Denote by  $A := (A_x, A_y)$  and  $B := (B_x, B_y)$  the Cartesian coordinates of the nearest parent to the typical user and his daughter, respectively. Denote by  $(R_2, \Theta)$  and  $(Z_2, \Psi)$  their corresponding polar coordinates, that is,

$$A_x = R_2 \cos \Theta, \quad A_y = R_2 \sin \Theta, \quad B_x = Z_2 \cos \Psi, \quad B_y = Z_2 \sin \Psi,$$

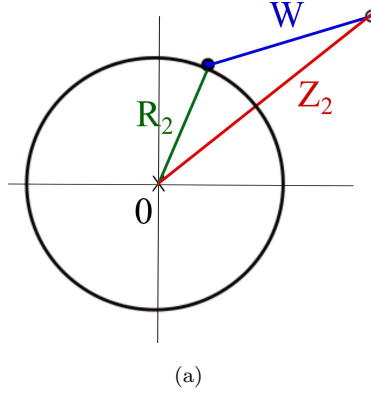
Define the random vector  $(C_x, C_y) := A - B$ , whose polar coordinates are denoted by  $(W, \Omega)$  (see Figure 5.5). We have the following transformation

$$\begin{aligned} A_x &= R_2 \cos \Theta, & A_y &= R_2 \sin \Theta, \\ C_x &= R_2 \cos \Theta - Z_2 \cos \Psi, & C_y &= R_2 \sin \Theta - Z_2 \sin \Psi. \end{aligned} \tag{5.13}$$

Denote by  $f_{A_x, A_y, C_x, C_y}$  the joint PDF of  $(A_x, A_y, C_x, C_y)$  and by  $f_{R_2, \Theta, Z_2, \Psi}$  the joint PDF of  $(R_2, \Theta, Z_2, \Psi)$ . The absolute value of the Jacobian of the transformation defined by equation (5.13) is  $R_2 Z_2$ . Thus, the change of variable Theorem [Ros09, pp. 274] states that

$$f_{R_2, \Theta, Z_2, \Psi}(r, \theta, z, \psi) = f_{A_x, A_y, C_x, C_y}(r \cos \theta, r \sin \theta, r \cos \theta - z \cos \psi, r \sin \theta - z \sin \psi) r z \tag{5.14}$$

As stated above, the random variable  $R_2$  is Rayleigh distributed, with scale parameters  $\zeta$ , and, as stated in Theorem 5,  $W$  is Rayleigh distributed, with scale parameter  $\alpha$ . On

Figure 5.5: The real random variables  $R_2$ ,  $Z_2$ , and  $W$ .

the other hand, the random angles  $\Theta$ ,  $\Psi$  and  $\Omega$  are considered uniformly distributed over  $[0, 2\pi)$ , given the isotropy of the PPP. Further, the random variables  $R_2$ ,  $\Theta$ ,  $W$ , and  $\Omega$  are considered to be independent between them, as in the PPP case. The cartesian coordinates of a point around a center, which has rayleigh radial distance from the origin and uniform angle, are distributed as an independent Gaussian vector [Ros09, pp. 276, Ex. 7b]. Hence,  $A_x, A_y$  are Normal distributed, with parameter  $(0, \zeta^2)$ , and  $C_x, C_y$  are Normal distributed, with parameters  $(0, \alpha^2)$ . Moreover,  $A_x, A_y, C_x, C_y$  are independent random variables. From equation (5.14) we have that

$$\begin{aligned} f_{R_2, \Theta, Z, \Psi}(r, \theta, z, \psi) &\stackrel{(a)}{=} \frac{rz}{(2\pi\alpha\zeta)^2} e^{-\left(\frac{r^2 \cos^2 \theta}{2\zeta^2} + \frac{r^2 \sin^2 \theta}{2\zeta^2} + \frac{(r \cos \theta - z \cos \psi)^2}{2\alpha^2} + \frac{(r \sin \theta - z \sin \psi)^2}{2\alpha^2}\right)} \\ &\stackrel{(b)}{=} \frac{rz}{(2\pi\alpha\zeta)^2} e^{-\left(\frac{r^2}{2} \left(\frac{1}{\alpha^2} + \frac{1}{\zeta^2}\right) + \frac{z^2}{2\alpha^2} - \frac{rz \cos(\theta - \psi)}{\alpha^2}\right)}, \end{aligned}$$

where (a) comes from the formula of the distribution of independent Gaussian random variables, and (b) follows from the trigonometric identities  $\cos^2 \theta + \sin^2 \theta = 1$  and  $\cos \theta \cos \psi + \sin \theta \sin \psi = \cos(\theta - \psi)$ . Since the random variables  $\Theta$  and  $\Psi$  are independent, uniform distributed over  $[0, 2\pi)$ , the joint PDF of  $(R_2, Z_2)$ , denoted by  $f_{R_2, Z_2}$  is given by the expression

$$\begin{aligned} f_{R_2, Z_2}(r, z) &\stackrel{(a)}{=} \frac{rz}{(\alpha\zeta)^2} e^{-\left(\frac{r^2}{2} \left(\frac{1}{\alpha^2} + \frac{1}{\zeta^2}\right) + \frac{z^2}{2\alpha^2}\right)} \frac{1}{2\pi} \int_0^{2\pi} e^{\frac{rz \cos w}{\alpha^2}} dw \\ &\stackrel{(b)}{=} \frac{rz}{(\alpha\zeta)^2} e^{-\left(\frac{r^2}{2} \left(\frac{1}{\alpha^2} + \frac{1}{\zeta^2}\right) + \frac{z^2}{2\alpha^2}\right)} I_0\left(\frac{rz}{\alpha^2}\right), \end{aligned}$$

where (a) comes from the change of variable  $w = \theta - \psi$  and (b) follows after considering the integral representation  $I_0(x) = \frac{1}{2\pi} \int_0^{2\pi} e^{x \cos w} dw$  [Leb65].

Finally, let us denote by  $f_{Z_2}$  the PDF of the random variable  $Z_2$  and by  $\eta = \left(\frac{1}{\alpha^2} + \frac{1}{\zeta^2}\right)$ .

To obtain  $f_{Z_2}$ , we integrate over  $[0, \infty)$  with respect to the variable  $r$  the preceding equation

$$\begin{aligned}
f_{Z_2}(z) &\stackrel{(a)}{=} \int_0^\infty \frac{rz}{(\alpha\zeta)^2} e^{-\left(\frac{r^2}{2}\eta + \frac{z^2}{2\alpha^2}\right)} \sum_{n=0}^\infty \frac{(1/4)^n}{(n!)^2} \left(\frac{rz}{\alpha^2}\right)^{2n} dr \\
&= \frac{z}{(\alpha\zeta)^2} e^{-\frac{z^2}{2\alpha^2}} \sum_{n=0}^\infty \frac{(1/4)^n}{(n!)^2} \left(\frac{z^2}{\alpha^4}\right)^n \int_0^\infty r^{2n} e^{-\frac{r^2}{2}\eta} r dr \\
&\stackrel{(b)}{=} \frac{z}{(\alpha\zeta)^2 \eta} e^{-\frac{z^2}{2\alpha^2}} \sum_{n=0}^\infty \frac{\left(\frac{z^2}{2\alpha^4 \eta}\right)^n}{n!} \\
&= \frac{z}{(\alpha\zeta)^2 \eta} e^{-\frac{z^2}{2\alpha^2}} e^{-\frac{z^2}{2\alpha^4 \eta}} \\
&\stackrel{(c)}{=} \frac{z}{\alpha^2 + \zeta^2} e^{-\frac{z^2}{2(\alpha^2 + \zeta^2)}},
\end{aligned}$$

where (a) comes from the series representation  $I_0(x) = \sum_{n=0}^\infty \frac{(1/4)^n}{(n!)^2} x^{2n}$  [Leb65], while (b) follows after the formula  $\int_0^\infty r^{2n} e^{-\frac{r^2}{2}\eta} r dr = \frac{2^n}{\eta^{n+1}} n!$ , and (c) after some algebraic manipulations and from the definition of  $\eta$ .





# Mutually Nearest Neighbors with resource constraints

This Chapter has given place to the following article, presented at WiOpt 2017, at Paris, France:

- Wireless Node Cooperation with Resource Availability Constraints.

## Abstract

Up to this point, the thesis has focused on clustering criteria based solely on geographic proximity. However, for the cooperation to be meaningful, each atom of a group of BSs should have sufficient available resources to share with the others. In this Chapter we consider an alternative distance to generate the mutually nearest neighbors and single BSs. The new distance takes into account both: Geographic proximity and available resources of the stations. When the network is modelled by a PPP, we derive an analytical expression on the probability of two atoms beings in cooperation. This leads into an interference analysis. The results illustrate that cooperation benefits depend strongly on the distribution of the available resources over the network.

## 6.1 The choice of the new distance

Along this Chapter, the available resources of each BS is quantified by a positive mark. The mark represents the amount of available resources itself (unused bandwidth, unoccupied OFDMA slots, etc), or a system indicator such as the residual capacity (see [DFMTT12]) or the coverage (one-minus-outage) probability [DGBA12, BG15, NMH14, TSAJ14, BK15, ABG11]. The higher its mark, the more available is a BS to serve additional users.

Our goal is to redefine the MNNR with a new distance. This distance should allow the formation of the cooperative pairs of BSs, with the following properties:

- (1) their locations are *Euclideanly* close, and

- (2) they have sufficient resources for the cooperation to be beneficial.

In this way, each BS is characterised by a 2-dimensional location, along with a positive mark (its available resources). Thus, we consider a BS in the 3-dimensional Euclidean space. As a result, we need to adjust the MNNR criterion in this larger space, with the aid of a distance that takes into consideration (1) and (2) appropriately.

The natural choice would be the 3-dimensional Euclidean norm. Unfortunately, this choice would allow cooperative pairs to be formed whose BSs can both have *an arbitrarily small amount* of available resources (whenever their location are geographically close). Therefore, the resulting cooperative pairs would not be reasonable for our particular purposes.

On the other hand, the 3-dimensional hyperbolic distance is actually a good candidate. Indeed, grouping the BSs according to their relative hyperbolic proximity (to be defined precisely in what follows) translates straightforwardly into network benefits: For the BSs in a cooperative pair, there is interference improvements, related to geographical proximity, while both BSs make use of their common available resources to serve the combined user load, implementing a type of *load balancing*. Such cooperative pairs can be used within the framework of C-RAN. Furthermore, when the BS locations are modeled by marked PPP, the hyperbolic distance makes possible the derivation of interesting analytic results.

The novel grouping criterion proposed in this Chapter, it is neither *dynamic*, since is not the user who directly selects the BSs for its service; nor entirely *static*, as the clusters can change to adjust to the resources of the BSs.

*Hyperbolic Geometry* was developed in the 19th century as an alternative to the discussion about the parallel postulate of Euclidean Geometry. During the 20th century, physicists found in it convenient tools to work in the fields of *mathematical physics* and *special relativity* [BEE96]. Nowadays, other applied fields such as *mathematical finance* and *option pricing* benefits also from it [HL08]. In recent years, important research in *communication networks* [SSKP16], *complex networks* [KPK<sup>+</sup>10], and *big network data* [SKP16] have also found in hyperbolic metric spaces an approach aspiring to radically change current practices.

## 6.2 Hyperbolic proximity

Let  $\mathbb{H}^3 = \{(x, y, z) \in \mathbb{R}^3 \mid z > 0\}$  denote the three dimensional hyperbolic half-space. Along this Chapter, the letters  $a$ ,  $b$ , and  $c$  denote atoms (BSs) in the hyperbolic space  $\mathbb{H}^3$ . For two atoms  $a = (x, y, z)$  and  $b = (\tilde{x}, \tilde{y}, \tilde{z})$  in  $\mathbb{H}^3$ , the vectors  $(x, y)$  and  $(\tilde{x}, \tilde{y})$  represent their corresponding 2-dimensional Euclidean position, and  $z > 0$  and  $\tilde{z} > 0$  their respective resources. Denote by

$$d_E^{(2)}(a, b) := \sqrt{(x - \tilde{x})^2 + (y - \tilde{y})^2},$$

the 2-dimensional Euclidean distance between  $a$  and  $b$  position, and the hyperbolic distance between  $a$  and  $b$  by the expression

$$d_{\mathbb{H}^3}(a, b) := \text{acosh} \left( \frac{d_E^{(2)}(a, b)^2}{2z\tilde{z}} + \frac{1}{2} \left( \frac{z}{\tilde{z}} + \frac{\tilde{z}}{z} \right) \right), \quad (6.1)$$

where  $\text{acosh}(\cdot)$  denotes the inverse of the hyperbolic cosine function [EGM98, Prop.1.6]. Before forming the cooperative pairs by means of hyperbolic proximity, we will analyse what it means for the atoms  $a$  and  $b$  to be hyperbolically close. Since  $\text{acosh}(\cdot)$  is an increasing function, it is sufficient to focus the analysis on the expression  $\frac{d_E^{(2)}(a, b)^2}{2z\tilde{z}} + \frac{1}{2} \left( \frac{z}{\tilde{z}} + \frac{\tilde{z}}{z} \right)$ .

The continuous function

$$(z, \tilde{z}, d_E^{(2)}(a, b)) \mapsto \frac{d_E^{(2)}(a, b)^2}{2z\tilde{z}}$$

attains its minimum value 0 at  $\{(z, \tilde{z}, 0) \mid z, \tilde{z} > 0\}$ . Hence, given  $z$  and  $\tilde{z}$ , this function is close to the minimum, when the values of  $d_E^{(2)}(a, b)$  are small. Given  $d_E^{(2)}(a, b)$ , the function is close to the minimum, when the value of the product  $z\tilde{z}$  is large, indicating one-out-of-two or both BS resources being large. On the other hand, for a given  $d_E^{(2)}(a, b)$ , the previous function explodes whenever the product  $z\tilde{z}$  is small, indicating one-out-of-two or both BS resources being small.

From the second term, the continuous function

$$(z, \tilde{z}) \mapsto \frac{1}{2} \left( \frac{z}{\tilde{z}} + \frac{\tilde{z}}{z} \right)$$

attains its global minimum value 1 at  $\{(z, z) \mid z > 0\}$ . Therefore, whenever  $z \approx \tilde{z}$ , the above function is close to its minimum. Thus, only the pairs of BSs whose resources are in balance would be candidates for cooperation. This term enforces a sort of *load balancing* among the BSs in cooperation.

With the above discussion, we summarize that two atoms  $a$  and  $b$  are hyperbolically close if all the three following conditions are satisfied:

- (1) they are geographically close (in the 2-dimensional sense),
- (2) the product of their resource indicators is not small,
- (3) the quantities of available resources of both are balanced.

### 6.3 Singles and cooperative pairs

In the previous Section we stated the potential benefits for a cooperative cellular network, whose BSs are grouped according to hyperbolic proximity. The next step is to give the rules to form these cooperative clusters of BSs.

Every configuration of points  $\phi$  over  $\mathbb{H}^3$  represents a topology for the BS locations, and a resource indicator for each one of them. Let  $\phi$  be a simple, locally-finite, configuration. For  $a$  and  $b$ , two different atoms in  $\phi$ , we say that  $a$  is in *Nearest Neighbor Relation in  $\mathbb{H}^3$  (NNR')* with  $b$ , with respect to  $\phi$ , if

$$b := \operatorname{argmin}_{c \in \phi \setminus \{a\}} d_{\mathbb{H}^3}(a, c),$$

and we write  $a \xrightarrow{\phi} b$ . When  $a$  is not in NNR' with  $b$ , we write  $a \not\xrightarrow{\phi} b$ .

Henceforth, we will only consider configurations fulfilling the uniqueness of the nearest neighbor. Even if this uniqueness is not true in general, as for the nearest neighbors in  $\mathbb{R}^d$ , when the atoms are modeled by a stationary point process, this condition holds  $\mathbb{P}$ -a.s. (see Section 6.6).

Consider a regular set  $\mathcal{D} \subset (0, \infty) \times (0, \infty)$ , which is symmetric, that is, if  $(z, \tilde{z}) \in \mathcal{D}$  then  $(\tilde{z}, z) \in \mathcal{D}$ . This set is thought to control even more the creation of the cooperating pairs, with respect to some specific criteria for the resources.

**Definition 8.** Two different atoms  $a$  and  $b$  in  $\phi$ , with resources  $z$  and  $\tilde{z}$ , respectively, are said to be in *Mutually Nearest Neighbor Relation in  $\mathbb{H}^3$  (MNNR')* if  $a \xrightarrow{\phi} b$ ,  $b \xrightarrow{\phi} a$ , and if  $(z, \tilde{z}) \in \mathcal{D}$ . We denote this by  $a \xrightarrow{\phi, \mathcal{D}} b$ . In telecommunication terms, the BSs  $a$  and  $b$  are in cooperation.

**Definition 9.** An atom  $a = (x, y, z)$  is said to be *single* if it is not in MNNR' (does not cooperate with any other atom in  $\phi$ ). That is, if for every  $b = (\tilde{x}, \tilde{y}, \tilde{z})$  in  $\phi \setminus \{a\}$  such that  $a \xrightarrow{\phi} b$ , then  $b \not\xrightarrow{\phi} a$  or  $(z, \tilde{z}) \notin \mathcal{D}$ .

In the following, we give an example of the use of the set  $\mathcal{D}$  to control the creation of cooperative pairs: Fix deployment of BSs, and assume that these have some users assigned. The available resources of each BS quantifies its residual capacity, *i.e.*, the remaining capacity after serving its assigned users. In this way, the resources being high, above some level  $\mathbf{H} > 0$ , is translated into a BS being assigned few users. Let B1 and B2 be two BSs geographically close, and suppose that the resources of both are high. Hence, B1 and B2 are hyperbolically close (see the previous subsection). If an operator considers appropriate to make B1 and B2 cooperate, it is sufficient to consider the MNNR', with the control set  $\mathcal{D} = (0, \infty) \times (0, \infty)$ . That is, without any extra constraint for the resources. On the other hand, suppose that this operator wants to minimize communication between the BSs, to prevent overburdening the backhaul/control channel. The available resources of B1 and B2 being high means that, under conventional conditions, each one can serve satisfactorily its own users. Hence, the operator might consider the cooperation between B1 and B2 unnecessary. To block their cooperation, simply apply the MNNR' criterion, with the control set chosen as follows,

$$\mathcal{D} = ((\mathbf{H}, \infty) \times (\mathbf{H}, \infty))^c, \quad (6.2)$$

where  $\cdot^c$  denotes the complement over  $(0, \infty) \times (0, \infty)$ .

### 6.3.1 Examples

Figure 6.1 illustrates a deployment of BSs, where the black numbers represent the resources block of each BS. A 0 means that this BS does not have a single available resource, and a 10 means that this BS has the maximum of resources block. Figure 6.1(a) shows the cooperative pairs and single BSs from the original MNNR, whereas Figure 6.1(b) shows those from the MNNR'. The most significant changes between the two models are highlighted within a green circle. From both Figures we appreciate that some pairs do not change, other disappear, and some others are created, with respect to the new criterion. For instance, there are two BSs in MNNR', with respective resource block 3 and 4, that actually are not in MNNR. This is explained because both BSs are close enough and, even though their respective amount of resources are not high, their resources are sufficient for their cooperation being beneficial. There are two other BSs, with respective resource block 3 and 8, that are in MNNR and also in MNNR'. Although the available resources of one are not high, the resources block of both BSs are balanced (with respect to our particular criterion). In this way, the cooperation is beneficial for the BS having 3 resources block, while the BS with 8 resources block is not really being affected, since the resources of its partner are not zero. On the other hand, all those cooperative pairs in MNNR for which one of its elements has zero resources block, then these union break in the hyperbolic model. This is justified for many reasons:

- An operator might find senseless to associate users to a BS not having resources block.
- Strictly speaking, a BS without resources block cannot cooperate with another BS: It will only take advantage of the resources of its pairing BS.
- Let us imagine that in a “cooperative” pair of BSs, one of its BSs has no resources block. If both have some users assigned, then these are going to be served only by the BSs with available resources. Therefore, all the resources of this BS are going to be consumed.

Thus, we confirm the statement from Section 6.2: two BSs are in cooperation, with respect to the hyperbolic distance, if (i) they are geographically close, (ii) both have enough resources to make possible and beneficial their *cooperation*, (iii) and their available resources are balanced. Actually, this example clarifies even more that the model proposed in the current Chapter relays strongly in the load balance between the BSs in a cooperative pair and, consequently, of the entire network.

Now suppose that an operator considers that two BSs both having resources block above  $\mathbf{H} := 7$  can serve satisfactorily each one their own users. Hence, the operator is not interested in to make these two BSs cooperate. Figure 6.2(a) shows the same deployment of BSs, and the cooperative pairs and single BSs from the MNNR', without any extra constraint for the resources. Whereas Figure 6.2(b) shows the cooperative pairs and single BSs from the MNNR', now considering the control set  $\mathcal{D}$  as in equation (6.2), for this particular choice of  $\mathbf{H}$ . The main differences between both approaches are highlighted within the green circles.

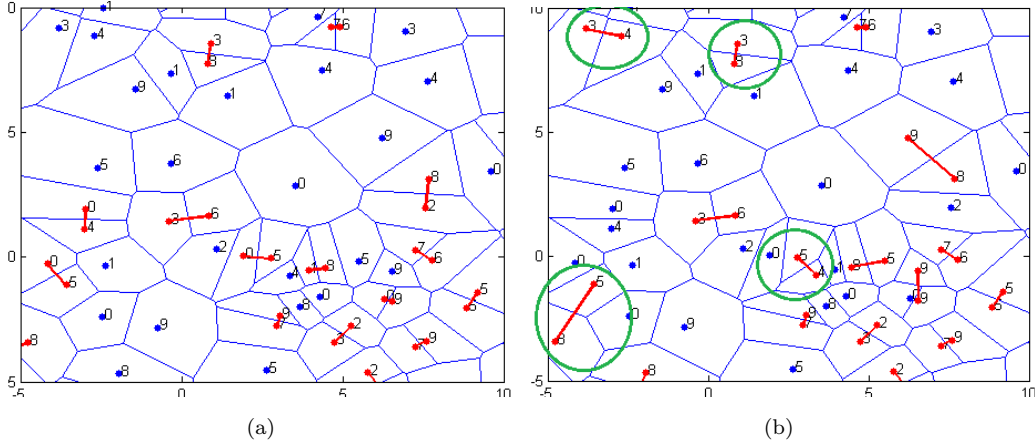


Figure 6.1: The MNNR (a) without constraints (b) with constraints.

Notice that the extra constraints imposed to the model break the pairs of BSs having both a large amount of available resources, as desired.

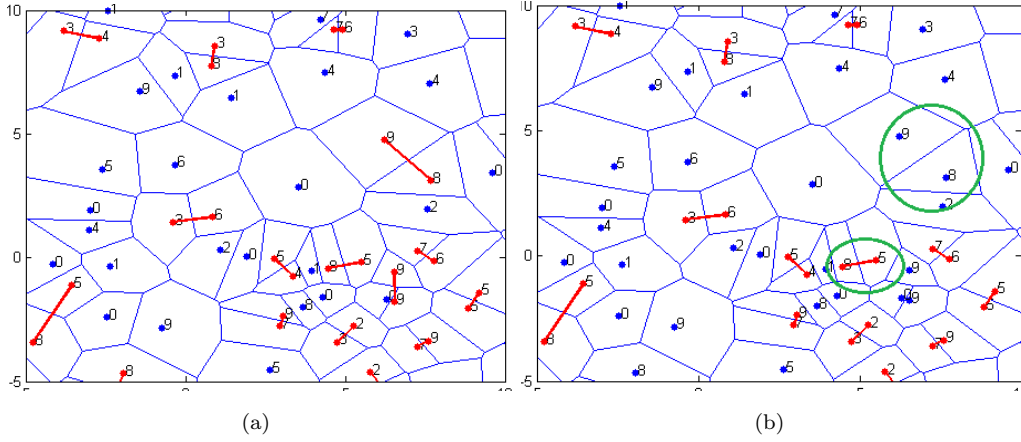


Figure 6.2: The MNNR (a) without extra constraints (b) with extra constraints

## 6.4 Analytic results

In the previous Sections we motivated and introduced the new model of mutually nearest neighbors, explaining its alternative benefits and versatility through some examples. This Section is devoted to the study of a cooperative cellular network, whose BSs are modeled by a PPP.

Consider an homogeneous and independently marked PPP  $\Phi$ . It models the positions of

the BSs over  $\mathbb{R}^2$ , with fixed density  $\lambda > 0$ . The marks lie in  $(0, \infty)$ , they follow a common distribution  $f(z)dz$ , and represent the available resources of each one of the BSs. This process turns out to be a PPP over  $\mathbb{R}^2 \times (0, \infty)$  [BB09], *stationary with respect to the BS positions*, whose intensity measure is

$$\Lambda(dxdydz) = \lambda dxdyf(z)dz. \quad (6.3)$$

Notice that this measure is absolutely continuous with respect to the Lebesgue measure on  $\mathbb{R}^2 \times (0, \infty)$ . From a different point of view, in  $\mathbb{H}^3$ , an hyperbolic volume measure  $v(dxdydz)$  arises naturally from the hyperbolic metric [EGM98],

$$v(dxdydz) = \frac{dxdydz}{z^3}.$$

If  $\Lambda(\cdot)$  was absolutely continuous with respect to  $v(dxdydz)$ , the resources of the BSs would be accumulated around the value  $z = 0$ ,  $\mathbb{P}$ -a.s., which is not realistic, from a telecommunication point of view. However, for the interested reader, the whole analysis presented in this Section stays the same in both cases: Just substitute  $f(z)$  for  $f^*(z) = \frac{f(z)}{z^3}$  in the formulas.

#### 6.4.1 A key property of the hyperbolic half-space

The assumption of the BSs being modeled by a PPP and the specific choice of the hyperbolic metric are the two elements granting the desired analysis. In particular, we will make use of a property of the hyperbolic half-space: Hyperbolic balls are described by Euclidean balls. For  $a \in \mathbb{H}^3$ , and  $\epsilon > 0$ , let

$$B_{\mathbb{H}^3}(\epsilon, a) := \{b \in \mathbb{H}^3 \mid d_{\mathbb{H}^3}(a, b) < \epsilon\}$$

be the hyperbolic ball, centered at  $a$ , with radius  $\epsilon$ . Suppose that  $a = (x, y, z)$ , let  $B_E^{(3)}(\epsilon, a)$  denote the 3-dimensional Euclidean ball, with center at  $(x, y, z \cosh(\epsilon))$ , and radius  $z \sinh(\epsilon) > 0$ . We have the following result.

**Proposition 7.** *The hyperbolic ball  $B_{\mathbb{H}^3}(\epsilon, a)$  is described in the 3-dimensional Euclidean space by the Euclidean ball  $B_E^{(3)}(\epsilon, a)$ .*

*Proof.* The atom  $b = (\tilde{x}, \tilde{y}, \tilde{z})$  belongs to  $B_{\mathbb{H}^3}(\epsilon, a)$  if, and only if,

$$\frac{d_E^{(2)}(a, b)^2}{2z\tilde{z}} + \frac{1}{2} \left( \frac{z}{\tilde{z}} + \frac{\tilde{z}}{z} \right) < \cosh(\epsilon).$$

After some simple manipulations, the previous inequality is equivalent to

$$d_E^{(2)}(a, b)^2 + \tilde{z}^2 - 2z\tilde{z}\cosh(\epsilon) + z^2 < 0.$$

Notice that

$$\begin{aligned} & z^2 - 2z\tilde{z}\cosh(\epsilon) + \tilde{z}^2 \\ &= z^2 - z^2 \cosh^2(\epsilon) + z^2 \cosh^2(\epsilon) - 2z\tilde{z}\cosh(\epsilon) + \tilde{z}^2 \\ &= z^2(1 - \cosh^2(\epsilon)) + (z\cosh(\epsilon) - \tilde{z})^2 \\ &= -z^2 \sinh^2(\epsilon) + (z\cosh(\epsilon) - \tilde{z})^2, \end{aligned}$$



where  $\sinh(\cdot)$  is the hyperbolic sine function, and the last equality holds after considering the hyperbolic trigonometric identity  $\cosh^2(\epsilon) - 1 = \sinh^2(\epsilon)$ . Since  $d_E^{(2)}(a, b)^2 = (x - \tilde{x})^2 + (y - \tilde{y})^2$ , we conclude that the atom  $b = (\tilde{x}, \tilde{y}, \tilde{z})$  belongs to  $B_{\mathbb{H}^3}(\epsilon, a)$  iff

$$(x - \tilde{x})^2 + (y - \tilde{y})^2 + (z \cosh(\epsilon) - \tilde{z})^2 < z^2 \sinh^2(\epsilon).$$

Notice that the previous equation describes the Euclidean ball centered at  $(x, y, z \cosh(\epsilon))$ , and with radius  $z \sinh(\epsilon) > 0$ ,  $B_E^{(3)}(\epsilon, a)$ .  $\square$

#### 6.4.2 The probability of two atoms being in cooperation

In this subsection, we present a result on which the whole analysis is based: *a tractable expression for the probability of two atoms being in cooperation*. For this task, fix  $a$  and  $b$ , two different atoms in  $\mathbb{H}^3$ , with respective resources  $z$  and  $\tilde{z}$ , and fix as well a control subset  $\mathcal{D}$ . Let

$$\begin{aligned} R &:= d_{\mathbb{H}^3}(a, b), \\ d &:= \sqrt{d_E^{(2)}(a, b)^2 + (z - \tilde{z})^2 \cosh^2(R)}, \\ r &:= z \sinh(R), \\ \tilde{r} &:= \tilde{z} \sinh(R), \\ c &:= z \cosh(R), \\ \tilde{c} &:= \tilde{z} \cosh(R), \\ h &:= \frac{(\tilde{r} - r + d)(r + \tilde{r} - d)}{2d}, \\ \tilde{h} &:= \frac{(r - \tilde{r} + d)(r + \tilde{r} - d)}{2d}, \\ \delta &:= \frac{\pi}{2} - a \sin\left(\frac{\tilde{c} - c}{d}\right), \\ \tilde{\delta} &:= \frac{\pi}{2} - a \sin\left(\frac{c - \tilde{c}}{d}\right). \end{aligned} \tag{6.4}$$

Notice that the variables  $R, d, r, \tilde{r}, c, \tilde{c}, h, \tilde{h}, \delta, \tilde{\delta}$ , are explicitly given as functions of  $d_E^{(2)}(a, b)$ ,  $z$  and  $\tilde{z}$ . We have the following result.

**Theorem 9.** *Let  $F : (0, \infty)^3 \rightarrow (0, \infty)$  be the measurable function, independent of the*

density  $\lambda$  and of the control set  $\mathcal{D}$ , given by the expression

$$\begin{aligned}
F(d_E^{(2)}(a, b), z, \tilde{z}) = & \\
& \lambda \pi \int_{-r}^r f(w+c)(r^2-w^2)dw - \lambda \int_{r-h}^r \int_0^{2\pi} \int_0^{\sqrt{r^2-w^2}} f(c+w\cos(\delta) - s\cos(\theta)\sin(\delta))sdsd\theta dw \\
& + \lambda \pi \int_{-r_2}^{r_2} f(w+\tilde{c})(\tilde{r}^2-w^2)dw - \lambda \int_{\tilde{r}-\tilde{h}}^{\tilde{r}} \int_0^{2\pi} \int_0^{\sqrt{\tilde{r}^2-w^2}} f(\tilde{c}+w\cos(\tilde{\delta}) - s\cos(\theta)\sin(\tilde{\delta}))sdsd\theta dw
\end{aligned} \tag{6.5}$$

Then,

$$\mathbb{P}^{a,b} \left( a \overset{\Phi, \mathcal{D}}{\leftrightarrow} b \right) = e^{-\lambda F(d_E^{(2)}(a,b), z, \tilde{z})} \mathbf{1}_{\{(z, \tilde{z}) \in \mathcal{D}\}} \tag{6.6}$$

For numerical purposes, it is fascinating to be able to calculate the expression  $\mathbb{P}^{a,b} \left( a \overset{\Phi, \mathcal{D}}{\leftrightarrow} b \right)$  only in function of the geographical distance between  $a$  and  $b$ , given by  $d_E^{(2)}(a, b)$ , and their corresponding available resources, given by  $z$  and  $\tilde{z}$ .

To prove the previous Theorem, we start by giving a purely geometric equivalence for the atoms  $a$  and  $b$  being in MNRR'. Consider the 3 dimensional Euclidean set

$$C(a, b) := B_E^{(3)}(R, a) \cup B_E^{(3)}(R, b). \tag{6.7}$$

We have the following Lemma

**Lemma 4.** *The probability of the atoms  $a$  and  $b$  being in MNRR is equal to*

$$\mathbb{P}^{a,b} \left( a \overset{\Phi, \mathcal{D}}{\leftrightarrow} b \right) = e^{-\Lambda(C(a,b))} \mathbf{1}_{\{(z, \tilde{z}) \in \mathcal{D}\}}, \quad \mathbb{P} - a.s., \tag{6.8}$$

where the measure  $\Lambda(\cdot)$  is given in equation (6.3), and  $\mathbb{P}^{a,b}$  is the two fold Palm measure of  $\Phi$ .

*Proof.* Suppose that the atoms  $a$  and  $b$  belong to a configuration  $\phi$ . The relation  $a \overset{\phi}{\rightarrow} b$  holds if, and only if, the Hyperbolic ball  $B_{\mathbb{H}^3}(R, a)$  is empty of atoms in  $\phi \setminus \{a\}$ . From Proposition 7, the latter happens if, and only if, the Euclidean ball  $B_E^{(3)}(R, a)$  is empty of atoms in  $\phi \setminus \{a\}$ . Thus, the relation  $a \overset{\phi, \mathcal{D}}{\leftrightarrow} b$  holds iff  $C(a, b)$  is empty of atoms in  $\phi \setminus \{a, b\}$ , and if  $(z, \tilde{z}) \in \mathcal{D}$ . Since  $\Lambda(\cdot)$  is the intensity measure of  $\Phi$ , after considering the empty space function of a PPP [BB09], we conclude that

$$\mathbb{P}^{a,b} \left( a \overset{\Phi, \mathcal{D}}{\leftrightarrow} b \right) = e^{-\Lambda(C(a,b))} \mathbf{1}_{\{(z, \tilde{z}) \in \mathcal{D}\}}, \quad \mathbb{P} - a.s.$$

□

Let us compare Lemma 1 (Chapter 4) with the previous Lemma. In Lemma 1, the two relevant balls lie in  $\mathbb{R}^2$ , they have the same radius, and their centers lie on the circumference

of each other. Furthermore, the intensity measure therein is actually the 2-dimensional Lebesgue measure. Hence, it is easy to compute the corresponding surface. On the other hand, in Lemma 4, we need to calculate the volume of  $C(a, b)$ , under the measure  $\Lambda(\cdot)$ . At this point, we only know that  $C(a, b)$  is the union of the 3-dimensional balls  $B_E^{(3)}(R, a)$  and  $B_E^{(3)}(R, b)$ , both having different radio, and their centers do not lie on the circumference of each other. Moreover, the intensity measure  $\Lambda(\cdot)$  is not the Lebesgue measure, which complicates the task. The subsection 6.4.7 is devoted to compute  $\Lambda(C(a, b))$ . Actually, we find that  $\Lambda(C(a, b)) = \lambda F(d_E(a, b), z, \bar{z})$ , where  $F(d_E(a, b), z, \bar{z})$  is given in equation (6.5).

### 6.4.3 Interference analysis

Theorem 9 allows to analyse the interference generated by the cooperative pairs, and single BSs. Their respective emitted signals, received at the typical user, correspond to directional BSs. That is, these signals depends on the positions of the group of BSs. For this duty, we use the projection map

$$\begin{aligned} \hat{\cdot} : \mathbb{H}^3 &\rightarrow \mathbb{R}^2 \\ a &\mapsto \hat{a} = (x, y) \end{aligned}$$

to obtain the 2-dimensional Euclidean position of every atom in  $\mathbb{H}^3$ . In this fashion, the letters  $\hat{a}$ ,  $\hat{b}$ , and  $\hat{c}$  denote elements of  $\mathbb{R}^2$ .

Via the dependent thinning defined in Section 6.3, we split the marked PPP  $\Phi$  into two new point processes.

**Definition 10.** *The process of singles and the process of cooperative pairs,  $\Phi^{(1)}$  and  $\Phi^{(2)}$ , are given by*

$$\begin{aligned} \Phi^{(1)} &:= \{a \in \Phi \mid a \text{ is single} \} \\ \Phi^{(2)} &:= \{a \in \Phi \mid a \text{ cooperates with another element of } \Phi \} \end{aligned}$$

Consider  $g : \mathbb{R}^2 \rightarrow [0, \infty)$  ( $k : \mathbb{R}^2 \times \mathbb{R}^2 \rightarrow [0, \infty)$ ), a generic random field, modeling the received signal to the typical user, emitted from a single (cooperative pair of) BS, as in Chapter 4. The interference fields generated by the processes of singles and pairs are denoted by

$$\begin{aligned} \mathcal{I}_g^{(1)} &:= \sum_{a \in \Phi^{(1)}} g(\hat{a}), \\ \mathcal{I}_k^{(2)} &:= \frac{1}{2} \sum_{a \in \Phi} \sum_{b \in \Phi \setminus \{a\}} k(\hat{a}, \hat{b}) \mathbf{1}_{\{a \overset{\Phi, \mathcal{P}}{\leftrightarrow} b\}}. \end{aligned} \tag{6.9}$$

The  $1/2$  in front of the summation in (6.9) prevents us from considering a pair twice.

In this section, for every two  $\hat{a}, \hat{b}$  in  $\mathbb{R}^2$ , we denote by  $d_E^{(2)}(\hat{a}, \hat{b})$  the two-dimensional Euclidean distance between them.

Applying the Campbell-Little-Mecke formula, Slivnyak-Mecke Theorem [BB09], and using the explicit expression provided by Theorem 9, we have the following result.

**Theorem 10.** *The expected value of the Interference generated by  $\Phi^{(1)}$  and  $\Phi^{(2)}$  is given by*

$$\begin{aligned}\mathbb{E} \left[ \mathcal{I}_g^{(1)} \right] &= 2\pi\lambda^2 \int_{\mathbb{R}^2} g(\hat{a}) d\hat{a} \int_0^\infty \left( 1 - \mathbb{E} \left[ e^{-\lambda F(s, Z, \tilde{Z})} \mathbf{1}_{\mathcal{D}}^{(Z, \tilde{Z})} \right] \right) s ds, \\ \mathbb{E} \left[ \mathcal{I}_k^{(2)} \right] &= \frac{\lambda^2}{2} \int_{\mathbb{R}^2} \int_{\mathbb{R}^2} k(\hat{a}, \hat{b}) \mathbb{E} \left[ e^{-\lambda F(d_E^{(2)}(\hat{a}, \hat{b}), Z, \tilde{Z})} \mathbf{1}_{\mathcal{D}}^{(Z, \tilde{Z})} \right] d\hat{a} d\hat{b},\end{aligned}\tag{6.10}$$

where  $Z$  and  $\tilde{Z}$  are two independent random variables, with common distribution  $f(z)dz$ , and  $F(s, z, \tilde{z})$  is defined in Theorem 9, equation (6.5).

*Proof.* Since the nearest neighbor is unique, for every atom  $a \in \Phi$ , we have that  $\mathbf{1}_{\{a \in \Phi^{(1)}\}} = \sum_{b \in \Phi \setminus \{a\}} \left( 1 - \mathbf{1}_{\{a \overset{\Phi, \mathcal{D}}{\leftrightarrow} b\}} \right)$ ,  $\mathbb{P}$ -a.s. Then,

$$\begin{aligned}\mathcal{I}_g^{(1)} &:= \sum_{a \in \Phi^{(1)}} g(\hat{a}), \\ &= \sum_{a \in \Phi} \sum_{b \in \Phi \setminus \{a\}} g(\hat{a}) \left( 1 - \mathbf{1}_{\{a \overset{\Phi, \mathcal{D}}{\leftrightarrow} b\}} \right), \quad \mathbb{P} - a.s.\end{aligned}$$

Using Campbell-Little-Mecke formula and Slivnyak-Mecke Theorem [BB09],

$$\begin{aligned}\mathbb{E} \left[ \mathcal{I}_g^{(1)} \right] &= \int_{\mathbb{H}^3} \int_{\mathbb{H}^3} \mathbb{E}^{a, b} \left[ g(\hat{a}) \left( 1 - \mathbf{1}_{\{a \overset{\Phi, \mathcal{D}}{\leftrightarrow} b\}} \right) \right] \Lambda(db) \Lambda(da) \\ &= \int_{\mathbb{H}^3} g(\hat{a}) \int_{\mathbb{H}^3} \left( 1 - \mathbb{P}^{a, b} \left( a \overset{\Phi, \mathcal{D}}{\leftrightarrow} b \right) \right) \Lambda(db) \Lambda(da).\end{aligned}$$

For two different atoms  $a$  and  $b$ , with marks  $z$  and  $\tilde{z}$ , respectively,

$$1 - \mathbb{P}^{a, b} \left( a \overset{\Phi}{\leftrightarrow} b \right) = 1 - e^{-\lambda F(d_E^{(2)}(a, b), z, \tilde{z})} \mathbf{1}_{\mathcal{D}}^{(z, \tilde{z})},$$

where  $F(s, z, \tilde{z})$  is defined in Theorem 9. After the change of variable to polar coordinates,

$$\begin{aligned}&\int_{\mathbb{H}^3} \left( 1 - \mathbb{P}^{a, b} \left( a \overset{\Phi}{\leftrightarrow} b \right) \right) \Lambda(db) \\ &= 2\pi\lambda \int_0^\infty \int_0^\infty \left( 1 - e^{-\lambda F(s, z, \tilde{z})} \mathbf{1}_{\mathcal{D}}^{(z, \tilde{z})} \right) s ds f(\tilde{z}) d\tilde{z} \\ &= 2\pi\lambda \int_0^\infty \left( 1 - \mathbb{E} \left[ e^{-\lambda F(s, z, \tilde{Z})} \mathbf{1}_{\mathcal{D}}^{(z, \tilde{Z})} \right] \right) s ds,\end{aligned}$$

where the last equality follows after considering a change of order of integration, and a random variable  $\tilde{Z}$ , with distribution  $f(z)dz$ . In the same fashion, consider a random

variable  $Z$ , independent of  $\tilde{Z}$ , with distribution  $f(z)dz$ , then

$$\begin{aligned} \mathbb{E} [\mathcal{I}_g^{(1)}] &= 2\pi\lambda^2 \int_{\mathbb{R}^2} g(\hat{a}) \int_0^\infty \left(1 - \mathbb{E} \left[ e^{-\lambda F(s, Z, \tilde{Z})} \mathbf{1}_{\mathcal{D}}^{(Z, \tilde{Z})} \right] \right) s ds d\hat{a} \\ &= 2\pi\lambda^2 \int_{\mathbb{R}^2} g(\hat{a}) d\hat{a} \int_0^\infty \left(1 - \mathbb{E} \left[ e^{-\lambda F(s, Z, \tilde{Z})} \mathbf{1}_{\mathcal{D}}^{(Z, \tilde{Z})} \right] \right) s ds. \end{aligned}$$

Again, using Campbell-Little-Mecke formula and Slivnyak-Mecke Theorem [BB09]

$$\begin{aligned} \mathbb{E} [\mathcal{I}_k^{(2)}] &= \frac{1}{2} \int_{\mathbb{H}^3} \int_{\mathbb{H}^3} \mathbb{E}^{a,b} \left[ k(\hat{a}, \hat{b}) \mathbf{1}_{\{a \overset{\Phi}{\leftrightarrow} b\}} \right] \Lambda(da) \Lambda(db) \\ &= \frac{1}{2} \int_{\mathbb{H}^3} \int_{\mathbb{H}^3} k(\hat{a}, \hat{b}) \mathbb{P}^{a,b} \left( a \overset{\Phi}{\leftrightarrow} b \right) \Lambda(da) \Lambda(db) \\ &= \frac{\lambda^2}{2} \int_{\mathbb{R}^2} \int_{\mathbb{R}^2} k(\hat{a}, \hat{b}) \mathbb{E} \left[ e^{-\lambda F(d_E^{(2)}(\hat{a}, \hat{b}), Z, \tilde{Z})} \mathbf{1}_{\mathcal{D}}^{(Z, \tilde{Z})} \right] d\hat{a} d\hat{b}. \end{aligned}$$

□

Notice that, to calculate the expected value of the interference generated by the process of singles, we need to compute the integral of  $g(\cdot)$  over  $\mathbb{R}^2$ , and then multiply it by another integral. However, to calculate the expected value of the interference generated by the process of cooperative pairs, we have to compute an integral over  $\mathbb{R}^2 \times \mathbb{R}^2$  of the function  $k(\cdot, \cdot)$  times another function that performs as a proportion of two points being in a cooperative pair.

#### 6.4.4 Intensity measure and the percentage of singles and pairs

Equation (6.6) is an expression for the probability of two given atoms being in cooperation. This expression is in function of their Euclidean distance and their corresponding available resources. Therefore, we can interpret Theorem 9 as a local result. We would like to go further, and give a global metric for the atoms in cooperative pairs, which does not depend on the position, similar to Corollary 2.

Denote by  $\mathcal{B}(\mathbb{R}^2)$  the Borel sigma-algebra, let  $M^{(1)}, M^{(2)} : \mathcal{B}(\mathbb{R}^2) \rightarrow [0, \infty)$  be the measures such that

$$\begin{aligned} M^{(1)}(A) &:= \mathbb{E} \left[ \sum_{a \in \Phi^{(1)}} \mathbf{1}_{\{\hat{a} \in A\}} \right], \\ M^{(2)}(A) &:= \mathbb{E} \left[ \sum_{a \in \Phi^{(2)}} \mathbf{1}_{\{\hat{a} \in A\}} \right], \end{aligned} \tag{6.11}$$

for every  $A \in \mathcal{B}(\mathbb{R}^2)$ . The number  $M^{(1)}(A)$  (respectively  $M^{(2)}(A)$ ) gives the average number of single (respectively cooperating) BSs, whose positions lie inside  $A$ . The following result gives an expression for the two preceding measures.

**Theorem 11.** *There exists a number  $P_{\mathcal{D}}(\lambda, f) \in [0, 1]$ , depending only on the density of the BSs  $\lambda$ , the density function of the marks  $f(z)$ , and the subset  $\mathcal{D}$ , such that, for every  $A \in \mathcal{B}(\mathbb{R}^2)$ ,*

$$\begin{aligned} M^{(1)}(A) &= (1 - P_{\mathcal{D}}(\lambda, f))\lambda\mathcal{S}^{(2)}(A), \\ M^{(2)}(A) &= P_{\mathcal{D}}(\lambda, f)\lambda\mathcal{S}^{(2)}(A). \end{aligned}$$

Furthermore,

$$P_{\mathcal{D}}(\lambda, f) = 2\pi\lambda \int_0^\infty \mathbb{E} \left[ e^{-\lambda F(s, Z, \tilde{Z})} \mathbf{1}_{\mathcal{D}}^{(Z, \tilde{Z})} \right] s ds, \quad (6.12)$$

where  $F(s, z, \tilde{z})$  is defined by Theorem 9, and  $Z$  and  $\tilde{Z}$  are two independent random variables, with common distribution  $f(z)dz$ .

*Proof.* Fix  $A \in \mathcal{B}(\mathbb{R}^2)$  and, for every  $a$  and  $b$  in  $\mathbb{H}^3$ , consider the function  $k(\hat{a}, \hat{b}) := 2\mathbf{1}_A^{\hat{a}}$ . Hence,

$$\begin{aligned} \mathcal{I}_k^{(2)} &= \frac{1}{2} \sum_{a \in \Phi} \sum_{b \in \Phi \setminus \{a\}} k(\hat{a}, \hat{b}) \mathbf{1}_{\{a \leftrightarrow b\}} \\ &= \sum_{a \in \Phi} \mathbf{1}_A^{\hat{a}} \sum_{b \in \Phi \setminus \{a\}} \mathbf{1}_{\{a \leftrightarrow b\}}, \\ &= \sum_{a \in \Phi^{(2)}} \mathbf{1}_{\{\hat{a} \in A\}}, \quad \mathbb{P} - a.s. \end{aligned}$$

where the preceding equality follows since the nearest neighbor is unique  $\mathbb{P}$ -a.s. Taking the expected value on the previous equation, we have that

$$M^{(2)}(A) = \mathbb{E} \left[ \mathcal{I}_k^{(2)} \right]. \quad (6.13)$$

On the other hand, applying Theorem 10 for this particular choice of  $k(\hat{a}, \hat{b})$ ,

$$\begin{aligned} \mathbb{E} \left[ \mathcal{I}_g^{(2)} \right] &= \lambda^2 \int_{\mathbb{R}^2} \mathbf{1}_{\hat{a} \in A} \left( \int_{\mathbb{R}^2} \mathbb{E} \left[ e^{-\lambda F(d_E^{(2)}(\hat{a}, \hat{b}), Z, \tilde{Z})} \mathbf{1}_{\mathcal{D}}^{(Z, \tilde{Z})} \right] d\hat{b} \right) d\hat{a} \\ &\stackrel{(a)}{=} \lambda^2 \int_{\mathbb{R}^2} \mathbf{1}_{\hat{a} \in A} \left( 2\pi \int_0^\infty \mathbb{E} \left[ e^{-\lambda F(s, Z, \tilde{Z})} \mathbf{1}_{\mathcal{D}}^{(Z, \tilde{Z})} \right] s ds \right) d\hat{a} \\ &= \lambda \int_{\mathbb{R}^2} \mathbf{1}_{\hat{a} \in A} d\hat{a} \left( \lambda 2\pi \int_0^\infty \mathbb{E} \left[ e^{-\lambda F(s, Z, \tilde{Z})} \mathbf{1}_{\mathcal{D}}^{(Z, \tilde{Z})} \right] s ds \right) \\ &= \lambda \mathcal{S}^{(2)}(A) \left( \lambda 2\pi \int_0^\infty \mathbb{E} \left[ e^{-\lambda F(s, Z, \tilde{Z})} \mathbf{1}_{\mathcal{D}}^{(Z, \tilde{Z})} \right] s ds \right), \end{aligned}$$

where equation (a) follows after considering the change of variable for polar coordinates. Define

$$P_{\mathcal{D}}(\lambda, f) := \lambda 2\pi \int_0^\infty \mathbb{E} \left[ e^{-\lambda F(s, Z, \tilde{Z})} \mathbf{1}_{\mathcal{D}}^{(Z, \tilde{Z})}(s) ds \right],$$

after considering equation (6.13), we have that

$$M^{(2)}(A) = P_{\mathcal{D}}(\lambda, f) \lambda \mathcal{S}^{(2)}(A).$$

Since the BSs locations follow a PPP with density  $\lambda$ ,

$$M^{(1)}(A) + M^{(2)}(A) = \lambda \mathcal{S}^{(2)}(A),$$

and then, the following identity holds

$$M^{(1)}(dxdy) = (1 - P_{\mathcal{D}}(\lambda, f)) \lambda dxdy.$$

We only have left to prove that  $P(\lambda, f)$  lies in  $[0, 1]$ . From the expression for  $P(\lambda, f)$ , it is clear that it is always positive. Further,

$$P_{\mathcal{D}}(\lambda, f) \lambda \mathcal{S}(A) = M^{(2)}(A) \leq \lambda \mathcal{S}(A),$$

for every  $A \in \mathcal{B}(\mathbb{R}^2)$ . This implies that  $P_{\mathcal{D}}(\lambda, f) \leq 1$ . □

Notice that the number  $P_{\mathcal{D}}(\lambda, f)$  does not depend on the surface  $A$ . The BS positions are modeled by a PPP, with intensity  $\lambda$ . Then, the previous Theorem states that the intensity of singles and cooperative pairs among the BSs is

$$\begin{aligned} (1 - P_{\mathcal{D}}(\lambda, f)) \lambda, \\ P_{\mathcal{D}}(\lambda, f) \lambda, \end{aligned}$$

respectively. Thus, the numbers  $(1 - P_{\mathcal{D}}(\lambda, f))$  and  $P_{\mathcal{D}}(\lambda, f)$  can interpret as a *the global proportion of singles and cooperative pairs*.

For numerical evaluation, notice that  $P_{\mathcal{D}}(\lambda, f)$  can be evaluated either (i) via Monte Carlo simulation, since

$$\mathbb{E} \left[ \mathbf{1}_{\mathcal{D}}^{(Z, \tilde{Z})} \int_0^\infty e^{-\lambda F(r, Z, \tilde{Z})} r dr \right] \approx \sum_{i=1}^N \frac{\mathbf{1}_{\mathcal{D}}^{(Z_i, \tilde{Z}_i)} \int_0^\infty e^{-\lambda F(r, Z_i, \tilde{Z}_i)} r dr}{N},$$

where  $(Z_i, \tilde{Z}_i)_{i=1}^N$  is an independent family of random vectors, with common distribution  $f(z)dz f(\tilde{z})d\tilde{z}$ , or (ii) via numerical integration, since

$$\mathbb{E} \left[ \mathbf{1}_{\mathcal{D}}^{(Z, \tilde{Z})} \int_0^\infty e^{-\lambda F(r, Z, \tilde{Z})} r dr \right] = \iint_{\mathcal{D}} \left( \int_0^\infty e^{-\lambda F(r, z, \tilde{z})} r dr \right) f(z) f(\tilde{z}) dz d\tilde{z}.$$

Until now, the parameters  $\lambda$  and  $f(z)$  have been presented as general. However, recall that the distribution of the marks  $f(z)dz$  models the resources of each BSs. Even if the resources do not depend on the position, they depend on the density  $\lambda > 0$  of the BSs : fixed a configuration of user, if the density is high (low), then we should expect that the resources are high (low) as well, and viceversa.

### 6.4.5 Proportion of singles and cooperative pairs

This subsection is devoted to study the class of cellular networks for which it is advisable to cluster the BSs with respect to their available resources, and the class of cellular networks for which the static criterion proposed in Chapter 4, by means only of Euclidean proximity, is enough.

We consider a density for the BSs  $\lambda = 1 [km^2]$ . For the following evaluations, we assume no extra constraint for the marks, that is, we choose  $\mathcal{D} = (0, \infty) \times (0, \infty)$ . From equations (6.5), (6.6), and (6.12), notice that the proportion of cooperative pairs depends strongly on the distribution of the marks. In Figure 6.3 we provide the numerical evaluation of  $P_{\mathcal{D}}(\lambda, f)$ . Specifically, in this example, the marks are distributed as a Beta random variable, with mean value  $\mu = 0.5$ . Recall that the Beta distribution is defined by its two first moments. The figure illustrates how *the percentage of stations in pair varies with the change of the variance of the marks*. Observe that, when the variance goes to zero, the value of  $P_{\mathcal{D}}(\lambda, f)$  tends to 0.6215, which is the average number of cooperative pairs in the strictly geometric model from Chapter 4 (see Theorem 3). On the other hand, when the variance is large, the value of  $P_{\mathcal{D}}(\lambda, f)$  differs from 0.6215 significantly.

To understand this better, suppose that  $\mu > 0$  is the mean value of the marks. If the variance is large, the available resources oscillate considerably around  $\mu$ . Equation (6.1) tells us that both the term involving the load balancing and the product of the available resources play a role in the formation of the cooperative pairs, instead of merely the Euclidean proximity between the BS positions, as in Chapter 4. On the other hand, consider a cellular network for which the available resources of the BSs do not vary considerably around  $\mu$ , that is, the resources are uniformly available throughout the network. Then, the load balancing term and the product of their available resources are practically constant in equation (6.1). Making clear that the 2-dimensional Euclidean distance between the BSs would be the most influential. In this case, we practically recover the model in Chapter 4.

### 6.4.6 Expected value of the interference field

This subsection is devoted to the evaluation of the integral expressions from Theorem 10. Since we are under a stationary framework, we suppose that the typical user is placed at the Euclidean origin  $\hat{0} := (0, 0)$ .

Given the position  $\hat{a}$  of a single BS, we suppose that it transmits a signal/interference  $s(\hat{a})$ , towards the typical user. For example, given a pathloss exponent  $\beta > 2$ , we can take  $s(\hat{a}) := \frac{1}{(d_E^{(2)}(\hat{a}, \hat{0}))^\beta}$ . Consider in equation (6.9) the function  $g(\hat{a}) := s(\hat{a})\mathbf{1}_{\{d_E^{(2)}(\hat{a}, \hat{0}) > R\}}$ , where  $R > 0$  is fixed. The indicator function serves to calculate the interference generated by the single BSs whose distance to the typical user is larger than  $R$ . The numerical evaluation of  $\mathbb{E}[\mathcal{I}_g^{(1)}]$ , using Theorem 10, is given in Figure 6.4. Notice that the expression in equation (6.10) gives almost identical results with the simulations.

To calculate the interference from pairs, we make the following choice of the function



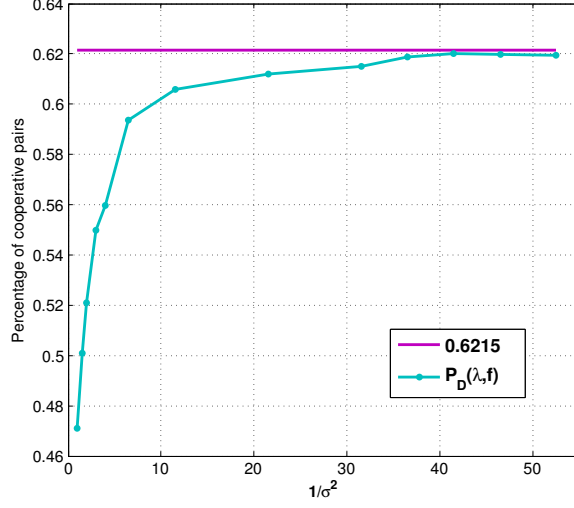


Figure 6.3: Percentage of cooperative pairs. The marks are Beta distributed, centered at 0.5, with different values for the variance  $\sigma^2$ .

$k(\cdot, \cdot)$ . For two BSs at 2-dimensional positions  $\hat{a}$  and  $\hat{b}$ , that form a cooperative pair, suppose that these transmit orthogonal signals, which are added at the typical user:  $s(\hat{a}) + s(\hat{b})$ . Given a pathloss exponent  $\beta > 2$ , we can take  $s(\hat{a}) := \frac{1}{(d_E^{(2)}(\hat{a}, \hat{0}))^\beta}$ . Then, consider in equation (6.9) the function

$$k(\hat{a}, \hat{b}) := s(\hat{a}) \mathbf{1}_{\{d_E^{(2)}(\hat{a}, \hat{0}) > R\}} + s(\hat{b}) \mathbf{1}_{\{d_E^{(2)}(\hat{b}, \hat{0}) > R\}},$$

where  $R > 0$  is fixed. After some calculations,

$$\mathbb{E}[I^{(2)}] = 2\pi\lambda^2 \int_{d(\hat{c}, \hat{0}) > R} s(\hat{c}) d\hat{c} \int_0^\infty \mathbb{E} \left[ e^{-\lambda \tilde{F}(s, Z, \tilde{Z})} \mathbf{1}_D^{(Z, \tilde{Z})} \right] s ds.$$

The numerical evaluation of  $\mathbb{E} \left[ I_k^{(2)} \right]$  is given in Figure 6.4. Again, the expression in equation (6.10) gives, as well, almost identical results with the simulations.

#### 6.4.7 The $\Lambda$ -volume of $C(a, b)$

The present subsection is devoted to compute the volume of  $C(a, b)$ , under the measure  $\Lambda(\cdot)$ , given by equation (6.3). This is the key point relating Lemma 4 with Theorem 9, on which the whole analysis is based.

As a starting point, we would like to reveal a little bit more on the topology of  $C(a, b)$ . From equation (6.4) and Figure 6.5, notice that:

- $d$  is the 3-dimensional Euclidean distance between the centers of  $B_E^{(3)}(R, a)$  and  $B_E^{(3)}(R, b)$ ,

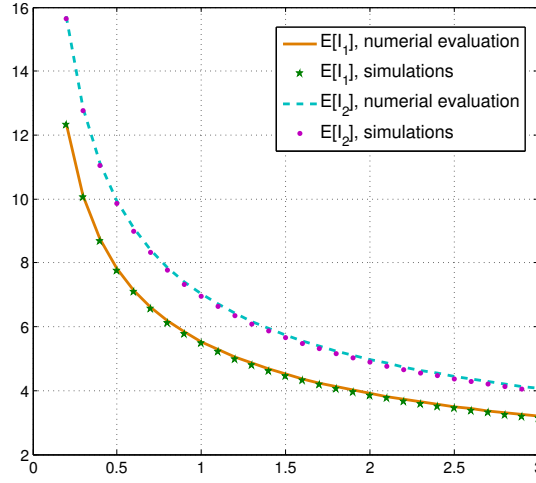


Figure 6.4: Expected value of the interference field generated by the singles and pairs, for  $\beta = 2.5$ . Numerical evaluations and simulations results.

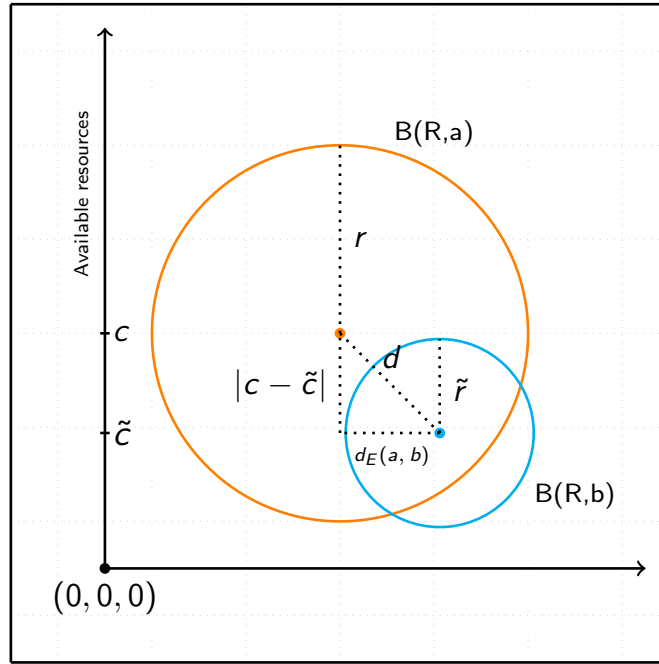


Figure 6.5: The set  $C(a, b)$ , along with its representative variables.

- $r$  and  $\tilde{r}$  are the correspondig radii of  $B_E^{(3)}(R, a)$  and of  $B_E^{(3)}(R, b)$ , and
- $c$  and  $\tilde{c}$  are the corresponding third coordinate of  $B_E^{(3)}(R, a)$  and  $B_E^{(3)}(R, b)$  centers.

We have the following result.

**Lemma 5.** *The 3 dimensional Euclidean balls  $B_E^{(3)}(R, a)$  and  $B_E^{(3)}(R, b)$  are never contained one within the other. Further, both balls always intersect each other, that is,  $C(a, b)$  is connected.*

*Proof.* The Euclidean ball  $B_E^{(3)}(R, a)$  is contained within  $B_E^{(3)}(R, b)$  if, and only if,  $d + r < \tilde{r}$ . Considering equation (6.4), the preceding inequality is equivalent to

$$d_E^{(2)}(a, b)^2 + (z - \tilde{z})^2 \cosh^2(R) < (\tilde{z} - z)^2 \sinh(R).$$

Since  $\cosh^2(R) \geq \sinh(R)$ , last inequality never holds. This implies that  $B_E^{(3)}(R, a)$  is never contained inside  $B_E^{(3)}(R, b)$ . By symmetry,  $B_E^{(3)}(R, b)$  is never contained within  $B_E^{(3)}(R, a)$  either.

From Figure 6.5, notice that the balls  $B_E^{(3)}(R, a)$  and  $B_E^{(3)}(R, b)$  intersect each other if, and only if,  $r + \tilde{r} > d$ . Considering the values of  $r, \tilde{r}, d$ , and using the identity  $\cosh^2(\epsilon) - 1 = \sinh^2(\epsilon)$ , the previous inequality is equivalent to

$$(z + \tilde{z})^2 (\cosh^2(R) - 1) > d_E^{(2)}(a, b)^2 + (z - \tilde{z})^2 \cosh^2(R).$$

For general values of  $z, \tilde{z}, R, d_E^{(2)}(a, b) > 0$ , this inequality does not always hold: choose small values of  $z, \tilde{z}$ , and  $R$ , and a large value of  $d_E^{(2)}(a, b)$ . In our particular situation,  $R$  is the hyperbolic distance between  $a$  and  $b$  (see equation 6.1). Hence,  $r + \tilde{r} > d$  holds if, and only if,

$$\begin{aligned} (z + \tilde{z})^2 \left( \left( \frac{d_E^{(2)}(a, b)^2}{2z\tilde{z}} + \frac{1}{2} \left( \frac{z}{\tilde{z}} + \frac{\tilde{z}}{z} \right) \right)^2 - 1 \right) \\ > d_E^{(2)}(a, b)^2 + (z - \tilde{z})^2 \left( \frac{d_E^{(2)}(a, b)^2}{2z\tilde{z}} + \frac{1}{2} \left( \frac{z}{\tilde{z}} + \frac{\tilde{z}}{z} \right) \right)^2 \end{aligned}$$

After some simple manipulations, the previous inequality is equivalent to

$$3(z - \tilde{z})^2 + \frac{d_E^{(2)}(a, b)^2}{2z\tilde{z}} + d_E^{(2)}(a, b)^2 \left( 2 \left( \frac{z}{\tilde{z}} + \frac{\tilde{z}}{z} \right) - 1 \right) + \frac{(z - \tilde{z})^4}{z\tilde{z}} > 0.$$

Since  $2 \left( \frac{z}{\tilde{z}} + \frac{\tilde{z}}{z} \right) > 2$ , the preceding inequality always holds.  $\square$

The previous Lemma and the inclusion-exclusion principle imply that

$$\Lambda(C(a, b)) = \Lambda(B_E^{(3)}(R, a)) + \Lambda(B_E^{(3)}(R, b)) - \Lambda(B_E^{(3)}(R, a) \cap B_E^{(3)}(R, b)). \quad (6.14)$$

The next Proposition computes  $\Lambda(B_E^{(3)}(R, a))$  and  $\Lambda(B_E^{(3)}(R, b))$ .

**Proposition 8.** *The volume of  $B_E^{(3)}(R, a)$  and  $B_E^{(3)}(R, b)$  under the measure  $\Lambda(\cdot)$ , given by equation (6.3), is*

$$\begin{aligned} \Lambda(B_E^{(3)}(R, a)) &= \lambda\pi \int_{-r}^r f(w + c)(r^2 - w^2)dw, \\ \Lambda(B_E^{(3)}(R, b)) &= \lambda\pi \int_{-\tilde{r}}^{\tilde{r}} f(w + \tilde{c})(\tilde{r}^2 - w^2)dw. \end{aligned} \quad (6.15)$$

*Proof.* Notice that the measure  $\Lambda(\cdot)$  is invariant under translations and rigid transformations, with respect to the  $xy$ -axis. Hence, we can suppose that  $a = (0, 0, z)$ , in particular,  $B_E^{(3)}(R, a)$  is centered at  $(0, 0, c)$ . Consider  $\tau : \mathbb{R}^3 \rightarrow \mathbb{R}^3$ , the translation sending  $(0, 0, c)$  to the origin. Then,  $\tau(B_E^{(3)}(R, a))$  is a 3-dimensional Euclidean ball, centered at the origin, with radius  $r$ . Given that  $|D\tau^{(-1)}| = 1$  (the absolute value of the Jacobian), the Lebesgue change of variable Theorem [Rud87, Th. 2.26] states that

$$\begin{aligned}\Lambda(B_E^{(3)}(R, b)) &= \iiint_{B_E^{(3)}(R, a)} \lambda f(w) dx dy dw \\ &= \iiint_{\tau(B_E^{(3)}(R, a))} \lambda f(w + c) dx dy dw.\end{aligned}$$

The set  $\tau(B_E^{(3)}(R, a))$  can be described in cylindrical coordinates. Thus,

$$\begin{aligned}\Lambda(B_E^{(3)}(R, a)) &= \lambda \int_{-r}^r \int_0^{2\pi} \int_0^{\sqrt{r^2 - w^2}} f(w + c) s ds d\theta dw \\ &= \lambda 2\pi \int_{-\tilde{r}}^r f(w + c) \int_0^{\sqrt{r^2 - w^2}} s ds dw \\ &= \lambda \pi \int_{-r}^r f(w + c) (r^2 - w^2) dw.\end{aligned}$$

In the same fashion,

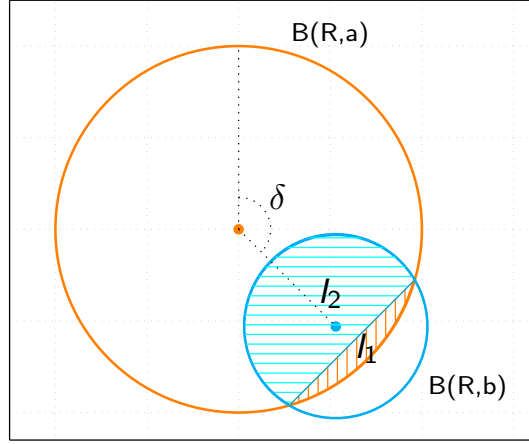
$$\Lambda(B_E^{(3)}(R, b)) = \lambda \pi \int_{-\tilde{r}}^{\tilde{r}} f(w + \tilde{c}) (\tilde{r}^2 - w^2) dw.$$

□

We only have left to calculate  $\Lambda(B_E^{(3)}(R, a) \cap B_E^{(3)}(R, b))$ .

**Proposition 9.** *The volume of  $B_E^{(3)}(R, a) \cap B_E^{(3)}(R, b)$  under the measure  $\Lambda(\cdot)$ , given by equation (6.3), is*

$$\begin{aligned}\Lambda(B_E^{(3)}(R, a) \cap B_E^{(3)}(R, b)) &= \lambda \int_{r-h}^r \int_0^{2\pi} \int_0^{\sqrt{r^2 - w^2}} f(c + w \cos(\delta) - s \cos(\theta) \sin(\delta)) s ds d\theta dw \\ &\quad + \lambda \int_{\tilde{r}-\tilde{h}}^{\tilde{r}} \int_0^{2\pi} \int_0^{\sqrt{\tilde{r}^2 - w^2}} f(\tilde{c} + w \cos(\tilde{\delta}) - s \cos(\theta) \sin(\tilde{\delta})) s ds d\theta dw.\end{aligned}\tag{6.16}$$

Figure 6.6: The angle  $\delta$  and the subsets  $I_1$  and  $I_2$ .

*Proof.* The measure  $\Lambda(\cdot)$  is invariant under translations and rigid transformations, with respect to the  $xy$ -axis. Then, we can suppose  $a = (0, 0, z)$  and  $b = (d_E^{(2)}(a, b), 0, \tilde{z})$ . In particular,  $B_E^{(3)}(R, a)$  and  $B_E^{(3)}(R, b)$  are centered at  $(0, 0, c)$  and  $(d_E^{(2)}(a, b), 0, \tilde{c})$ , respectively. Denote by  $I_1$  ( $I_2$ ) the lens defined by the intersection of  $B_E^{(3)}(R, a)$  ( $B_E^{(3)}(R, b)$ ) with  $B_E^{(3)}(R, b)$  ( $B_E^{(3)}(R, a)$ ) (See Figure 6.6). Since  $\Lambda(\cdot)$  is absolutely continuous with respect to the Lebesgue measure,

$$\Lambda(B_E^{(3)}(R, a) \cap B_E^{(3)}(R, b)) = \Lambda(I_1) + \Lambda(I_2).$$

To compute  $\Lambda(I_1)$ , we consider the transformation that rotates  $\delta$ -degrees the vector described by the centers of the balls about the  $x - z$  axis (see Figure 6.6),

$$R_\delta = \begin{pmatrix} \cos(\delta) & 0 & -\sin(\delta) \\ 0 & 1 & 0 \\ \sin(\delta) & 0 & \cos(\delta) \end{pmatrix}.$$

Given the position of the centers,  $\delta := \arcsin\left(\frac{c - \tilde{c}}{d}\right) + \frac{\pi}{2}$ . Consider  $\tau : \mathbb{R}^3 \rightarrow \mathbb{R}^3$ , the translation sending  $(0, 0, c)$  to the origin, and define  $T : \mathbb{R}^3 \xrightarrow{R_\delta} \mathbb{R}^3 \xrightarrow{\tau} \mathbb{R}^3$ . Since  $|DT^{(-1)}| = 1$ , the Lebesgue change of variable Theorem [Rud87, Th. 2.26] states that

$$\begin{aligned} \Lambda(I_1) &= \iiint_{I_1} \lambda f(w) dx dy dw \\ &= \iiint_{T(I_1)} \lambda f(c + w \cos(\delta) - x \sin(\delta)) dx dy dw, \end{aligned}$$

where the last equality follows from the fact that

$$(x, y, w) \xrightarrow{T^{(-1)}} (x \cos(\delta) + w \sin(\delta), y, c + w \cos(\delta) - x \sin(\delta))$$

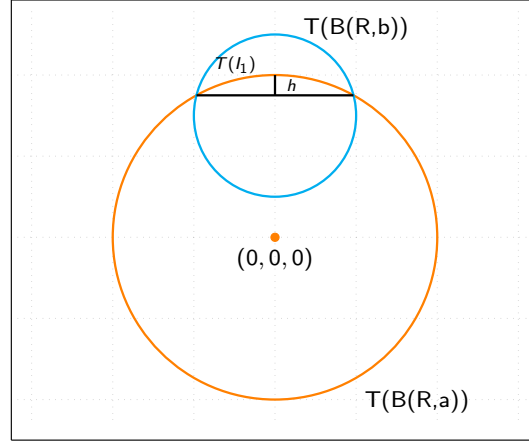


Figure 6.7: The height  $h$  of the lens  $T(I_1)$ , and the sets  $T(B_E^{(3)}(R, a))$ , and  $T(B_E^{(3)}(R, b))$ .

Remark that we can describe  $T(I_1)$  in cylindrical coordinates (see Figure 6.7). Therefore,

$$\begin{aligned} \Lambda(I_1) &= \lambda \int_{r-h}^r \int_0^{2\pi} \int_0^{\sqrt{r^2-w^2}} f(c + w \cos(\delta) - s \cos(\theta) \sin(\delta)) \, ds \, d\theta \, dw, \end{aligned}$$

where  $h = \frac{(\tilde{r}-r+d)(r+\tilde{r}-d)}{2d}$  is the height of the lens defined by  $I_1$  (see the Appendix). In the same fashion,

$$\begin{aligned} \Lambda(I_2) &= \lambda \int_{\tilde{r}-\tilde{h}}^{\tilde{r}} \int_0^{2\pi} \int_0^{\sqrt{\tilde{r}^2-w^2}} f(\tilde{c} + w \cos(\tilde{\delta}) - s \cos(\theta) \sin(\tilde{\delta})) \, ds \, d\theta \, dw, \end{aligned}$$

where

$$\begin{aligned} \tilde{h} &:= \frac{(r - \tilde{r} + d)(r + \tilde{r} - d)}{2d}, \\ \tilde{\delta} &:= \frac{\pi}{2} - a \sin\left(\frac{c - \tilde{c}}{d}\right). \end{aligned}$$

□

To give an expression for  $C(a, b)$ , we only need to consider equation (6.14), and the expressions for  $\Lambda(B_E^{(3)}(R, a))$ ,  $\Lambda(B_E^{(3)}(R, b))$ , and  $\Lambda(B_E^{(3)}(R, b) \cap B_E^{(3)}(R, a))$  from equations (6.15) and (6.16).

## 6.5 Conclusions

In this Chapter, we proposed a novel grouping criterion of BSs, resulting in single BSs and cooperative pairs. To form the cooperative pairs, the criterion favors the BSs which are geographically close, and, at the same time, have both enough resources. In this way, their cooperation is meaningful and beneficial. When the BSs are modeled by a PPP, an analysis of the probability of two BSs being in a cooperative pair is provided, followed by an interference analysis. In particular, for cellular networks where the available resources of the BSs vary a lot, the cooperative pairs differs considerably from the purely geometrically model from Chapter 4. On the other hand, for cellular networks where the available resources of the BSs stay almost constant throughout the network, the cooperative pairs of both model are practically the same.

## 6.6 Additional material

### 6.6.1 Uniqueness of the hyperbolic nearest neighbor

Let  $\Phi$  be a point process stationary point process on  $\mathbb{R}^2$ , with density  $0 < \lambda < \infty$ , independently marked over  $(0, \infty)$ , and whose marks have  $f(z)dz$  as their common distribution. Its intensity measure  $\Lambda(\cdot)$  has the same representation as in equation (6.3) [BB09]. Consider the mapping

$$\begin{aligned} \mathbb{H}^3 \times \mathbb{H}^3 &\rightarrow \mathbb{H}^3 \\ (b, a) &\mapsto (b \ominus a) \end{aligned}$$

such that, for every two atoms  $a = (x, y, z)$  and  $b = (\tilde{x}, \tilde{y}, \tilde{z})$ ,  $(b \ominus a) = (\tilde{x} - x, \tilde{y} - y, \tilde{z})$ . Notice that this mapping is not symmetric. Fixed  $a \in \mathbb{H}^3$ , for every simple and locally finite configuration  $\phi = \{b_n\}_{n=1}^\infty$ , we consider the following notation as in [BB09]

$$\phi - a := \{b_n \ominus a\}_{n=1}^\infty, \quad (6.17)$$

Suppose that  $a, b, c$  are three different atoms in  $\Phi$ . The stationarity of the process allows us to consider  $a = (x, y, z)$ ,  $b = (\tilde{x}, \tilde{y}, \tilde{z})$ , and  $c = (0, 0, z^*)$ . In particular,

$$\begin{aligned} d_{\mathbb{H}^3}(a, c) &= \frac{x^2 + y^2}{2zz^*} + \frac{1}{2} \left( \frac{z}{z^*} + \frac{z^*}{z} \right) \\ d_{\mathbb{H}^3}(b, c) &= \frac{\tilde{x}^2 + \tilde{y}^2}{2\tilde{z}z^*} + \frac{1}{2} \left( \frac{z^*}{\tilde{z}} + \frac{\tilde{z}}{z^*} \right) \\ &= \frac{(\tilde{x} - x + x)^2 + (\tilde{y} - y + y)^2}{2\tilde{z}z^*} + \frac{1}{2} \left( \frac{z^*}{\tilde{z}} + \frac{\tilde{z}}{z^*} \right) \end{aligned}$$

Hence, the equality  $d_{\mathbb{H}^3}(a, c) = d_{\mathbb{H}^3}(b, c)$  holds if, and only if,

$$\frac{x^2 + y^2}{z} - \frac{(\tilde{x} - x + x)^2 + (\tilde{y} - y + y)^2}{\tilde{z}} = z^* \left( \frac{z}{z^*} + \frac{z^*}{z} - \left( \frac{z^*}{\tilde{z}} + \frac{\tilde{z}}{z^*} \right) \right) \quad (6.18)$$

Let  $\alpha : \mathbb{H}^3 \times \mathbb{H}^3 \rightarrow \mathbb{H}^3$  and  $\beta : \mathbb{H}^3 \times \mathbb{H}^3 \times \mathbb{H}^3 \rightarrow \mathbb{H}^3$  be two functions such that, for every  $a = (x, y, z)$ ,  $b = (\tilde{x}, \tilde{y}, \tilde{z})$ , and  $c = (x^*, y^*, z^*)$ ,

$$\begin{aligned}\alpha(a, b) &:= \frac{x^2 + y^2}{z} - \frac{(\tilde{x} + x)^2 + (\tilde{y} + y)^2}{\tilde{z}}, \\ \beta(a, b, c) &:= z^* \left( \frac{z^*}{\tilde{z}} + \frac{\tilde{z}}{z^*} - \frac{z}{z^*} - \frac{z^*}{z} \right).\end{aligned}\tag{6.19}$$

From equation (6.18) and equation (6.19),  $d_{\mathbb{H}^3}(a, c) = d_{\mathbb{H}^3}(b, c)$  happens if, and only if,  $\alpha(a, b \ominus a) - \beta(a, b, c) = 0$ . Let

$$\begin{aligned}\mathcal{B} &:= \{\text{There exist different } a, b, c \in \Phi, \text{ such that } d_{\mathbb{H}^3}(a, c) = d_{\mathbb{H}^3}(b, c)\} \\ &= \{\text{There exist different } a, b, c \in \Phi, \text{ such that } \alpha(a, b \ominus a) - \beta(a, b, c) = 0\} \\ &\stackrel{(a)}{=} \bigcup_{a \in \Phi} \bigcup_{b \in \Phi} \bigcup_{c \in \Phi} \{(b \hat{\ominus} a) \neq 0, (c \hat{\ominus} a) \neq 0, b \neq c, \alpha(a, b \ominus a) - \beta(a, b, c) = 0\}, \mathbb{P} - a.s.\end{aligned}$$

where (a) follows after considering that the distribution of the available resources is absolutely continuous. This representation of  $\mathcal{B}$  is the one that allows us to prove that  $\mathbb{P}(\mathcal{B}) = 0$ . For this task, consider the application such that, for every  $a \in \mathbb{H}^3$  and every simple, and locally finite cofiguration  $\phi$  on  $\mathbb{H}^3$ ,

$$g(a, \phi) := \sum_{b \in \phi} \sum_{c \in \phi} \mathbf{1}_{\{\hat{b} \neq 0, \hat{b} \neq 0, b \neq c, \alpha(a, b) - \beta(a, b, c) = 0\}}.\tag{6.20}$$

In particular,

$$\begin{aligned}g(a, \phi - a) &= \sum_{b \in \phi - a} \sum_{c \in \phi - a} \mathbf{1}_{\{\hat{b} \neq 0, \hat{b} \neq 0, b \neq c, \alpha(a, b) - \beta(a, b, c) = 0\}} \\ &\stackrel{(a)}{=} \sum_{b \in \phi} \sum_{c \in \phi} \mathbf{1}_{\{(b \hat{\ominus} a) \neq 0, (c \hat{\ominus} a) \neq 0, b \neq c, \alpha(a, b \ominus a) - \beta(a, b, c) = 0\}},\end{aligned}\tag{6.21}$$

where (a) follows from equation (6.17), and from the fact that the function  $\beta(a, b, c)$  only depends on the resources of the atoms, not on their position. Denote by  $\mathbb{E}^0$  the Palm



measure of  $\Phi$ . Hence, the reduced Campbell's formula gives

$$\begin{aligned}
\mathbb{P}(\mathcal{B}) &= \mathbb{P}\left(\bigcup_{a \in \Phi} \bigcup_{b \in \Phi} \bigcup_{c \in \Phi} \{(b \hat{\ominus} a) \neq 0, (c \hat{\ominus} a) \neq 0, b \neq c, \alpha(a, b \ominus a) - \beta(a, b, c) = 0\}\right) \\
&= \mathbb{E}\left[\mathbf{1}_{\bigcup_{a \in \Phi} \bigcup_{b \in \Phi} \bigcup_{c \in \Phi} \{(b \hat{\ominus} a) \neq 0, (c \hat{\ominus} a) \neq 0, b \neq c, \alpha(a, b \ominus a) - \beta(a, b, c) = 0\}}\right] \\
&\leq \mathbb{E}\left[\sum_{a \in \Phi} \sum_{b \in \Phi} \sum_{c \in \Phi} \mathbf{1}_{\{(b \hat{\ominus} a) \neq 0, (c \hat{\ominus} a) \neq 0, b \neq c, \alpha(a, b \ominus a) - \beta(a, b, c) = 0\}}\right] \\
&\stackrel{(a)}{=} \mathbb{E}\left[\int_{\mathbb{H}^3} g(a, \Phi - a) \Phi(da)\right] \\
&= \int_{\mathbb{H}^3} \mathbb{E}^0[g(a, \Phi)] \Lambda(da) \\
&\stackrel{(b)}{=} \int_{\mathbb{H}^3} \mathbb{E}^0\left[\sum_{b \in \Phi} \sum_{c \in \Phi} \mathbf{1}_{\{\hat{b} \neq 0, \hat{c} \neq 0, b \neq c, \alpha(a, b) - \beta(a, b, c) = 0\}}\right] \Lambda(da) \\
&\stackrel{(c)}{=} \mathbb{E}^0\left[\sum_{b \in \Phi} \sum_{c \in \Phi} \int_{\mathbb{H}^3} \mathbf{1}_{\{\hat{b} \neq 0, \hat{c} \neq 0, b \neq c, \alpha(a, b) - \beta(a, b, c) = 0\}} \Lambda(da)\right],
\end{aligned}$$

where (a) follows from equation (6.21), (b) follows from equation (6.20), and (c) after considering Tonelli's Theorem.

For fixed  $b$  and  $c$ , from equation (6.19), notice that the transformation  $a \mapsto \alpha(a, b) - \beta(a, b, c) = 0$  defines a 2-dimensional surface in  $\mathbb{H}^3$ . Since  $\Lambda(\cdot)$  is absolutely continuous with respect to the Lebesgue measure, then, for every  $a \in \mathbb{H}^3$ ,

$$\begin{aligned}
0 &= \Lambda(\{a \mid \alpha(a, b) - \beta(a, b, c) = 0\}) \\
&= \int_{\mathbb{H}^3} \mathbf{1}_{\{\hat{b} \neq 0, \alpha(a, b) - \beta(a, b, c) = 0\}} \Lambda(da).
\end{aligned}$$

We conclude that  $\mathbb{P}(\mathcal{B}) = 0$ .

### 6.6.2 The height of a lens

For this subsection, capital letters denote points in the Euclidean space, and small letters denote length of segments.

Let  $\tau_1$  and  $\tau_2$  be two Euclidean spheres, both intersecting each other (see Figure 6.8). Suppose that their respective centers,  $A$  and  $B$ , and their respective radii,  $r$  and  $r'$ , are known. In particular, the value of  $d$  (the length of the segment  $\overline{AB}$ ) is known as well. Denote by  $h$  the length of the upper height of the lens described by the Intersection of  $\tau_1$  and  $\tau_2$  (again, see Figure 6.8). The aim of this subsection is to give an expression for  $h$  in function of  $r$ ,  $r'$ , and  $d$ .

Denote by  $\triangle ABC$  the 2-dimensional Euclidean triangle defined by  $A$ ,  $B$ , and  $C$ , and by  $(ABC)$  its 2-dimensional Euclidean surface. Observe that the segment  $\overline{CD}$  is the height of





# Generalisation for clusters larger than pairs, a discussion

## Abstract

This final Chapter is devoted to discuss a way to generalise the cluster formation for larger groups. The model proposed is an extension of the MNNR, with maximum clustersize larger than 2. It is constructed iteratively: At each iteration, it adds to each cluster the best possible atom, according to the nearest neighbor criterion, in case it exists. The resulting cooperative groups are subclusters of the NNM, and are easily simulated. Allowing to obtain results via simulations.

## 7.1 The $K$ -NNM

The model proposed in this Section is called the *Kth-Nearest Neighbor Model* ( $K$ -NNM). It is generated (i) by means of proximity between the BSs, (ii) independently of the BS density, and (iii) with a fixed maximum clustersize, denoted by  $K \geq 2$ . The corresponding clusters consist of, at most,  $K$  atoms connected by their respective nearest neighbors. The rest remain single.

The MNNR, as discussed in Chapter 3, is the best criterion to form clusters, with the above properties, for a maximum clustersize 2. For  $K > 2$ , we generate the clusters of  $K$ -NNM iteratively. The idea is simple: we add, at most, one of the remaining single atoms to each one of the clusters from  $(K - 1)$ -NNM. In this way, the new clusters have, at most,  $K$  atoms. The appropriate choice of the single atom being added to a given cluster guarantees its closeness to the rest of atoms conforming this cluster, independently of the BS density. Having said that, now we explain the choice of the single atom being added. Let  $A_{K-1}$  be the set of single atoms, for the  $(K - 1)$ -NNM. Given a cooperative cluster from the  $(K - 1)$ -NNM,  $B = \{x_1, \dots, x_m\}$ , in particular,  $m \leq K - 1$ . Consider the single atoms whose nearest neighbor is an element of  $B$ . We add to  $B$  the one that is closer to its nearest neighbor, in case it exists. Otherwise,  $B$  remains the same. The algorithm is described as follows:

1. Let

$$C := \{x \in A \mid \text{an element of } B \text{ is the nearest neighbor of } x\}$$

2. If  $C = \emptyset$ , there are no more nearest neighbors to add to this cluster. **Return**  $B$ .

3. Otherwise,  $C$  must be finite, since the configurations we consider are locally finite. Suppose that  $C = \{y_1, \dots, y_l\}$ .

- Consider the vector  $\hat{v} = (v_1, \dots, v_l)$ , where the entry  $v_i$  is the distance from  $y_i$  to its nearest neighbor:

$$v_i := \min_{j=1, \dots, m} \|x_j - y_i\|$$

- Let  $j := \operatorname{argmin}_{i=1, \dots, l} v_i$ , the index of the element of  $C$  with the minimum distance to its nearest neighbor.

- **Return**  $B \cup \{y_j\}$ .

Notice that we have chosen the best single atom for  $B$  to be added, according to the nearest neighbor criterion. Since the nearest neighbor is independent of the BS density, the new cluster is independent of the BS density as well. Moreover, being the nearest neighbor unique, the resulting clusters are always the same, no matter the order on which we implement the algorithm to the different clusters of the  $(K-1)$ -NNM. Thus, besides this procedure being the most natural way to enlarge the clusters, it generates a unique family of cooperative clusters, with the desired properties, and a new set of single BSs.

Figure 7.1 shows a deployment of BSs, and the evolution of the  $K$ -NNM, for different the values of  $K$ . The clusters are connected with lines, according to the nearest neighbor criterion, where the dashed lines indicate the single point being added during the current iteration. Notice that from  $K = 7$  the set of single atoms is empty, implying that for  $K > 7$ ,  $K$ -NNM is the same as 7-NNM.

## 7.2 Properties

Given a finite configuration, let us consider the corresponding  $K$ -NNM, for different values of  $K$ . Notice that, after a finite number of iteration ( $K$ ), there are no more single points to add. Therefore, there exists  $K^* \geq 2$ , such that, for every  $K \geq K^*$ , the clusters of  $K$ -NNM and  $K^*$ -NNM are the same. Moreover, for this finite configuration, for every  $K \geq K^*$  the corresponding clusters of  $K$ -NNM and those from the NNM coincide.

However, the latter does not hold always for infinite configurations: Consider a PPP and denote by  $\rho(n)$  the probability of having a cluster from the NNM with, at least,  $n$  atoms. The authors in [KMN06] prove that, there exist constants  $C_1, C_2, N^* \in (0, \infty)$  such that,

$$e^{-C_1 n \log(n)} \leq \rho(n) \leq e^{-C_2 n \log(n)}, \text{ for } n \geq N^*. \quad (7.1)$$

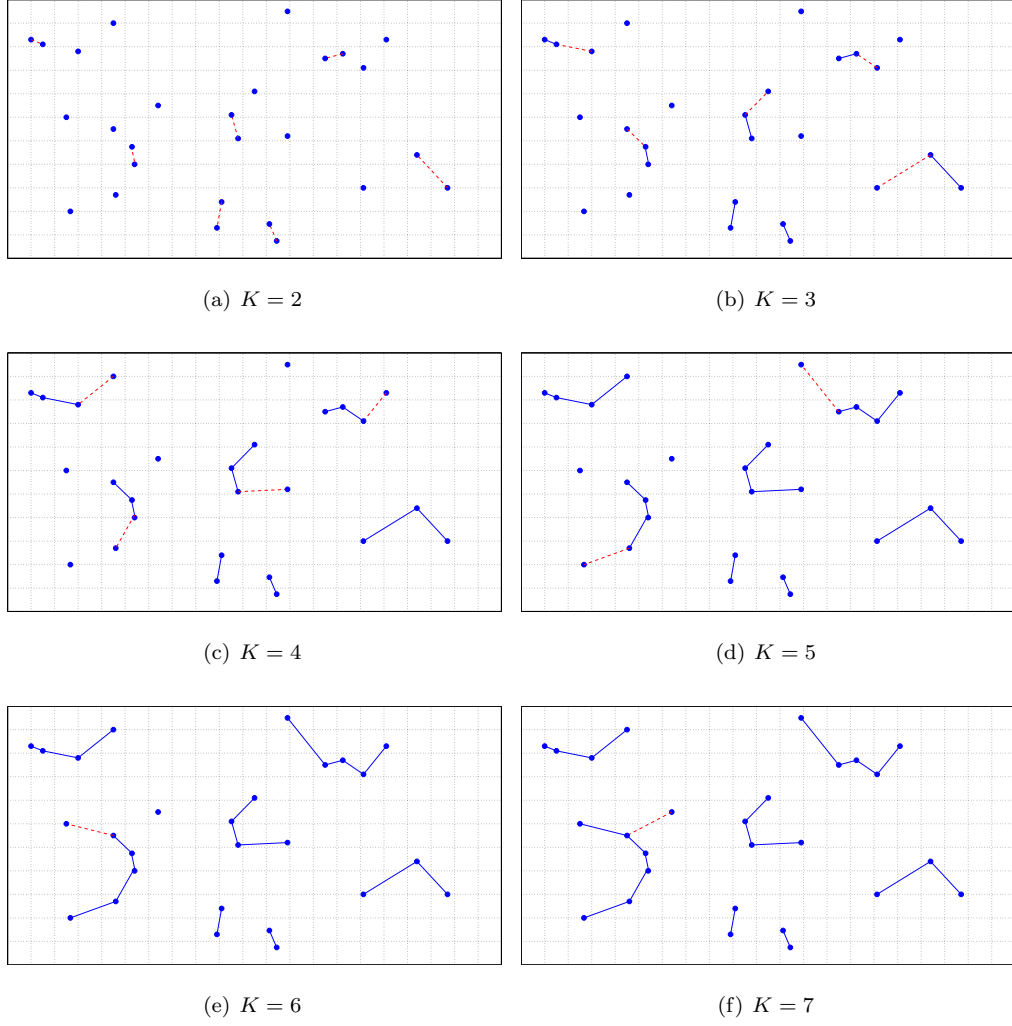


Figure 7.1: A deployment of atoms (blue dots) and the cooperative clusters generated by the corresponding  $K$ -NNM.

Hence, there exists a cluster from the NNM, with at least  $N$  atoms with positive probability. If  $N > K$ , this cluster, evidently, does not belong to the  $K$ -NNM. On the other hand, given  $N > 2$ , by definition, every cooperative cluster from the NNM with exactly  $N$  atoms belongs to  $K$ -NNM, for every  $K \geq N$ . Thus, for the PPP, we would expect that  $K$ -NNM converges towards the NMM, as  $K$  goes to infinity.

From equation (7.1) notice that, for the NNM of a PPP, the probability of having large clusters goes to zero exponentially. Table 7.2 shows the expected proportion of singles, pairs, triplets, etc., for different values of  $K \geq 2$ . The results, obtained via simulations, are independent of the BS density. Notice that, from  $K = 9$ , there are practically no more single points to add. Hence, for  $K > 9$ , the percentage of clusters having at least 10 atoms is practically zero. Notice also that, for large values of  $K$ , most of the clusters have size 3, followed by those of size 4 and size 2.

$K$	1	2	3	4	5	6	7	8	9	10
2	38%	63%	0%	0%	0%	0%	0%	0%	0%	0%
3	18%	23%	59%	0%	0%	0%	0%	0%	0%	0%
4	8%	23%	28%	41%	0%	0%	0%	0%	0%	0%
5	3%	23%	28%	22%	24%	0%	0%	0%	0%	0%
6	2%	23%	28%	22%	14%	12%	0%	0%	0%	0%
7	1%	23%	28%	22%	14%	7%	5%	0%	0%	0%
8	1%	23%	28%	22%	14%	7%	3%	2%	0%	0%
9	0%	23%	28%	22%	14%	7%	3%	1%	1%	0%
10	0%	23%	28%	22%	14%	7%	3%	1%	1%	0%

### 7.3 Non tractability of the $K$ -NNM and related problems

The results from table 7.2 were obtained via simulations, due to the lack of tractability of the expressions of the model. Indeed, let us consider a fixed  $K > 2$ , the position of  $K$  atoms, and a point configuration. These  $K$  atoms belong to a cooperative group of size  $K$  from the  $K$ -NNM, with respect to this configuration, if, and only if,

- (1) The  $K$  atoms are connected between them via its nearest neighbor, and
- (2) each one of the  $K$  balls, centered at each atom and whose radius is the distance to its nearest neighbor, is empty of atoms from the configuration.

To dig a little bit more into the analysis, let us deal first with property (1). Figure 7.2 shows two random sets of  $K = 6$  atoms for which (1) does not hold. Actually, as opposed to the case  $K = 2$ , for larger values of  $K$ , the property (1) is not always fulfilled, complicating a lot the analysis from the beginning. Hence, given the position of  $K$  atoms, we need to verify if these fulfill property (1). In case they do not, the required probability is zero,

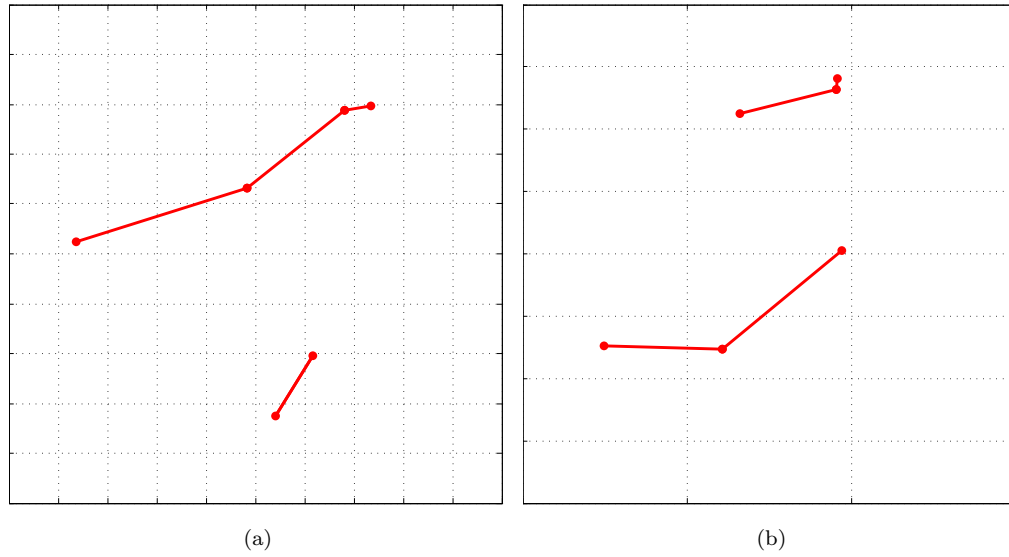


Figure 7.2: Two different sets of  $K = 6$  atoms, for which the property (1) does not hold. (a) None of the atoms from the pair in MNNR are the nearest neighbor of the remaining atoms. Hence, this pair is not connected to the rest. (b) The atoms of each triplet have their nearest neighbor within the same group. Hence, the atoms of one triplet are not connected with those from the other triplet.



otherwise, we proceed to deal with property (2). Figure 7.3 shows two random deployment of  $K = 6$  atoms, for which (1) holds, and the corresponding balls. Notice that the planar area, defined by the union of the balls, depends strongly on the position of the atoms, and not only on their relative distance. A difficulty presented for every  $K > 2$ . The empty space function of a PPP allows to give a theoretical representation, similar to the one in equation (6.8), of the required probability. Until now, however, there is no known method to obtain a tractable expression of the union of  $K > 2$  balls, with different radii and centers lying on the circumference of one of the other atoms. As opposed to the case  $K = 2$ , for which it was an easy task (see Lemma 1), or to the analysis in subsection 6.4.7, a little more arduous, yet feasible.

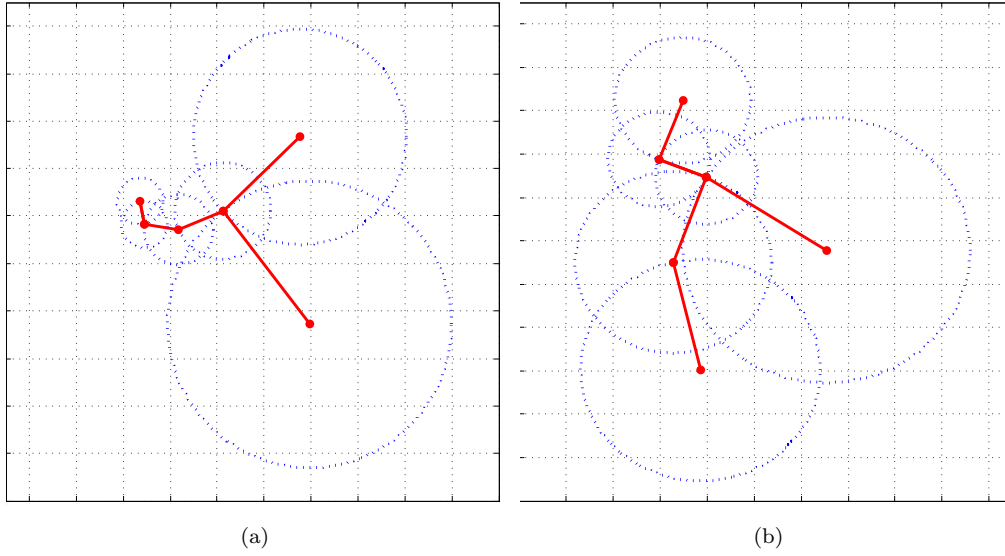


Figure 7.3: Two different sets of  $K = 6$  atoms, for which the property (1) holds. Each atom with its corresponding nearest neighbor ball.

As if this were not sufficient, additionally, for  $1 < k \leq K$ , the analysis to compute the probability of  $k$  given atoms being in a cooperative cluster of size  $k$  is even more complicated. For instance, consider  $K = 3$  and  $k = 2$ . Given the positions of two atoms, these two belong to a cooperative pair if, and only if,

- (i) they are in MNNR,
- (ii) no other atom of the configuration has as one of these two as its nearest neighbor.

The task of describing when these two properties hold is analogous to the proof of Proposition 3: to find the required probability, we must find the conditional probability of an intricate set, conditioned to the fact that two balls are empty. The latter makes the required duty harder than the case  $k = K$ , described above.

From the above discussion, we conclude that, for  $K > 2$ , a similar analysis as those from Chapter 4 and Chapter 5, are very complicated, if not impossible. Thus, the only known way to study cooperative networks, following the  $K$ -NNM, is via simulations. The algorithm described in Section 7.1, even though being computationally expensive, it is quite useful. For instance, to obtain the proportion of cooperative clusters from table 7.2. These percentages are closely related to the *generation number* and the *ancestor number*, concepts introduced in [KMN06, Gio16]. The authors study the PDF of these numbers and generate upper and lower bounds. Although the bounds are not tight, their computation represents a profound insight to the problem's geometrical nature and, probably, it is the only way to obtain analytical results.

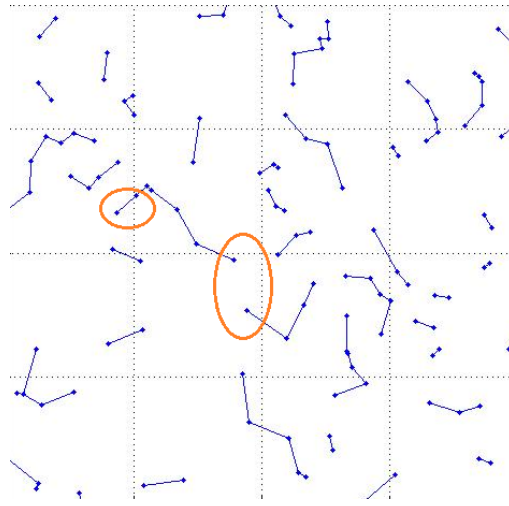


Figure 7.4: A deployment of atoms (blue dots) and the cooperative clusters generated by the corresponding  $K$ -NNM, for  $K = 9$ .

Another problem presented in the  $K$ -NNM is that, for large values of  $K$ , the model allows the formation of clusters which are questionable for our particular purposes. Figure 7.4 shows a deployment of BSs, and the cooperative clusters generated by the  $K$ -NNM, for  $K = 9$ . There are two clusters highlighted, one with 7 atoms, denoted by  $C_1$ , and the other one with 4 atoms, denoted  $C_2$ . Notice that there are atoms in  $C_1$  closer to  $C_2$  than to other atoms in  $C_1$ . The same situation is presented in other clusters within the same Figure. This is explained since the atoms within a cluster are connected by each atom nearest neighbor. Hence, the atoms within a large cluster do not necessarily need to be close to each other. The best way to prevent this inconvenient is keeping a low maximum clustersize. Figure 7.5 shows the same deployment of atoms, with the clusters generated by the  $K$ -NNM, for  $K = 3$  and  $K = 4$ . For these lower values of  $K$ , this inconvenience is less present for  $K = 4$ , and practically nonexistent for  $K = 3$ .

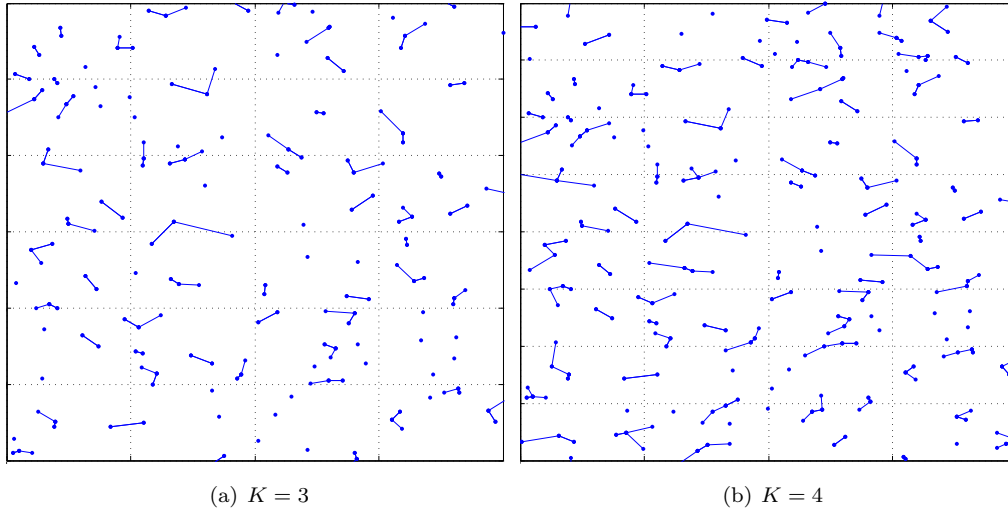


Figure 7.5: A deployment of atoms (blue dots) and the cooperative clusters generated by the corresponding  $K$ -NNM, for (a)  $K = 3$  (b) and  $K = 4$ .

## 7.4 Conclusions

In this Chapter, we presented a clustering criterion, generalizing the MNMR, with maximum clustersize  $K > 2$ . It is constructed by enlarging the pairs of mutually nearest neighbors, according to the nearest neighbor criterion. The corresponding groups are subclusters of the NNM. In spite of the lack of tractability of the model, it is possible to obtain results via simulations. These results could serve to study cooperative networks with large clusters, formed according to proximity. The later along with the implementation of different cooperation schemes for the cooperative groups, could reveal even greater potentials.

# General conclusions

## 8.1 Summary

This thesis focus in four different modes, based on node proximity, for the study of cooperative networks.

- We started by proposing a clustering methodology to generate cooperative pairs of BSs in MNNR, and the rest of the BSs remain single. When a point process models the BS positions, this dependent thinning results into the process of singles and the process of cooperative pairs. We provided structural properties for both of them, mostly when the original point process is a PPP. Each one of the expressions for these results presents different challenges for its numerical tractability. This is due to the fact that the thinning defining the singles and pairs strongly depends on the configuration. All the analysis constitute a novel toolbox towards the understanding and analysis of static cooperative networks.
- With the aid of the results from the former model, it is possible to provide a complete analysis of the coverage probability. We proposed an alternative model that imitates the structure of the single atoms and cooperative pairs. It allows to obtain explicit and tractable formulas of the coverage probability, for two different user-to-BS associations. Compared with non cooperative case, the coverage benefits of the model can reach a 15% of absolute gain. Different cooperative schemas resulted in different coverage benefits. Meaning that the coverage benefits depend on the clustering criterion and the signals emitted by the cooperative clusters.
- We modified the MNNR. To create the cooperative pairs, the new criterion favors the BSs which are geographically close and, at the same time, have both enough resources for their cooperation being meaningful. When the BSs are modeled by a PPP, an analysis of such cooperative networks is provided. In particular, if the resources of the BSs do not vary, the cooperative pairs from this model and those from the purely geometry model are practically the same. On the other hand, if the resources of the BSs vary considerably, the corresponding pairs between both models differ.

- Finally, we presented a clustering criterion, with maximum clustersize larger than 2. It is constructed by enlarging the pairs of mutually nearest neighbors, adding the best single point, according to the nearest neighbor criterion. Until now, the only way to obtain results is via simulations. The lack of tractability of the model is due to overlapping circles throughout the analysis, a complication presented all over the thesis.

## 8.2 Future work

The models proposed along the thesis leave a lot of open windows, being for generalize the ideas, apply them, or both.

### The MNNR for larger classes of cellular networks

To apply a similar analysis to other classes of point processes, we should be able to obtain a similar result to Lemma 1, under the correspondings two-fold Palm probability and empty space function. The first choice is, of course, the non-stationary PPP, with an intensity measure absolutely continuous with respect to the Lebesgue measure. In this way, the corresponding singles and cooperative are well defined (Corollary 1). Moreover, the Campbell-Litte-Mecke formula and Slyvniak Theorem allow us to obtain the non-stationary versions of Lemma 1, Theorem 3, Theorem 6, Corollary 2, and Theorem 8. Similar results to the rest of the ones presented in Chapter 4, however, are more complicated. For example, Theorem 4 uses the stationary structure of the process. Additionally, a coverage analysis for such cooperative networks, as the one from Chapter 5, it is for sure more tricky. On the other hand, the MNNR with resource constraints should requires a much more detailed analysis, since Chapter 7 relies completely on the stationarity of the BS positions.

For the Ginibre point process, we could use the results in [Gol10, DZH15] about its Palm measure and empty space function. The expressions will not be as tractable as in the PPP case, but still numerically feasible.

## Dimensioning

An interesting question, that arises naturally, is about the resources block of the BSs, for cellular networks under the MNNR, compared with the non-cooperative case. Since the MNNR is based on node proximity, a good start would be a local approach, describing cells of mutually nearest neighbors serving some users, and make the analysis considering different cooperation schemes.

### **Robustness of the model**

The pathloss exponent is the most significative parameter in our model. In real life situations, it is difficult to calibrate. Under specific propagation environments, we only know the ranges where it lies. Thus, it is imperative to analyse if our model is robust, to protect an operator wanting to use the MNNR, against the error of estimation.

### **Larger dimensions**

The model presented in Chapter 7 gives a first insight of whether or not it is useful/meaningful to consider the MNNR in spaces larger than the 2-dimensional Euclidean space. The distance to form the cooperative pairs was crucial to answer this question. It would be interesting, as well, to take the direction proposed by the authors in [BGRS98].

### **Other application fields**

The theory of point process and stochastic geometry has a wide interaction with other branches of mathematics and applied sciences. Thus, it would be interesting to study the benefits of the MNNR for theoretical purposes or for other applied fields than telecommunications. Since proximity is important everywhere, we are sure that the possible gains are countless.



# Appendix

## 9.1 List of publications

- *Analyzing Interference from Static Cellular Cooperation using the Nearest Neighbor Model.* Anastasios Giovanidis, Luis David Alvarez Corrales, Laurent Decreusefond. WIOPT-SPASWIN 2015, Mumbai, India.
- *Coverage Gains from the Static Cooperation of Mutually Nearest Neighbours.* Luis David Alvarez Corrales, Anastasios Giovanidis, Philippe Martins. IEEE GLOBE-COM, 2016, Washington D.C., USA.
- *Analysis of Static Cellular Cooperation between Mutually Nearest Neighboring Nodes.* Luis David Alvarez Corrales, Anastasios Giovanidis, Philippe Martins, Laurent De-creusefond. Submitted Journal paper, arXiv:1611.02614v1.
- *Wireless Node Cooperation with Resource Availability Constraints.* Luis David Alvarez Corrales, Anastasios Giovanidis, Philippe Martins, Laurent De-creusefond. WIOPT-SPASWIN 2017, Paris, France.



## 9.2 Table of Abbreviations

Abbreviation	Explanation
BS	Base Station
CCDF	The tail probability distribution functions
CoMP	Coordinated Multipoint
C-RAN	Centralized-RAN
HetNet	Heterogeneous Network
LLM	Lilypond Model
MIMO	Multiple-Input Multiple-Output
NNM	Nearest Neighbor Model
PDF	The probability density function
PPP	Poisson Point Process
RRG	Random Geometri Graph
SINR	Signal-to-Interference-plus-Noise-Ratio
r.v.	Random variable

### 9.3 Table of Figures

Figure	Page	Explanation
1.1	8	A deployment of BSs (blue dots) and users (asterisks). (a) Each user is served by all the surrounding BSs around a fixed radio. (b) Each user is served by its three closest BSs.
1.2	9	A deployment of BSs (blue dots) and users (asterisks). The BSs lying within a square-area belong to a cooperative cluster. A user is served by the cluster defined by the square-area where it is placed.
1.3	10	A deployment of BSs (blue dots) and the clusters defined by the RGG for two different values of $R$ . The value for $R$ in (a) is smaller than the corresponding value of $R$ in (b) .
1.4	12	A deployment of BSs (blue dots) and the clusters defined by the (a) LLM and (b) NNM.
1.5	15	Consider a static clustering criterion forming cooperative pairs of mutually nearest neighbors, and the rest of the atoms remain single. (a) The atoms $a$ and $b$ belong to a cooperative pair, since $a$ is the nearest neighbor of $b$ , and $b$ is the nearest neighbor of $a$ . Since $a$ is the nearest neighbor of $c$ , but $c$ is not the nearest neighbor of $a$ , then $c$ remains single. (b) If $a$ and $b$ serve a large number of users, the asterisks, the available remaining resources of both are low. If $c$ does not serve as many users, it has a considerable amount of unused resources. Since $c$ is close to $a$ , their alternative cooperation can allow users of $a$ to be partly served from both $a$ and $c$ , while the signals from $c$ can be sufficiently strong, due to proximity.
2.1	21	A deployment of BSs (blue dots) and the clusters defined by the NNM. The atoms connected by the red-dashed lines are the mutually nearest neighbors.
2.2	23	A deployment of BSs (blue dots) and the corresponding NNM. The atoms connected by the red-dashed lines are the pair of mutually nearest neighbors within each one of the clusters defined by the NNM.
4.1	32	(Up) The atoms $x$ and $y$ are mutually nearest neighbors, so, they work in pair. The atom $x$ is the nearest neighbor of $w$ , but $w$ is not the closest atom to $x$ , thus $w$ is single. (Down) A Poisson realisation with its corresponding Voronoi diagram. The asterisks are the single BSs, the connected dots are the cooperating pairs.
4.2	35	Figures (a) and (b) show, respectively, the hexagonal grid model without perturbation and with the center being perturbed after a random experiment. On the other hand, figures (c) and (d) present, respectively, in the vertical axis the average percentages of singles and pairs, for the hexagonal grid model, against different values for the parameter $Q > 0$ in the horizontal axis.

Figure	Page	Explanation
4.3	40	(a) The J function of the processes $\Phi^{(1)}$ . (b) The J function of the processes $\Phi^{(2)}$ .
4.4	46	Expected value of the interference generated by the single atoms, outside a radius $R$ , (b) and by the cooperative pairs, outside a radius $R$ .
4.5	46	The LT for the (a) process of singles and (b) the process of cooperative pairs.
5.1	50	Two cooperating BSs, where $r$ and $Z_r$ are their distances from the origin, and $W$ is the distance between them.
5.2	56	Closeness of the approximation between the superposition and the Nearest Neighbor model, $\beta = 3$ . (a) Fixed transmitter and (b) closest transmitter.
5.3	56	Validity of the analysis for the superposition model for the fixed single transmitter. (a) $\beta = 2.5$ (b) $\beta = 4$ .
5.5	62	The real random variables $R_2$ , $Z_2$ , and $W$ .
6.1	70	The MNNR (a) without constraints vs (b) with constraints.
6.2	70	Different types of constraints.
6.3	80	Percentage of cooperative pairs. The marks are Beta distributed, centered at 0.5, with different values for the variance $\sigma^2$ .
6.4	81	Expected value of the interference field generated by the singles and pairs, for $\beta = 2.5$ . Numerical evaluations and simulations results.
6.5	81	The set $C(a, b)$ , along with its representative variables.
6.6	84	The angle $\delta$ and the subsets $I_1$ and $I_2$ .
6.7	85	The height $h$ of the lens $T(I_1)$ , and the sets $T(B_E^{(3)}(R, a))$ , and $T(B_E^{(3)}(R, a))$ .
6.8	89	The angle $\delta$ and the subsets $I_1$ and $I_2$ .
7.1	93	A deployment of atoms (blue dots) and the cooperative clusters generated by the corresponding $K$ -NNM.
7.2	95	Two different sets of $K = 6$ atoms, for which the property (1) does not hold. (a) None of the atoms from the pair in MNNR is the nearest neighbor of the remaining atoms. Hence, this pair is not connected to the rest of the atoms. (b) The atoms of each triplet have their nearest neighbor within the same group. Hence, the atoms of one triplet are not connected with those from the other one.
7.3	96	Two different sets of $K = 6$ atoms, for which the property (1) holds. Each atom with its corresponding ball.
7.4	97	A deployment of atoms (blue dots) and the cooperative clusters generated by the corresponding $K$ -NNM, for $K = 9$ .

## 9.4 Table of Symbols

Symbol	Explanation
$\phi$	Simple, locally finite, point configuration
$\Phi$	Point Process
$\mathbb{R}^d$	$d$ -dimensional Euclidean space
$\ \cdot\ _d$	$d$ -dimensional Euclidean distance
$\operatorname{argmin}$	Arguments of the minimum
$x \xrightarrow{\phi} y$	The atom $y$ is the nearest neighbor of $x$ , with respect to the configuration $\phi$
$\mu^p(\mathbb{R}^d)$	The space of point configuration over $\mathbb{R}^d$
$\mathbb{P}^{x!}$	Palm measure
$\mathbb{E}^{x!}$	The expected value under the Palm measure $\mathbb{P}^{x!}$
$\emptyset$	The empty set
$\mathcal{M}^{n \times n}(\mathbb{R})$	the space of square matrices.
$\mathcal{S}^{(2)}(\cdot)$	The 2-dimensional Euclidean surface.
$B_E^{(3)}(x, r)$	2-dimensional Euclidean ball, centered at $x$ , and radius $r > 0$ .
$\stackrel{(d)}{=}$	Equality in distribution.
$\mathbb{H}^3$	The 3-dimensional hyperbolic half-space.
$d_{\mathbb{H}^3}(a, b)$	The 3-dimensional hyperbolic distance between $a$ and $b$ .
$d_E^{(2)}(a, b)$	The 2-dimensional distance between the position of $a$ and $b$ .
$B_{\mathbb{H}^3}(\epsilon, a)$	The hyperbolic ball, centered at $a$ , with radius $\epsilon$ .
$B_E^{(3)}(\epsilon, a)$	The 3-dimensional Euclidean ball described by $B_{\mathbb{H}^3}(\epsilon, a)$ .
$\mathcal{B}(\mathbb{R}^2)$	The Borel sigma-algebra.



# Bibliography

- [ABG11] J. G. Andrews, F. Baccelli, and R. K. Ganti. A Tractable Approach to Coverage and Rate in Cellular Networks. *IEEE Trans. on Communications*, 59(11):3122–3134, 2011.
- [ACGM16] L. David Álvarez Corrales, A. Giovanidis, and P. Martins. Coverage Gains from the Static Cooperation of Mutually Nearest Neighbours. *IEEE Globecom*, 2016.
- [ACGMD16] L. David Álvarez Corrales, A. Giovanidis, P. Martins, and L. Decreusefond. Analysis of Static Cellular Cooperation between Mutually Nearest Neighboring Nodes. *arXiv:1611.02614*, 2016.
- [ADC16] M. Afshang, H.S. Dhillon, and P.H.J. Chong. Fundamentals of Cluster-Centric Content Placement in Cache-Enabled Device-to-Device Networks. *IEEE Trans. on Communications*, 2016.
- [AH13] S. Akoum and R. W. Heath. Interference Coordination: Random Clustering and Adaptive Limited Feedback. *IEEE Trans. on Signal Processing*, 61(7):1822–1834, 2013.
- [Arn92] V. Arnol’d. *Ordinary Differential Equations*. Springer-Verlag, third edition, 1992.
- [Bad07] A.J. Baddeley. *Spatial Point Processes and their Applications*. Lecture Notes in Mathematics: Stochastic Geometry, Springer Verlag ,Berlin Heidelberg, 2007.
- [BB03] F. Baccelli and P. Brémaud. *Elements of Queueing Theory*. Springer, second edition edition, 2003.
- [BB09] F. Baccelli and B. Błaszczyszyn. *Stochastic Geometry and Wireless Networks, Volume I — Theory*, volume 3, No 3–4 of *Foundations and Trends in Networking*. NoW Publishers, 2009.
- [BEE96] J. Beem, P. Ehrlich, and K. Easley. *Global Lorentzian Geometry*. Chapman & Hall/CRC, 1996.
- [BG15] F. Baccelli and A. Giovanidis. A Stochastic Geometry Framework for Analyzing Pairwise-Cooperative Cellular Networks. *IEEE Trans. on Wireless Communications*, 14(2):794–808, 2015.
- [BGRS98] K. Beyer, J. Goldstein, R. Ramakrishnan, and U. Shaft. *When Is “Nearest Neighbo” Meaningful?* Lecture Notes in Computer Science. Springer, 1998.
- [BK15] B. Błaszczyszyn and H. P. Keeler. Studying the SINR Process of the Typical User in Poisson Networks Using its Factorial Moment Measures. *IEEE Trans. on Information Theory*, 61(12):6774–6794, 2015.
- [BKF14] P. Buchholz, J. Kriege, and I. Felko. *Input Modeling with Phase-Type Distributions and Markov Models: Theory and Applications*. Springer, 2014.

- [BKK15] B. Blaszczyszyn, M. K. Karray, and H. P. Keeler. Wireless networks appear Poissonian due to strong shadowing. *IEEE Transaction on Wireless Communication*, 2015.
- [BP14] M. Brandonjić and W. Perkins. On Sharp Thresholds in Random Geometric Graphs. *arXiv:1308.1084v2 [math.PR]*, 2014.
- [CCY<sup>+</sup>15] A. Checko, H. Christiansen, Y. Yan, L. Scolari, G. Kardaras, M. S. Berger, and L. Dittmann. Cloud RAN for Mobile Networks—A Technology Overview. *IEEE Communications Surveys and Tutorials*, 17:405–426, 2015.
- [CHC14] A. Checko, H. Holm, and H. Christiansen. Optimizing small cells deployment by the use of C-RANs. *European Wireless 2014*, 2014.
- [Cox69] H.S.M. Coxeter. *Introduction to Geometry*. John Wiley & Sons, Inc, 2nd edition, 1969.
- [dBCvKO08] M. de Berg, O. Cheong, M. van Kreveld, and M. Overmars. *Computational Geometry: Algorithms and Applications*. Springer-Verlag, 3rd rev. ed. 2008.
- [DFMTT12] L. Decreusefond, E. Ferraz, P. Martins, and V. Thanh-Tung. Robust methods for LTE and WiMAX dimensioning. *Valuetools*, pages 74–82, 2012.
- [DGBA12] H.S. Dhillon, R.K. Ganti, F. Baccelli, and J.G. Andrews. Modeling and analysis of K-tier downlink heterogeneous cellular networks. *IEEE JSAC*, vol. 30, no. 3, pp. 550–560, Apr., 2012.
- [DST16] L. Decreusefond, M. Schulte, and C. Thäle. Functional Poisson approximation in Kantorovich-Rubinstein distance with applications to U-statistics and stochastic geometry. *Annals of Probability*, 44, 2016.
- [DV15] L. Decreusefond and A. Vasseur. Asymptotics of superposition of point processes. *Geometry of Science Information*, October 2015.
- [DZH15] N. Deng, W. Zhou, and M. Haenggi. The Ginibre Point Process as a Model for Wireless Networks With Repulsion. *IEEE Transactions on Wireless Communications*, 14, 2015.
- [EGM98] J. Elstrodt, F. Grunewald, and J. Mennicke. *Groups Acting on Hyperbolic Space*. Springer, 1998.
- [GHH<sup>+</sup>10] D. Gesbert, S. Hanly, H. Huang, S. Shamai-Shitz, O. Simeone, and W. Yu. Multi-Cell MIMO Cooperative Networks: A New Look at Interference. *IEEE JSAC*, 28(9), 2010.
- [Gio16] A. Giovanidis. How to group wireless nodes together? *arXiv:1602.03906v1*, 2016.
- [GKB12] A. Giovanidis, J. Krolkowski, and S. Brueck. A 0-1 program to form minimum cost clusters in the downlink of cooperating base stations. In *WCNC*, pages 940–945, 2012.
- [Gol10] A. Goldman. The Palm measure and the Voronoi tessellation for the Ginibre process. *The Annals of Probability*, 20(1):90–128, 2010.
- [GS62] D. Gale and L.S. Shapley. College Admissions and the Stability of Marriage. *The American Mathematical Monthly*, 69, no. 1:9–15, Jan. 1962.
- [GZHZ16] Anjin Guo, Yi Zhong, M. Haenggi, and Wenyi Zhang. The Gauss-Poisson Process for Wireless Networks and the Benefits of Cooperation. In *IEEE Trans. on Wireless Communications*, 2016.

- [HA11] H. Huang and J. Andrews. A Stochastic Geometry Approach to Coverage in Cellular Networks With Multi-Cell Cooperation. *Global Telecommunications Conference*, 2011.
- [HL08] P. Henry-Labordère. *Analysis, Geometry, and Modeling in Finance*. Chapman & Hall/CRC, 2008.
- [HM96] O. Häggström and R. Meester. Nearest neighbour and hard sphere models in continuum percolation. *Wiley Random Struct. Alg.*, 9(3):295–315, 1996.
- [IDM<sup>+</sup>11] R. Irmer, H. Droste, P. Marsch, S. Brueck, H. P. Mayer, L. Thiele, and V. Jungnickel. Coordinated Multipoint: Concepts, Performance, and Field Trials Results. *IEEE Communications Magazine*, 49:102–111, 2011.
- [Irv85] R.W. Irving. An efficient algorithm for the "stable roommates" problem. *Journal of Algorithms*, 6:577–595, 1985.
- [JJT<sup>+</sup>08] V. Jungnickel, S. Jaeckel, L. Thiele, L. Jiang, U. Krüger, A. Brylka, and C. Helmont. Capacity Measurements in a Cooperative MIMO Network. *IEEE Transactions on Vehicular Communications*, 58:2392 – 2405, Jun 2008.
- [JMZ<sup>+</sup>14] V. Jungnickel, K. Manolakis, W. Zirwas, B. Panzner, V. Braun, M. Lossow, M. Sternad, Apelfröjd R., and T. Svensson. The Role of Small Cells, Coordinated Multipoint, and Massive MIMO in 5g. *IEEE Communications Magazine*, 52(44-51), 2014.
- [Kal84] Olav Kallenberg. *Random Measures*. Academic Pr, 1984.
- [Ker13] P. Kerret. *Transmission coopérative dans les réseaux sans-fil avec feedback distribué*. Réseaux et télécommunications, Télécom ParisTech, 2013.
- [KG13] P. Kerret and D. Gesbert. CSI Sharing Strategies for Transmitter Cooperation in Wireless Networks. *IEEE Wireless Communications*, 20:43–49, 2013.
- [KMN06] I. Kozakova, R. Meester, and S. Nanda. The size of components in continuum nearest-neighbor graphs. *The Annals of Probability*, 34, no.2:528–538, 2006.
- [KPK<sup>+</sup>10] D. Krioukov, F. Papadopoulos, M. Kitsak, A. Vahdat, and M. Boguñá. Hyperbolic Geometry of Complex Networks. *Phys Rev E*, 82:036106, 2010.
- [LAL16] M. Lyazidi, N. Aitsaadi, and R. Langar. Dynamic resource allocation for Cloud-RAN in LTE with real-time BBU/RRH assignment. *IEEE International Conference on Communications (ICC)*, 2016.
- [LBDA15] Y. Li, F. Baccelli, H. Dhillon, and J. Andrews. Statistical Modeling and Probabilistic Analysis of Cellular Networks With Determinantal Point Processes. *IEEE Trans. on Communications*, 63, 2015.
- [Leb65] N. Lebedev. *Special Functions and Their Applications*. Pretince Hall, 1965.
- [LHA13] A. Lozano, R. Heath, and J. Andrews. Fundamental Limits of Cooperation. *IEEE Transactions on Information Theory*, 59:5213–5226, 2013.
- [LMR14] F. Lavancier, J. Moller, and E. Rubak. Determinantal point process models and statistical inference : Extended version. *arXiv:1205.4818*, 2014.
- [MR96] R. Meester and R. Roy. *Continuum Percolation*. Cambridge University Press, 1996.



- [NMH14] G. Nigam, P. Minero, and M. Haenggi. Coordinated Multipoint Joint Transmission in Heterogeneous Networks. *IEEE Trans. on Communications*, 62(11):4134–4146, 2014.
- [Pen03] M. Penrose. *Random Geometric Graphs*. Oxford Studies in Probability, 2003.
- [PGH08] A. Papadogiannis, D. Gesbert, and E. Hardouin. A Dynamic Clustering Approach in Wireless Networks with Multi-Cell Cooperative Proocessing. *ICC*, 2008.
- [PLH16] J. Park, N. Lee, and R. W. Heath. Cooperative Base Station Coloring for Pair-wise Multi-Cell Coordination. *IEEE Trans. on Wireless Communications*, 2016.
- [RC04] C. Robert and G. Casella. *Monte Carlo Statistical Methods*. Springer Texts in Statistics. Springer, 2nd edition, 2004.
- [Ros09] Sheldon M. Ross. *A first course in probability*. Pearson Pretince Hall, 8th edition, 2009.
- [Rud87] W. Rudin. *Real and Complex Analysis*. McGraw-Hill International editions, third edition, 1987.
- [She07] D.J. Sheskin. *Handbook of parametric and nonparametric statistical procedures*. Chapman & Hall/CRC, 4th Edition, 2007.
- [SKP16] E. Stai, V. Karyotis, and S. Papavassiliou. A Hyperbolic Space Analytics Framework for Big Network Data and Their Applications. *IEEE Network*, pages 11–17, January 2016.
- [SSKP16] E. Stai, K. Sotiropoulos, V. Karyotis, and S. Papavassiliou. Hyperbolic Traffic Load Centrality for Large-Scale Complex Communications Networks. *International Conference on Telecommunications (ICT)*, June 2016.
- [TSAJ14] R. Tanbourgi, S. Singh, J. G. Andrews, and F. K. Jondral. A Tractable Model for Noncoherent Joint-Transmission Base Station Cooperation. *IEEE Trans. on Wireless Communications*, 13(9):4959–4973, 2014.
- [VKG17] S. Veetie, K. Kuchi, and R. Ganti. Coverage Analysis of Cloud Radio Networks With Finite Clustering. *IEEE Trans. on Wireless Communications*, 16:594–606, 2017.